THE WORLD BANK
IBRD • IDA | WORLD BANK GROUP

ESMAP
Energy Sector Management Assistance Program

SOLAR RESOURCE AND PV POTENTIAL OF THE MALDIVES

12 MONTH SOLAR RESOURCE REPORT

June 2017

This report was prepared by Solargis, under contract to The World Bank.

It is one of several outputs from the solar resource mapping component of the activity "Renewable Energy Resource Mapping and Geospatial Planning – Maldives" [Project ID: P146018]. This activity is funded and supported by the Energy Sector Management Assistance Program (ESMAP), a multi-donor trust fund administered by The World Bank, under a global initiative on Renewable Energy Resource Mapping. Further details on the initiative can be obtained from the ESMAP website.

This document is an **interim output** from the above-mentioned project, and the content is the sole responsibility of the consultant authors. Users are strongly advised to exercise caution when utilizing the information and data contained, as this may include preliminary data and/or findings, and the document has not been subject to full peer review. Final outputs from this project will be marked as such, and any improved or validated solar resource data will be incorporated into the Global Solar Atlas.

Washington DC 20433
Telephone: +1-202-473-1000
Internet: www.worldbank.org

Annual Solar Resource Report

for solar meteorological stations after completion of 12 months of measurements

Republic of Maldives

Reference No. 129-06/2017
Date: 7 June 2017

Customer

World Bank
Energy Sector Management Assistance Program
Contact: Mr. Oliver J. Knight
1818 H St NW, Washington DC, 20433, USA
Phone: +1-202-473-3159
E-mail: mailto:oknight@worldbank.org
http://www.esmap.org/RE_Mapping

Consultant

Solargis s.r.o.
Contact: Mr. Marcel Suri
Mytna 48, 811 07 Bratislava, Slovakia
Phone +421 2 4319 1708
E-mail: marcel.suri@solargis.com
http://solargis.com

TABLE OF CONTENTS

ACRONYMS

AP	Atmospheric Pressure
CFSR	Climate Forecast System Reanalysis. The meteorological model operated by the US service NOAA (National Oceanic and Atmospheric Administration)
CFS v2	Climate Forecast System Version 2 CFSv2 model is the operational extension of the CFSR (NOAA, NCEP)
DIF	Diffuse Horizontal Irradiation, if integrated solar energy is assumed. Diffuse Horizontal Irradiance, if solar power values are discussed
DNI	Direct Normal Irradiation, if integrated solar energy is assumed. Direct Normal Irradiance, if solar power values are discussed.
GFS	Global Forecast System. The meteorological model operated by the US service NOAA (National Oceanic and Atmospheric Administration)
GHI	Global Horizontal Irradiation, if integrated solar energy is assumed. Global Horizontal Irradiance, if solar power values are discussed.
MACC	Monitoring Atmospheric Composition and Climate – meteorological model operated by the European service ECMWF (European Centre for Medium-Range Weather Forecasts)
Meteosat IODC (MFG)	Meteosat satellites operated by EUMETSAT organization. MFG: Meteosat First Generation. For this report the data from the Meteosat IODC are used. The satellite is positioned over the Indian Ocean.
PWAT	Precipitable water (water vaour)
RH	Relative Humidity at 2 metres
TEMP	Air Temperature at 2 metres
WD	Wind Direction at 10 metres
WS	Wind Speed at 10 metres

GLOSSARY

Aerosols	Small solid or liquid particles suspended in air, for example desert sand or soil particles, sea salts, burning biomass, pollen, industrial and traffic pollution.
All-sky irradiance	The amount of solar radiation reaching the Earth's surface is mainly determined by Earth-Sun geometry (the position of a point on the Earth's surface relative to the Sun which is determined by latitude, the time of year and the time of day) and the atmospheric conditions (the level of cloud cover and the optical transparency of atmosphere). All-sky irradiance is computed with all factors taken into account
Bias	Represents systematic deviation (over- or underestimation) and it is determined by systematic or seasonal issues in cloud identification algorithms, coarse resolution and regional imperfections of atmospheric data (aerosols, water vapour), terrain, sun position, satellite viewing angle, microclimate effects, high mountains, etc.
Clear-sky irradiance	The clear sky irradiance is calculated similarly to all-sky irradiance but without taking into account the impact of cloud cover.
Long-term average	Average value of selected parameter (GHI, DNI, etc.) based on multiyear historical time series. Long-term averages provide a basic overview of solar resource availability and its seasonal variability.
P50 value	Best estimate or median value represents 50% probability of exceedance. For annual and monthly solar irradiation summaries it is close to average, since multiyear distribution of solar radiation resembles normal distribution.
P90 value	Conservative estimate, assuming 90% probability of exceedance (with the 90% probability the value should be exceeded). When assuming normal distribution, the P90 value is also a lower boundary of the 80% probability of occurrence. P90 value can be calculated by subtracting uncertainty from the P50 value. In this report, we apply a simplified assumption of normal distribution of yearly values.
Root Mean Square Deviation (RMSD)	Represents spread of deviations given by random discrepancies between measured and modelled data and is calculated according to this formula: $$RMSD = \sqrt{\frac{\sum_{k=1}^{n}\left(X^{k}{}_{measured} - X^{k}_{modeled}\right)^{2}}{n}}$$ On the modelling side, this could be low accuracy of cloud estimate (e.g. intermediate clouds), under/over estimation of atmospheric input data, terrain, microclimate and other effects, which are not captured by the model. Part of this discrepancy is natural - as satellite monitors large area (of approx. 3.3 x 3.4 km for MSG satellite), while sensor sees only micro area of approx. 1 sq. centimetre. On the measurement side, the discrepancy may be determined by accuracy/quality and errors of the instrument, pollution of the detector, misalignment, data loggers, insufficient quality control, etc.
Solar irradiance	Solar power (instantaneous energy) falling on a unit area per unit time [W/m^2]. Solar resource or solar radiation is used when considering both irradiance and irradiation.
Solar irradiation	Amount of solar energy falling on a unit area over a stated time interval [Wh/m^2 or kWh/m^2].
Uncertainty of estimate, U_{est}	Is a parameter characterizing the possible dispersion of the values attributed to an estimated irradiance/irradiation values. In this report, uncertainty assessment of the solar resource model estimate is based on a detailed understanding of the achievable accuracy of the solar radiation model and its data inputs (satellite, atmospheric and other data), which is confronted by an extensive data validation experience. The second source of uncertainty is ground measurements. Their quality depends on accuracy of instruments, their maintenance and data quality control. Third contribution to the uncertainty is from the site adaptation method where ground-measured and satellite-based data are correlated.

1 INTRODUCTION

1.1 Background

This report is prepared within Phase 1 of the project *Renewable Energy Resource Mapping for the Republic of the Maldives*. This part of the project focuses on solar resource mapping and measurement services as part of a technical assistance in the renewable energy development implemented by the World Bank in Maldives. It is being undertaken in close coordination with the Ministry of Environment and Energy (MEE) of Maldives, the World Bank's primary country counterpart for this project. This project is funded by the *Energy Sector Management Assistance Program* (ESMAP) and *Asia Sustainable and Alternative Energy Program* (ASTAE), both administered by the World Bank and supported by bilateral donors.

This report summarizes results of first 12 months of the measuring campaign by the project ESMAP at four solar meteorological stations, installed in Maldives as part of the World Bank's ESMAP mission in Maldives. This report describes delivery of site-specific data, site adaptation of solar model, data uncertainty and statistical summary.

This report accompanies delivery of site-specific solar resource and meteorological data for four sites, where solar meteorological stations have been operated. As a result of high-quality operation of the meteorological sits, and site adaptation the Solargis model, reliable historical time series and TMY data is computed. **The delivered time series and Typical Meteorological Year data is ready for use for bankable evaluation of solar energy projects.**

The measurements at four sites, located in Maldives, are provided by Suntrace company (Germany). The model data for the same sites and related works, together with this report are supplied by Solargis (Slovakia).

1.1 Delivered data sets

The site specific data, provided as part of this delivery, include:

- Solar and meteorological easurements, after second level quality assessment (first level was delivered by Suntrace)
- Time series, representing last 18 years (1999 to 2016)
- Typical Meteorological Year data, also representing last 18 years

The data is delivered in formats ready to use in energy simulation software. This report provides detailed insight of the methodologies and reuslts.

Table 1.1 Delivered data characterstics

Feature	Time coverage	Primary time step	Delivered files
Measurements (Suntrace)	Dec 2015 to Dec 2016 Analytical tasks consider only a period from Jan to Dec 2016	1 minute	Quality controlled measurements – 1- minute
Model data – original (Solargis)	Jan 1999 to Dec 2016	30 minutes	Time series – hourly Time series – monthly Time series – yearly
Model data – site dadapted (Solargis)	Jan 1999 to Dec 2016	30 minutes	Time series – hourly Time series – monthly Time series – yearly Typical Meteorological Year P50 – hourly Typical Meteorological Year P90 – hourly

Table 1.2 Parameters in the delivered site-adapted time series and TMY data (hourly time step)

Parameter	Acronym	Unit	TS	TMY P50	TMY P90
Global horizontal irradiance	GHI	W/m^2	X	X	X
Direct normal irradiance	DNI	W/m^2	X	X	X
Diffuse horizontal irradiance	DIF	W/m^2	X	X	X
Global tilted irradiance (at optimum angle)	GHI	W/m^2	X	-	-
Solar azimuth	SA	°	X	X	X
Solar elevation	SE	°	X	X	X
Air temperature at 2 metres	TEMP	°C	X	X	X
Wind speed at 10 metres	WS	m/s	X	X	X
Wind direction at 10 metres	WD	°	X	X	X
Relative humidity	RH	%	X	X	X
Air Pressure	AP	hPa	X	X	X
Precipitable Water	PWAT	kg/m^2	X	X	X

1.2 Information included in this report

This report presents:

- Solar resource and meteorological measurements after 12 months of operation
  - Review and quality check of the measured data
  - Calibration procedures and results
  - List and explanation of the occurred disturbances and failures
- Comparison of the measurements to the model and uncertainty analysis
  - Comparison of solar and meteo measurements with the model data
  - Site adaptation of satellite data based on ground measurements and uncertainty estimate
  - Estimate of data uncertainty
- Data analysis (measured vs. modelled)
  - Monthly summaries of solar and meteorological parameters captured at the site
  - Variability of measured solar parameters
  - Frequency of occurrence of GHI and DNI 1-minute and 30-minute values
  - Frequency of occurrence of GHI and DNI 1-minute and 30-minute ramps

2 POSITION OF SOLAR METEOROLOGICAL SITES

In Maldives, four measuring stations were installed within the ESMAP Solar initiative. All of them have been located at the airports within the premises of Maldives Meteorological Service (Figure 2.1, Table 2.1).

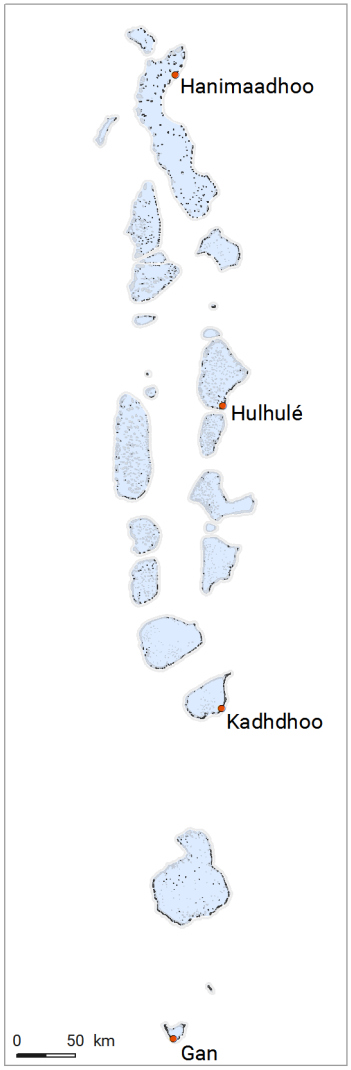

Figure 2.1: Position of solar meteorological stations in Maldives

Table 2.1 Overview information on the solar meteorological stations installed in Maldives

Site name (airport)	Site ID	Latitude [°]	Longitude [°]	Altitude [m a.s.l.]	Measurement station host
Hanimaadhoo	MVHAQ	6.7482°	73.1696°	2	Hanimaadhoo International Airport
Hulhulé	MVMLE	4.1927°	73.5281°	2	Male International Airport
Kadhdhoo	MVKDO	1.8599°	73.5203°	2	Kadhdhoo Airport
Gan	MVGAN	-0.6911°	73.1599°	2	Gan International Airport

Besides the good geographical distribution within the territory of Maldives, the locations fit well to the population centres, where solar installations can be primarily deployed.

In addition to geographical and socio-economic criteria, the sites fulfil the criteria for the operation and maintenance of the solar measuring stations:

- Availability of free horizon,
- Availability of GSM networks,
- Availability of local work force for maintenance,
- Easy to access and high level of security

During the first year of the measurements, the measured data was analysed and harmonized with the objective to acquire reference solar radiation data for reducing the uncertainty of the model Chapter 6). The quality data from four Tier-2 meteorological stations are available for this assessment (Chapter 3).

Position and detailed information about measurement sites is available also on Global Solar Atlas website: http://globalsolaratlas.info/?c=4.850154,73.146973,6&e=1

3 GROUND MEASUREMENTS IN MALDIVES

3.1 Instruments and measured parameters

Basic information about measurements sites is in Table 3.1. Solar parameters at all stations are measured by high (SR20, for measurements of GHI) and medium (RSP, for GHI, DNI and DIF) accuracy equipment (Table 3.2 and 3.3). The measurement campaign in Maldives has been performed by Suntrace GmbH company (Germany).

Table 3.1 Overview information on measurement stations operated in the region

ID	Site name (airport)	Site ID	Latitude [°]	Longitude [°]	Altitude [m a.s.l.]	Installation date
1	Hanimaadhoo	MVHAQ	6.7482°	73.1696°	2	10 Dec 2015
2	Hulhulé	MVMLE	4.1927°	73.5281°	2	08 Dec 2015
3	Kadhdhoo	MVKDO	1.8599°	73.5203°	2	14 Dec 2015
4	Gan	MVGAN	-0.6911°	73.1599°	2	13 Dec 2015

Table 3.2 Instruments installed at the solar meteorological stations

Site name	GHI 1	GHI 2	DNI	DIF	Temp	RH	WS	AP
Hanimaadhoo	SR20 - T1	RSP 4G	RSP 4G	RSP 4G	DKRF 400	DKRF 400	First Class	-
Hulhulé	SR20 - T1	RSP 4G	RSP 4G	RSP 4G	DKRF 400	DKRF 400	First Class	-
Kadhdhoo	SR20 - T1	RSP 4G	RSP 4G	RSP 4G	DKRF 400	DKRF 400	First Class	-
Gan	SR20 - T1	RSP 4G	RSP 4G	RSP 4G	DKRF 400	DKRF 400	First Class	-

Table 3.3 Technical parameters and accuracy class of the instruments

Parameter	Instrument	Type	Manufacturer	Uncertainty
GHI 1	Secondary standard pyranometer	SR20 - T1	Hukseflux	< ±2.0 % (daily)
GHI 2	Rotating Shadowband Irradiometer	RSP 4G	Reichert GmbH	Indicatively ±5 %
DIF	Rotating Shadowband Irradiometer	RSP 4G	Reichert GmbH	Indicatively ±8 %
DNI	Rotating Shadowband Irradiometer	RSP 4G	Reichert GmbH	Indicatively ±5 %
TEMP	Temperature probe	DKRF 400	Driesen und Kern	± 1.5 °C
RH	Relative humidity probe	DKRF 400	Driesen und Kern	± 3.5 % RH
WS	Wind speed sensor (WS at 3.0 m height)	First Class	Thies Clima	< ±1 %
AP	Barometric pressure sensor	Not provided	-	-
-	Data logger	blueberry	Wilmers GmbH	-

3.2 Station operation and calibration of instruments

In this report, data from the first year of 2-year measurement campaign is analysed. As the measurement stations have been installed during December 2015, the **period considered for the data analysis starts in January 2016 and ends in December 2016 for all four stations**. Overview of the data availability, time step and measured parameters is shown in Tables 3.4 and 3.5.

Table 3.4 Overview information on solar meteorological stations operating in the region

Site name(airport)	Site ID	First measurement period	Primary time step
Hanimaadhoo	MVHAQ	11 Dec 2015 to 31 Dec 2016	1 minute
Hulhulé	MVMLE	09 Dec 2015 to 31 Dec 2016	1 minute
Kadhdhoo	MVKDO	15 Dec 2015 to 31 Dec 2016	1 minute
Gan	MVGAN	14 Dec 2015 to 31 Dec 2016	1 minute

Table 3.5 Period of measurements analysed in this report

Year, month	2015												2016												2017											
Station	1	2	3	4	5	6	7	8	9	10	11	12	1	2	3	4	5	6	7	8	9	10	11	12	1	2	3	4	5	6	7	8	9	10	11	12
Hanimaadhoo																																				
Hulhulé																																				
Kadhdhoo																																				
Gan																																				

During the measurement campaign, local staff of Maldives Meteorological Service was fully trained by Suntrace, and participating on daily inspection and cleaning of instruments. Local partner Renewable Energy Maldives, performed detailed visits and station maintenance after 6 and 12 months of operation. Instruments field verification, i.e. one day long comparative measurements of solar radiation parameters and cross check with the instruments from the spare station to proof that sensitivities (calibration constants) remained stable within the instrument specifications, was performed by Suntrace GmbH after one year of operation (Table 3.6).

Table 3.6 Meteorological stations maintenance and instruments field verification

Site name (airport)	Site ID	Instruments cleaning interval	Annual verification visit	Instruments field verification	Comments
Hanimaadhoo	MVHAQ	daily	23 to 24 Nov 2016	SR20 - T1 RSP 4G	No issues
Hulhulé	MVMLE	daily	22 to 23 Nov 2016	SR20 - T1 RSP 4G	No issues
Kadhdhoo	MVKDO	daily	27 to 28 Nov 2016	SR20 - T1 RSP 4G	No issues
Gan	MVGAN	daily	25 to 26 Nov 2016	SR20 - T1 RSP 4G	No issues

To perform a verification of the measurements, the spare instruments were connected to the spare station logger. The timestamp of both data has been synchronized to be able to perform a valid inter-comparison. For the RSP values the corresponding calibration factors and corrections have been applied. Values below 50 W/m^2 have been discarded. Results of field instruments verification are listed in Table 3.7. According to the results of filed check of the instruments, the calibration coefficients at Gan, Kadhdhoo and Hulhulé solar meteorological

stations has been updated. Detailed results and discussion is supplied in *Annual maintenance visit reports* delivered separately for each meteorological station in February 2017.

Table 3.7 Results of field instruments verification at the respective stations

Site name (airport)	Site ID	Relative bias [%]			
		SR20 GHI	RSP 4G GHI	RSP 4G DNI	RSP 4G DIF
Hanimaadhoo	MVHAQ	-0.7	2.6	14.8*	1.2
Hulhulé	MVMLE	-2.3	-3.5	4.5	-5.5
Kadhdhoo	MVKDO	-0.8	0.8	5.7	-2.0
Gan	MVGAN	0.0	2.3	15.2*	-0.6

* Verification affected by prevailing cloud weather

3.3 Quality control of measured solar resource data

Prior to correlation with satellite-based solar data, the ground-measured solar radiation was quality-controlled by Solargis. Quality control (QC) was based on methods defined in SERI QC procedures and Younes et al. [1, 2] and the in-house developed tests. The ground measurements were inspected also visually, mainly for identification of shading and other error patterns such as RSP shading ring malfunction.

Figures 3.1 to 3.7 show results of quality control for individual stations. The colours in Figures 3.1, 3.3, 3.5 and 3.7 indicate the following flags:

- Blue: data excluded by visual inspection - mainly shading, shading ring issues
- Green: data passed all tests
- Grey: sun below horizon
- White and brown strips: missing data
- Red and violet: GHI, DNI and DIF consistency problem or problems with physical limits

The data records not passing the quality control test were flagged and excluded from the further processing. The results show relatively small amount of excluded data readings (Tables 3.9, 3.11, 3.13 and 3.15). Most serious is the DNI degradation due to shadowband issues.

3.3.1 Hanimaadhoo Airport

Table 3.8 Occurrence of data readings for Hanimaadhoo meteorological station

Data availability	GHI SR20		GHI, DNI RSP	
Sun below horizon	276 509	49.6%	276 509	49.6%
Sun above horizon	280 770	50.4%	280 770	50.4%
Total data readings	557 279	100.0%	557 279	100.0%

Table 3.9 Excluded ground measurements after quality control (Sun above horizon) in Hanimaadhoo

Type of test	Occurrence of data samples (Sun above horizon)					
	GHI SR20		DNI RSP		GHI RSP	
Physical limits test	237	0.1%	0	0.0%	1 288	0.5%
Consistency test (GHI – DNI – DIF)	-	-	135	0.0%	135	0.0%
Visual test (incorrect data)	12 886	4.6%	17 995	6.4%	12 462	4.4%
Other (non valid data)	98	0.0%	166	0.1%	166	0.1%
Total excluded data samples	13 221	4.7%	18 296	6.5%	14 051	5.0%
Total samples	280 770	100.0%	280 770	100.0%	280 770	100.0%

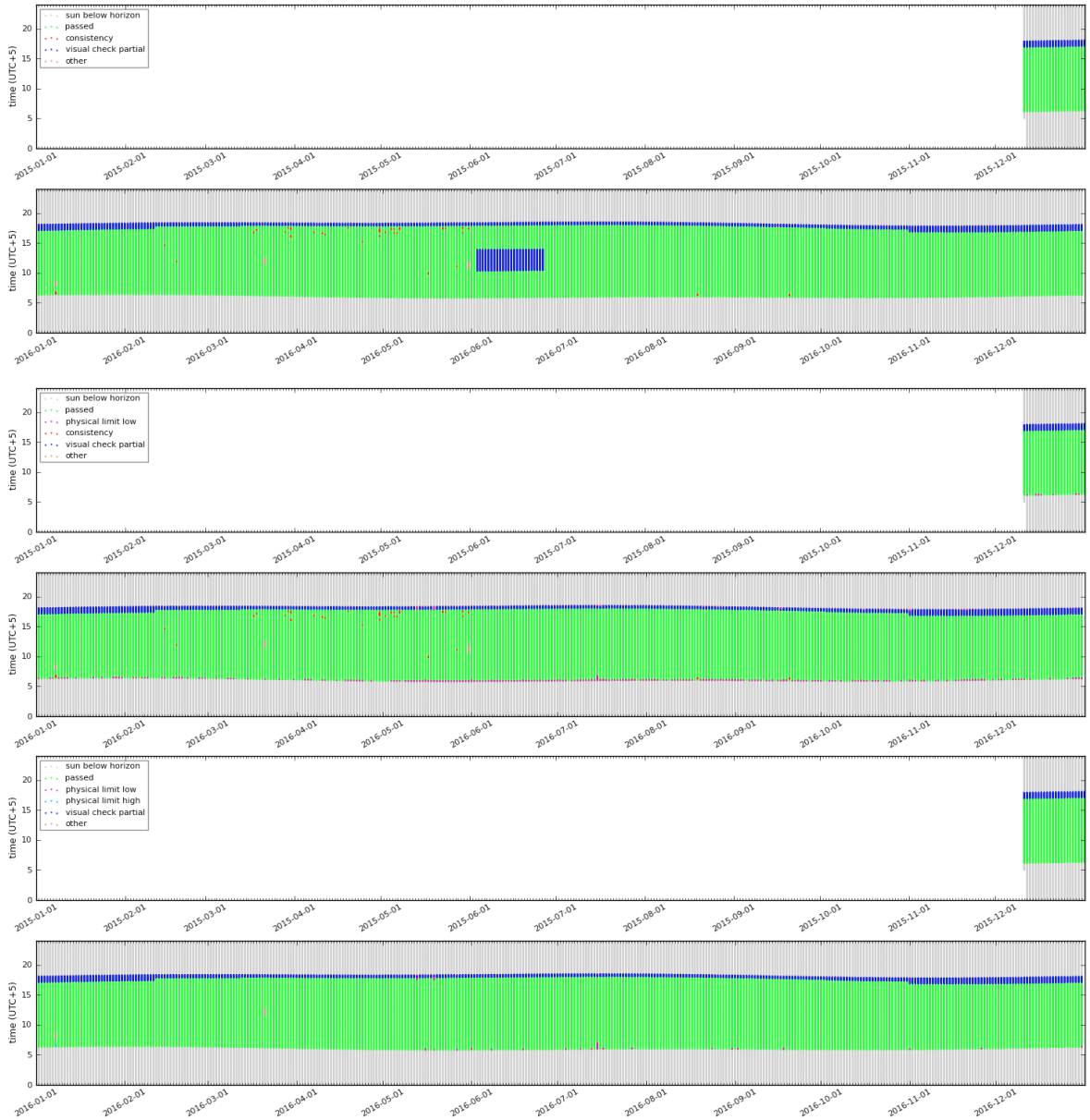

Figure 3.1 Results of GHI and DNI quality control in Hanimaadhoo.
Green – data passing all tests; grey – sun below horizon; red – consistency issue, violet – physical limit, blue excluded by visual inspection. Top: DNI (RSP); middle: GHI (RSP); bottom: GHI (SR20)

Main findings:

- Shadowband malfunction. Due to specific location of measurement stations close to the Equator the rotating shadowband may not in some periods sufficiently shade the sensor. This insufficient shading results in degraded DNI and DIF measurements. This problem was identified for period a from 3 to 26 June 2016 around the noon. Approximately 1.8% of DNI and DIF measurements were excluded.
- A systematic difference between GHI measurements from secondary standard pyranometer SR20-T1 and RSP (Figure 3.4). GHI from SR20 is in average higher by 4.4% than GHI from RSP. In the noon time, it can exceed 6%.
- Late afternoon shading from surrounding objects
- GHI measurements from SR20 were replaced by data from RSP in case of shading from wind mast.

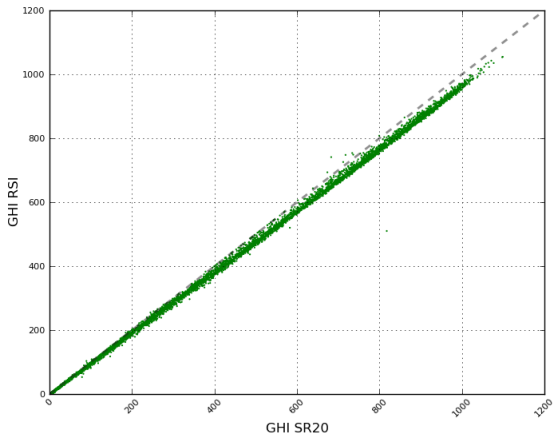

Figure 3.2 Systematic difference between GHI from SR20 and RSP – Hanimaadhoo.

3.3.2 Hulhulé Airport

Table 3.10 Occurrence of data readings for Hulhulé meteorological station

Data availability	GHI SR20		GHI, DNI RSP	
Sun below horizon	277 856	49.6%	277 856	49.6%
Sun above horizon	282 303	50.4%	282 303	50.4%
Total data readings	560 159	100.0%	560 159	100.0%

Table 3.11 Excluded ground measurements after quality control (Sun above horizon) in Hulhulé

Type of test	Occurrence of data samples (Sun above horizon)					
	GHI SR20		DNI RSP		GHI RSP	
Physical limits test	278	0.1%	0	0.0%	1 211	0.4%
Consistency test (GHI – DNI – DIF)	-	-	52	0.0%	52	0.0%
Visual test (incorrect data)	12 796	4.5%	24 692	8.7%	12 436	4.4%
Other (non valid data)	101	0.0%	5 687	2.0%	853	0.3%
Total excluded data samples	13 175	4.7%	30 431	10.8%	14 552	5.2%
Total samples	282 303	100.0%	282 303	100.0%	282 303	100.0%

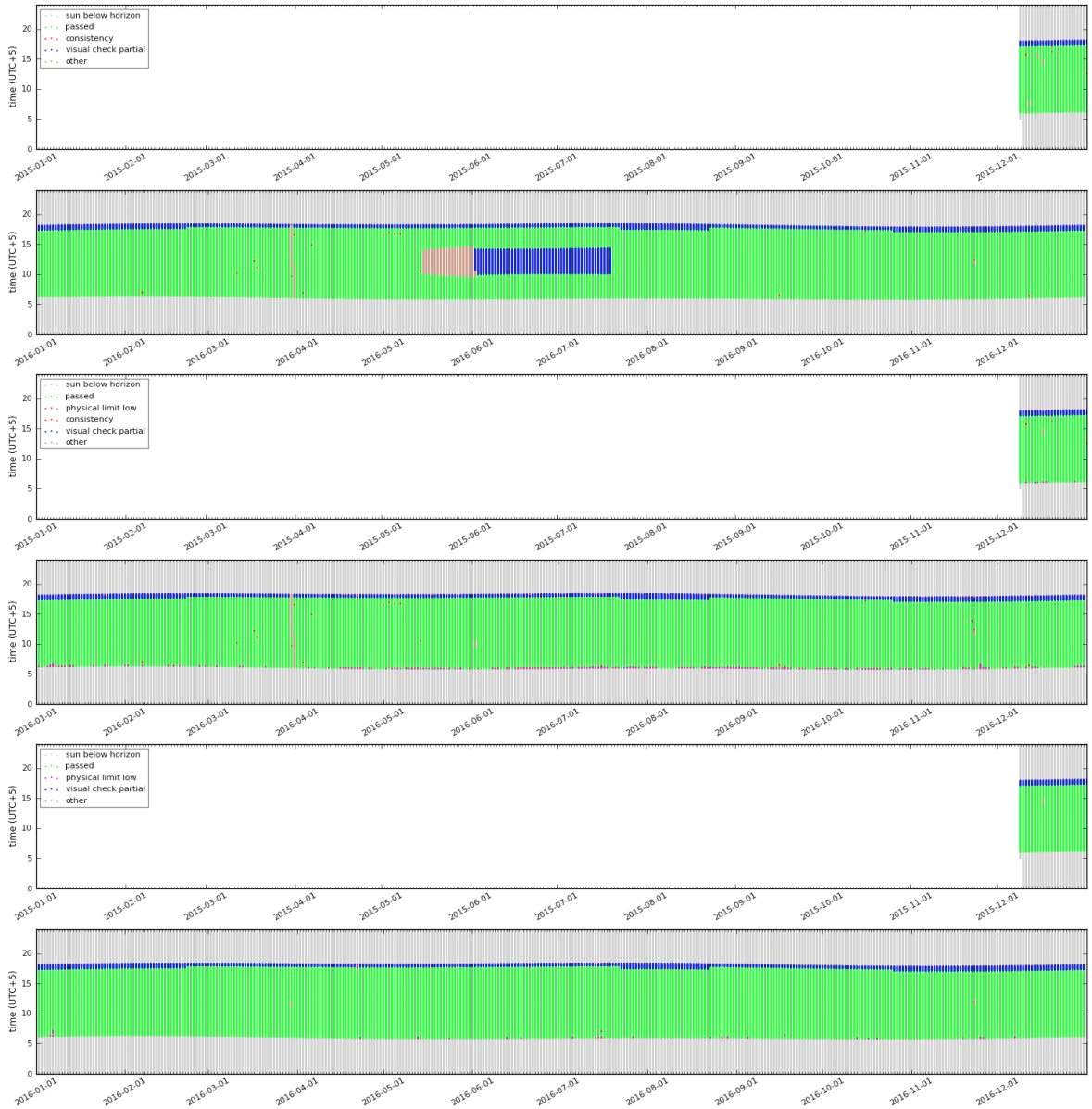

Figure 3.3 Results of GHI and DNI quality control in Hulhulé.
Green – data passing all tests; grey – sun below horizon; red – consistency issue, violet – physical limit issue, blue excluded by visual inspection; brown – missing data.
Top: DNI (RSP); middle: GHI (RSP); bottom: GHI (SR20)

Main findings:

- Shadowband malfunction (Figure 3.4). This issue was identified for a period from 15 May to 19 July 2016 around the noon. Affected data readings in May were excluded by data provider, readings from June and July were excluded by quality control. Approximately 6.2% of DNI and DIF measurements were excluded in total.
- A systematic difference between GHI measurements from secondary standard pyranometer SR20-T1 and RSP (Figure 3.5). GHI from SR20 is in average higher by 6.6% than GHI from RSP. In the noontime the difference can exceed 8%.
- Late afternoon shading from surrounding objects
- GHI measurements from SR20 were replaced by data from RSP in case of shading from wind mast.

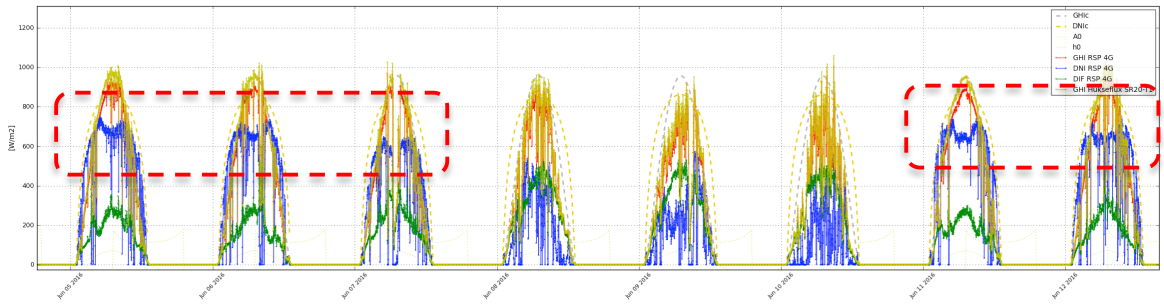

Figure 3.4 Effect of RSP shadowband issues – drop of DNI in Hulhulé.
Blue: DNI RSP; yellow: GHI SR20; red: GHI RSP; green: DIF RSP; dashed: theoretical clear-sky profile

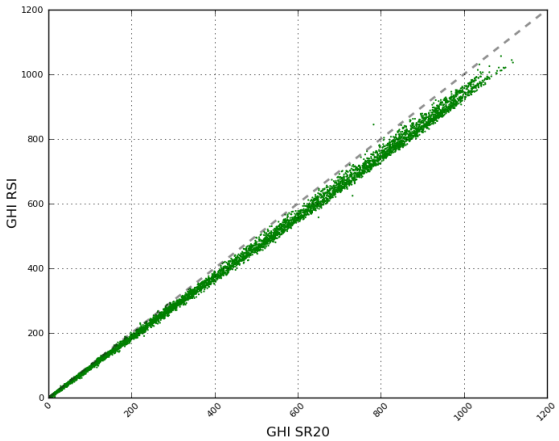

Figure 3.5 Systematic difference between GHI from SR20 and RSP - Hulhulé.

3.3.3 Kadhdhoo Airport

Table 3.12 Occurrence of data readings for Kadhdhoo meteorological station

Data availability	GHI SR20		GHI, DNI RSP	
Sun below horizon	273 387	49.6%	273 387	49.6%
Sun above horizon	278 132	50.4%	278 132	50.4%
Total data readings	551 519	100.0%	551 519	100.0%

Table 3.13 Excluded ground measurements after quality control (Sun above horizon) in Kadhdhoo

Type of test	Occurrence of data samples (Sun above horizon)					
	GHI SR20		DNI RSP		GHI RSP	
Physical limits test	381	0.1%	0	0.0%	1 089	0.4%
Consistency test (GHI – DNI – DIF)	-	-	66	0.0%	66	0.0%
Visual test (incorrect data)	23 762	8.5%	41 994	15.1%	23 011	8.3%
Other (non valid data)	48	0.0%	102	0.0%	101	0.0%
Total excluded data samples	24 191	8.7%	42 162	15.2%	24 267	8.7%
Total samples	278 132	100.0%	278 132	100.0%	278 132	100.0%

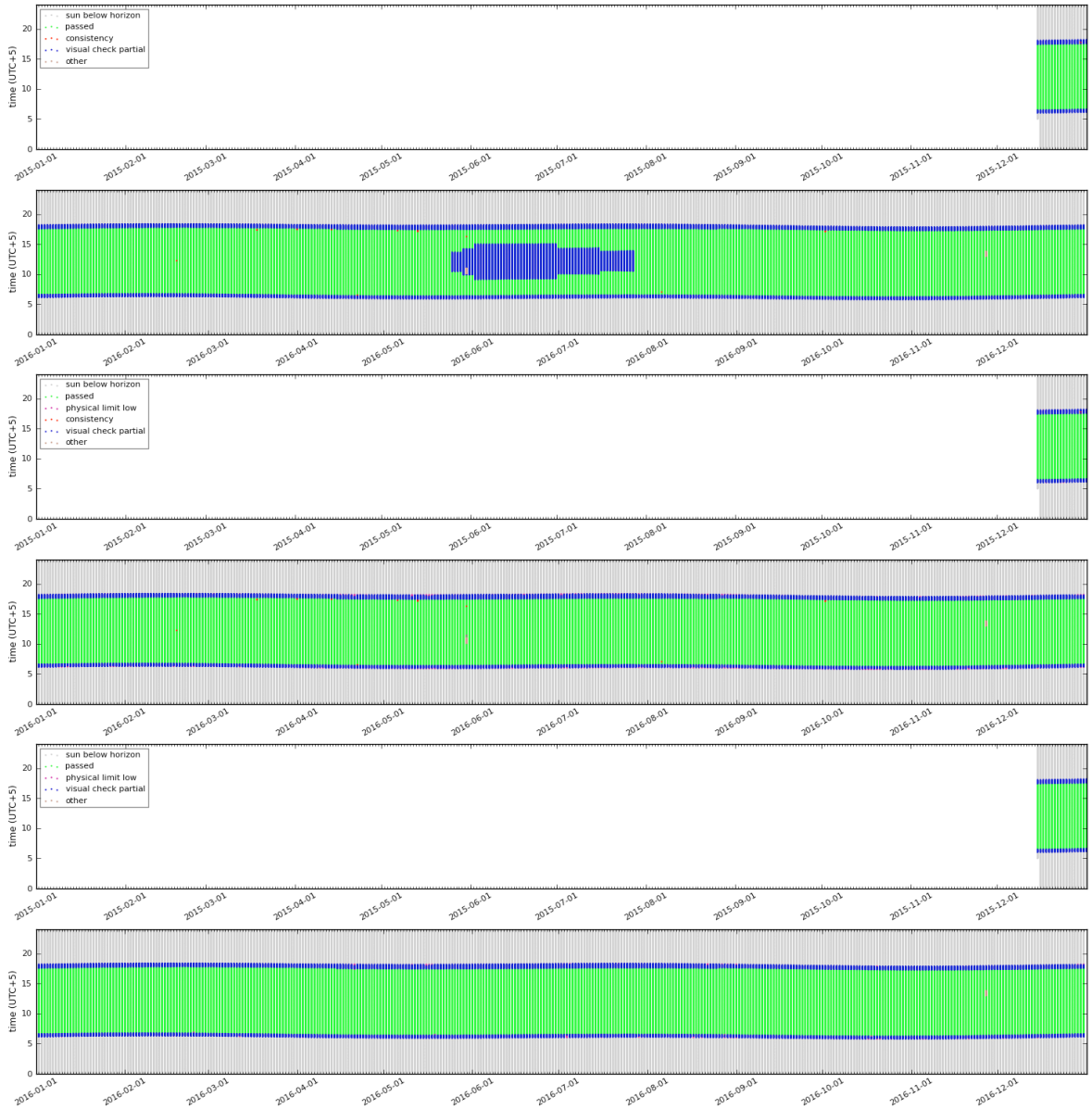

Figure 3.6 Results of GHI and DNI quality control – Kadhdhoo.
Green – data passing all tests; grey – sun below horizon; red – consistency issue, violet – physical limit issue, blue excluded by visual inspection. Top: DNI (RSP); middle: GHI (RSP); bottom: GHI (SR20)

Main findings:

- Shadowband malfunction (Figure 3.7). This issue was identified for a period from 25 May to 7 July 2016 around the noon. Affected data readings from June and July were excluded by quality control. Approximately 6.8% of DNI and DIF measurements were excluded in total.
- A systematic difference between GHI measurements from secondary standard pyranometer SR20-T1 and RSP (Figure 3.8). GHI from SR20 is in average higher by 4.3% than GHI from RSP. In the noon time it can exceed 7%.
- Late afternoon and early morning shading from surrounding objects
- GHI measurements from SR20 were replaced by data from RSP in case of shading from wind mast.

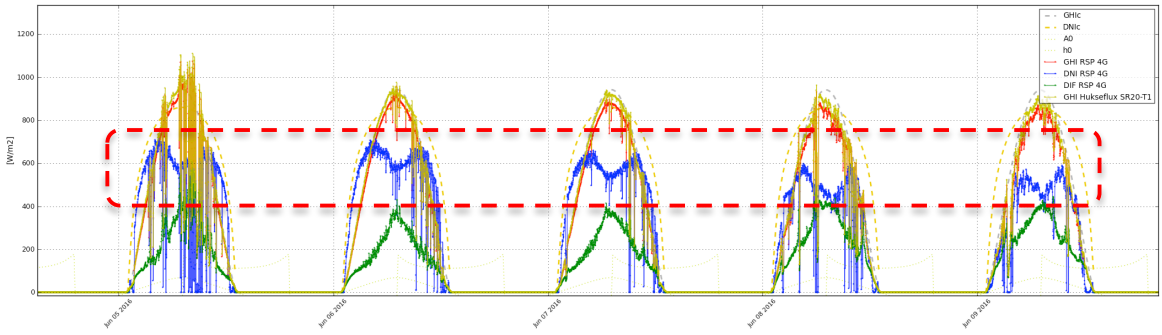

Figure 3.7 Effect of RSP shadowband issues – drop of DNI in Kadhdhoo.
Blue: DNI RSP; yellow: GHI SR20; red: GHI RSP; green: DIF RSP; dashed: theoretical clear-sky profile

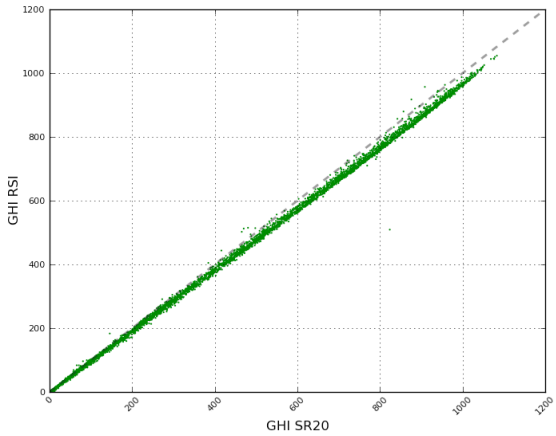

Figure 3.8 Systematic difference between GHI from SR20 and RSP – Kadhdhoo.

3.3.4 Gan Airport

Table 3.14 Occurrence of data readings for Gan meteorological station

Data availability	GHI SR20		GHI, DNI RSP	
Sun below horizon	273 987	49.5%	273 987	49.5%
Sun above horizon	278 972	50.5%	278 972	50.5%
Total data readings	552 959	100.0%	552 959	100.0%

Table 3.15 Excluded ground measurements after quality control (Sun above horizon) in Gan

Type of test	Occurrence of data samples (Sun above horizon)					
	GHI SR20		DNI RSP		GHI RSP	
Physical limits test	393	0.1%	0	0.0%	1 168	0.4%
Consistency test (GHI – DNI – DIF)	-	-	144	0.1%	144	0.1%
Visual test (incorrect data)	0	0.0%	14 843	5.3%	0	0.0%
Other (non valid data)	98	0.0%	17 194	6.2%	328	0.1%
Total excluded data samples	491	0.2%	32 181	11.5%	1 640	0.6%
Total samples	278 972	100.0%	278 972	100.0%	278 972	100.0%

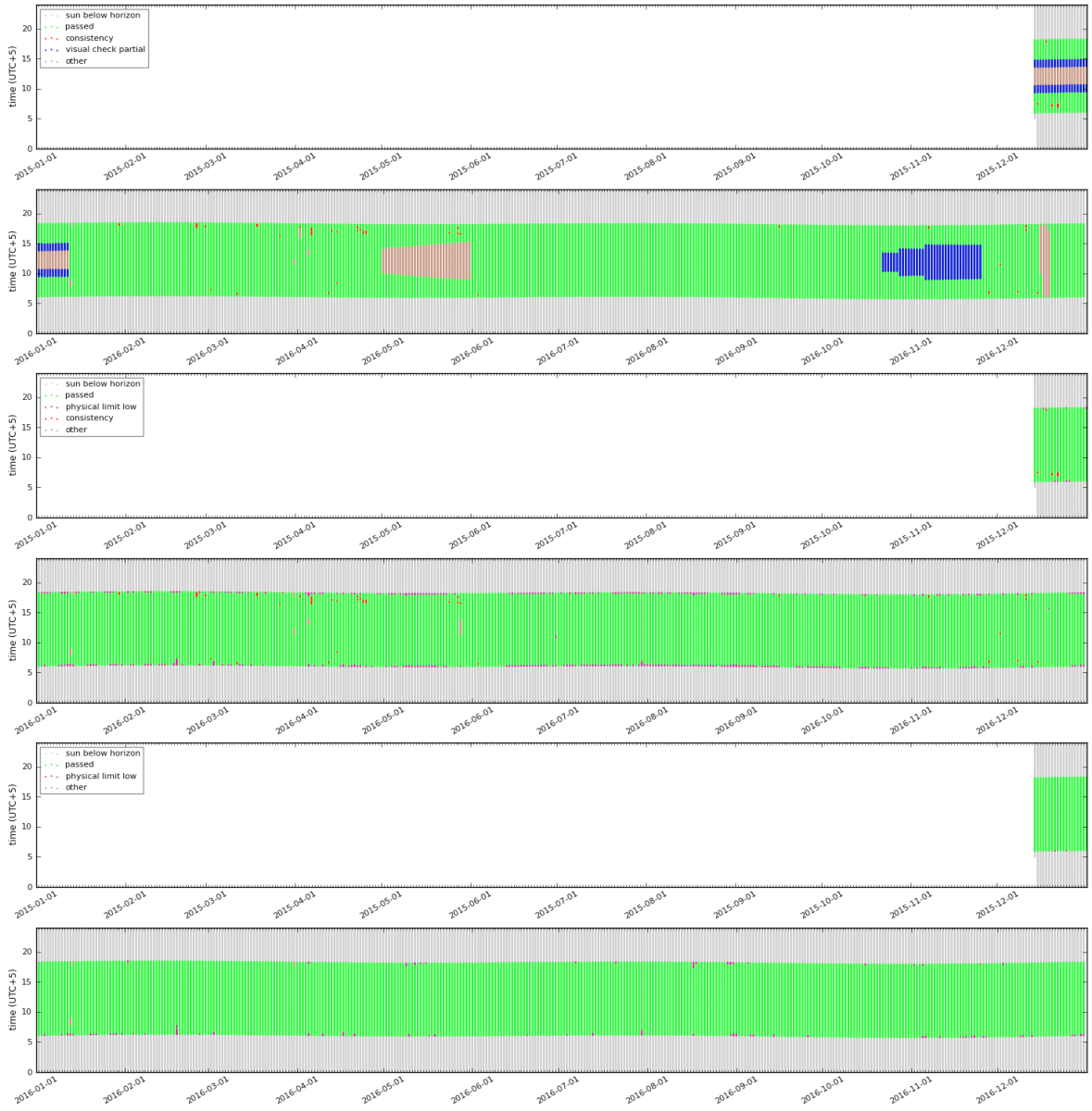

Figure 3.9 Results of GHI and DNI quality control – Gan.
Green – data passing all tests; grey – sun below horizon; red – consistency issue, violet – physical limit issue, blue excluded by visual inspection; brown – missing data.
Top: DNI (RSP); middle: GHI (RSP); bottom: GHI (SR20)

Main findings:

- Shadowband malfunction (Figure 3.10). This issue was identified for several periods (from 14 December 2015 to 12 January 2016; from 1 May to 31 May 2016 and from 22 October to 25 November 2016) around the noon. Affected data readings were excluded partly by data provider and partly by quality control. Approximately 11% of DNI and DIF measurements were excluded in total.
- A systematic difference between GHI measurements from secondary standard pyranometer SR20-T1 and RSP (Figure 3.11). GHI from SR20 is in average higher by 4.5% than GHI from RSP. In the noon time it can exceed 6%.
- GHI measurements from SR20 were replaced by data from RSP in case of shading from wind mast (Figure 3.12).

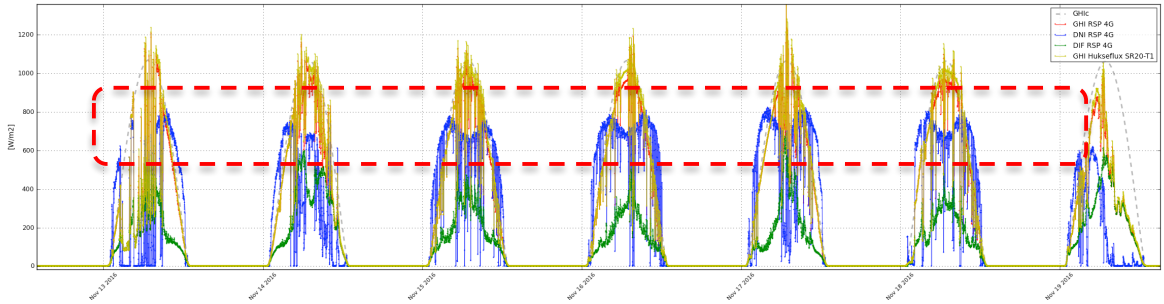

Figure 3.10 Effect of RSP shadowband issues – drop of DNI in Gan.
Blue: DNI RSP; yellow: GHI SR20; red: GHI RSP; green: DIF RSP; dashed: theoretical clear-sky profile

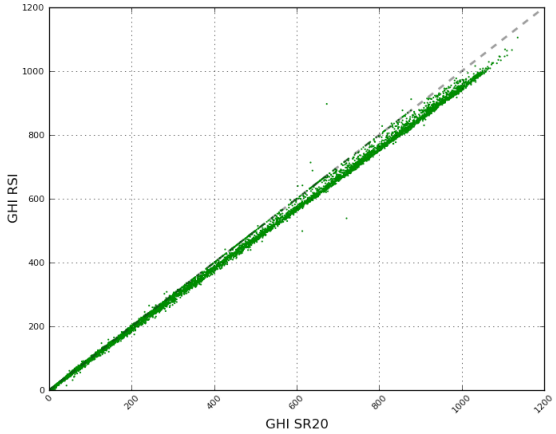

Figure 3.11 Systematic difference between GHI from SR20 and RSP - Gan.

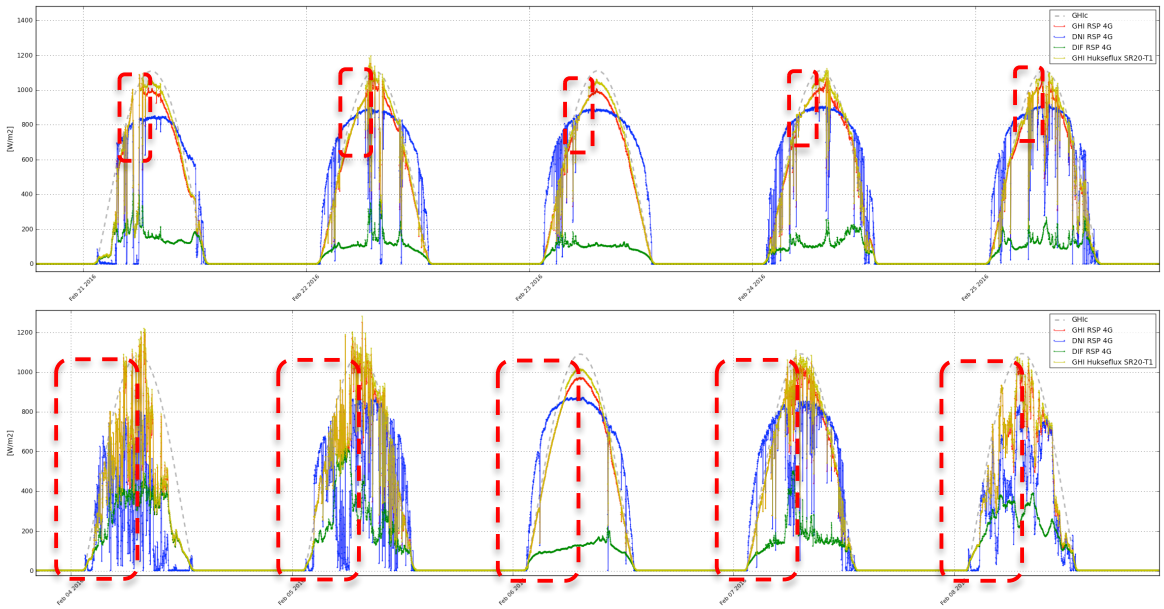

Figure 3.12 Replacement of SR20 GHI by RSP GHI due to wind mast shading in Gan.
Blue: DNI RSP; yellow: GHI SR20; red: GHI RSP; green: DIF RSP; dashed: theoretical clear-sky profile

3.4 Recommendations on the operation and maintenance of the sites

Based on the results of quality control (Table 3.16), we conclude that the solar radiation measurements come from the high (SR20) and medium (RSP) accuracy equipment that is professionally operated and maintained. Some issues were identified during the data quality control:

- Degraded DNI and DIF measurements due to shadowband malfunction. These data were flagged and excluded from further processing
- Higher systematic difference between GHI from SR20 and RSP (up to 6.6% in Hulhulé). This is known effect that should relate only to GHI instrument calibration. Due to this issue, the GHI from RSP was not considered for site-adaptation

For future works, we recommend:

- Adopt measures to avoid the shadowband problems, where possible.
- Identify and fix source of systematic difference between SR20 and RSP

Table 3.16 Quality control summary (all sites)

Description		
Station description, metadata		Installation report for all stations available
Instrument accuracy		Secondary standard instrument SR20-T1
		Rotating Shadowband Irradiometer RSP 4G
Instrument calibration		Instruments were calibrated
Data structure		Clear
Cleaning and maintenance information		Diligent daily cleaning
Time reference		Correct and clear time reference
Quality control complexity		RSP data, full QC SR20 data, without (GHI-DNI-DIF) consistency test
Quality control results		Shadowband temporary technical issues Larger systematic difference between GHI from SR20 and RSP (this is known issue)
Period		Almost 13 months
Other issues		

Legend: Quality marker

Very good	Good	Sufficient	Problematic	Insufficient	Not specified

4 SOLAR RESOURCE MODEL DATA

4.1 Solar model

Solar radiation is calculated by Solargis model, which are parameterized by a set of inputs characterizing the cloud transmittance, state of the atmosphere and terrain conditions. A comprehensive **overview of the Solargis model** is made available in the recent book publication [3]. The methodology is also described in [4, 5]. The related uncertainty and requirements for bankability are discussed in [6, 7].

In Solargis approach, the **clear-sky irradiance** is calculated by the simplified SOLIS model [8]. This model allows fast calculation of clear-sky irradiance from the set of input parameters. Sun position is deterministic parameter, and it is described by the algorithms with satisfactory accuracy. Stochastic variability of clear-sky atmospheric conditions is determined by changing concentrations of atmospheric constituents, namely aerosols, water vapour and ozone. Global atmospheric data, representing these constituents, are routinely calculated by world atmospheric data centres:

- In Solargis, the new generation **aerosol data set** representing Atmospheric Optical Depth (AOD) is used. The calculation accuracy is strongly determined by quality of aerosols, especially for cloudless conditions. The aerosol data implemented by MACC-II/CAMS and MERRA-2 projects are used [9, 10].
- **Water vapour** is also highly variable in space and time, but it has lower impact on the values of solar radiation, compared to aerosols. The GFS and CFSR databases (NOAA NCEP) are used in Solargis, and the data represent the daily variability from 1999 to the present time [11, 12, 13].
- **Ozone** absorbs solar radiation at wavelengths shorter than 0.3 μm, thus having negligible influence on the broadband solar radiation.

The clouds are the most influencing factor, modulating clear-sky irradiance. Effect of clouds is calculated from the satellite data in the form of a **cloud index** (cloud transmittance). The cloud index is derived by relating radiance recorded by the satellite in spectral channels and surface albedo to the cloud optical properties. In Solargis, the modified calculation scheme of Cano has been adopted to retrieve cloud optical properties from the satellite data [14].

To calculate **all-sky irradiance** in each time step, the clear-sky global horizontal irradiance is coupled with cloud index. Direct Normal Irradiance (DNI) is calculated from Global Horizontal Irradiance (GHI) using modified Dirindex model [15]. Diffuse irradiance for tilted surfaces, which is calculated by Perez model [16]. The calculation procedure includes also terrain disaggregation, the spatial resolution is enhanced with use of the digital terrain model to 250 meters [17]. Solargis model version 2.1 has been used. Table 4.1 summarizes technical parameters of the model inputs and of the primary data outputs.

Table 4.1 Input data used in the Solargis and related GHI and DNI outputs for Maldives

Inputs into the Solargis model	Source of input data	Time representation	Original time step	Approx. grid resolution
Cloud index	Meteosat IODC satellites (EUMETSAT)	1999 to date	30 minutes	2.8 x 3.2 km
Atmospheric optical depth (aerosols)*	MACC-II/CAMS* (ECMWF)	2003 to date	3 hours	75 km and 125 km
	MERRA-2 (NASA)	1999 to 2002	1 hour	50 km
Water vapour	CFSR/GFS (NOAA)	1999 to date	1 hour	35 and 55 km
Elevation and horizon	SRTM-3 (SRTM)	-	-	250 m
Solargis primary data outputs (GHI and DNI)	-	1999 to date	30 minutes	250 m

** Aerosol data for 2003-2012 come from the reanalysis database; the data representing years 2013-present are derived from near-real time operational model*

4.2 Site adaptation of the solar model – method

The fundamental difference between a satellite observation and a ground measurement is that signal received by the satellite radiometer integrates a large area, while a ground station represents a pinpoint measurement. This results in a mismatch when comparing instantaneous values from these two observation instruments, mainly during intermittent cloudy weather and changing aerosol load. Nearly half of the hourly Root Mean Square Deviation (RMSD) for GHI and DNI can be attributed to this mismatch (value at sub-pixel scale), which is also known as the "nugget effect" [18].

The satellite pixel is not capable describing the inter-pixel variability in complex regions, where within one pixel diverse natural conditions mix-up (e.g. fog in narrow valleys or along the coast). In addition, the coarse spatial resolution of atmospheric databases such as aerosols or water vapour is not capable to describe local patterns of the state of atmosphere. These features can be seen in the satellite DNI data by increased bias due to imperfect description of aerosol load. Satellite data have inherent inaccuracies, which have certain degree of geographical and time variability.

Especially DNI is strongly sensitive to variability of cloud information, aerosols, water vapour, and terrain shading. The relation between uncertainty of global and direct irradiance is nonlinear. Often, a negligible error in global irradiance may have high counterpart in the direct irradiance component.

The solar energy projects require representative and accurate GHI and DNI time series. The satellite-derived databases are used to describe long-term solar resource for a specific site. However, their problem when compared to the high-quality ground measurements is a slightly higher bias and partial disagreement of frequency distribution functions, which may limit their potential to record the occurrence of extreme situations (e.g. very low atmospheric turbidity resulting in a high DNI and GHI). A solution is to correlate satellite-derived data with ground measurements to understand the source of discrepancy and subsequently to improve the accuracy of the resulting time series.

The Solargis satellite-derived data are correlated with ground measurement data with two objectives:

- Improvement of the overall bias (removal of systematic deviations)
- Improvement of the fit of the frequency distribution of values.

The relation between uncertainty of global and direct irradiance is nonlinear. Often, a negligible error in the global horizontal irradiance may trigger higher error in the direct irradiance component. Limited spatial and temporal resolution of the input data and simplified nature of the models results in the occurrence of systematic and random deviations of the model outputs when compared to the ground observations. The deviations in the satellite-computed data, which have *systematic nature*, can be reduced by site adaptation or regional adaptation methods.

The terminology related to the procedure improving accuracy of the satellite data is not harmonized, and various terms are used:

- Correlation of ground measurements and satellite-based data;
- Calibration of the satellite model (its inputs and parameters);
- Site adaptation or regional adaptation of satellite based data.

The term *site adaptation* is more general and best explains the concept of adapting the satellite-based model (by correlation, calibration, fitting and recalculation) to the ground measured data. **Site adaptation** aims to adapt the characteristics of the satellite-based time series to the site-specific conditions described by local measurements.

Three conditions are important for successful adaptation of the satellite-based model:

1. High quality DNI and GHI ground measurements for at least 12 months must be available; optimally data for 2 or 3 years should be used;
2. High quality satellite data must be used, with consistent quality over the whole period of data;
3. There must be identified a systematic difference between both data sources.

Systematic difference can be measured by two characteristics:

- Bias (offset)
- Systematic deviation in the distribution of hourly or daily values (in the histogram)

Systematic difference can be stable over the year or it can slightly change seasonally for certain meteorological conditions (e.g. typical cloud formation during a day, seasonal air pollution). The data analysis should distinguish systematic differences from those arising at occasional events, such as extreme sand storms or forest fires. The episodically-occurring differences may mislead the results of adaptation, especially if short period of ground measurements is only available.

If one of the three above-mentioned conditions is not fulfilled, site adaptation (regional adaptation) will not provide the expected results. On the contrary, such an attempt may provide worse results.

For the quantitative assessment of the accuracy enhancement procedures, the following metrics is used:

- Metrics based on the comparison of all pairs of the hourly daytime data values: Mean Bias, and Root Mean Square Deviation (RMSD), histogram, in an absolute and relative form (divided by the daytime mean DNI values);
- Metrics based on the difference of the cumulative distribution functions: KSI (Kolmogorov-Smirnov test Integral) [19]

The normalized KSI is defined as an integral of absolute differences of two cumulative distribution functions *D* normalized by the integral of critical value $a_{critical}$:

$$KSI\% = \frac{\int_{x\,\min}^{x\,\max} D_n dx}{a_{critical}} * 100$$

$$a_{critical} = V_c * (x_{\max} - x_{\min})$$

$$V_c = \frac{1.63}{\sqrt{N}}, \quad N \geq 35$$

where critical value depends on the number of the data pairs *N*. As the KSI value is dependent on the size of the sample, the KSI measure may be used only for the relative comparison of fit of cumulative distribution of irradiance values.

For the accuracy enhancement of solar resource parameters in this study, a combination of two methods was used. First, systematic deviations due to influence of aerosols were partially removed. Afterwards, to improve the distribution of values, the fitting of cumulative frequency distribution curves of ground measurements and satellite data was used.

The site-adaptation procedure first identifies the sources of discrepancies by comparing the ground-measured data with Solargis model data, for the period of the overlap between both data sets. Based on this analysis, correction coefficients to improve the fit between the measured and the model Solargis data are developed. In the second step, these coefficients are used for the adaptation of the full (18 years) time series.

The satellite data is available in 30-minute time step and the ground measurements in 1-minute time step. To partially remove the conceptual difference of point and satellite pixel measurements, prior to site adaptation, all the measures are calculated using aggregated data in the hourly time step.

The adaptation was based on measured DNI data from RSP 4G instrument and GHI data from the secondary standard SR20-T1 instrument. GHI measured by the RSP 4G was not used because of higher uncertainty of the outputs (Chapter 3.3)

4.3 Results of the model adaptation at four sites

The original Solargis data show a regional pattern of slight overestimation, compared to the ground measurements – mainly for DNI. The GHI fits the ground measurements very well. The model adaptation allowed removing large part of mismatch between satellite-based data and ground measurements.

Tables 4.2 to 4.5 summarize validation of the site-adaptation results for all solar measuring stations.

Table 4.2 Direct Normal Irradiance: bias and KSI before and after model site-adaptation

Meteo station	Original DNI data			DNI after regional adaptation		
	Bias	Bias	KSI	Bias	Bias	KSI
	[kWh/m^2]	[%]	[-]	[kWh/m^2]	[%]	[-]
Hanimaadhoo	10	2.8	61	0	0.1	45
Hulhulé	22	6.0	78	0	0.0	63
Kadhdhoo	19	5.1	83	0	0.0	71
Gan	21	5.3	92	0	0.0	83
Mean	18	4.8	79	0	0.0	66
Standard deviation	5.5	1.4		0.1	0.0	

Table 4.3 Global Horizontal Irradiance: bias and KSI before and after model site-adaptation

Meteo station	Original GHI data			GHI after regional adaptation		
	Bias	Bias	KSI	Bias	Bias	KSI
	[kWh/m^2]	[%]	[-]	[kWh/m^2]	[%]	[-]
Hanimaadhoo	3	0.6	29	0	0.0	26
Hulhulé	-1	-0.1	31	0	0.0	29
Kadhdhoo	0	0.0	30	0	0.0	29
Gan	3	0.7	41	0	0.0	32
Mean	1	0.3	33	0	0.0	29
Standard deviation	2.1	0.4		0.0	0.0	

Table 4.4 Direct Normal Irradiance: RMSD before and after model site-adaptation

Meteo station	RMSD of original DNI data			RMSD of DNI after regional adaptation		
	Hourly	Daily	Monthly	Hourly	Daily	Monthly
	[%]	[%]	[%]	[%]	[%]	[%]
Hanimaadhoo	31.4	17.0	6.2	31.4	16.8	5.4
Hulhulé	35.5	19.7	7.4	34.9	19.0	4.8
Kadhdhoo	36.4	18.6	6.4	36.0	18.0	3.8
Gan	33.8	17.3	6.9	33.4	16.7	4.4
Mean	34.3	18.1	6.7	33.9	17.6	4.6

Table 4.5 Global Horizontal Irradiance: RMSD before and after model site-adaptation

Meteo station	RMSD of original GHI data			RMSD of GHI after regional adaptation		
	Hourly	Daily	Monthly	Hourly	Daily	Monthly
	[%]	[%]	[%]	[%]	[%]	[%]
Hanimaadhoo	15.2	6.8	2.4	15.2	6.8	2.4
Hulhulé	16.2	7.0	2.1	16.3	7.0	2.2
Kadhdhoo	16.8	6.7	1.5	16.8	6.7	1.5
Gan	15.1	6.3	2.0	15.1	6.2	1.9
Mean	15.9	6.7	2.0	15.9	6.7	2.0

As a result, at the level of individual measurement sites in Maldives, the mean bias of the adapted values was reduced to zero. The values of RMSD and KSI accuracy parameters are also reduced, especially for DNI.

The effect of the site adaptation is presented in a detail for all sites (Figures 4.1 to 4.4). The changes are very small as the original data have good fit to ground measurements.

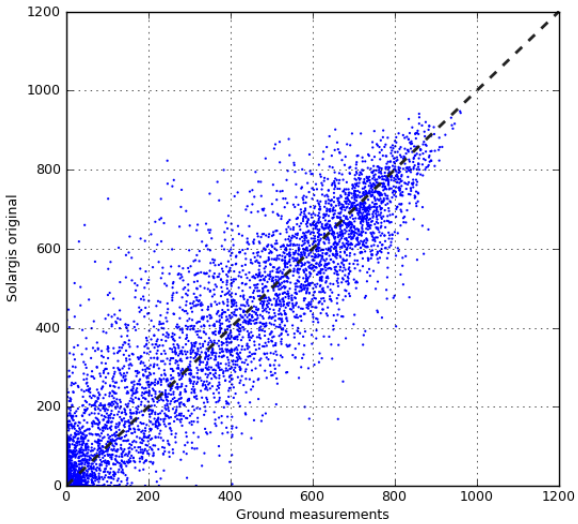

Hanimaadhoo: Original DNI

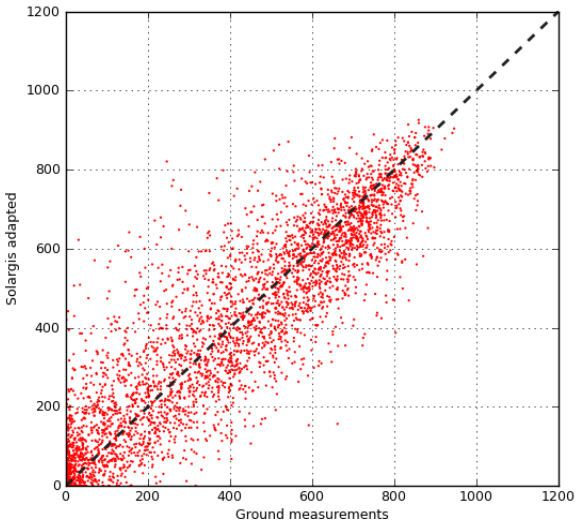

Hanimaadhoo: DNI after adaptation

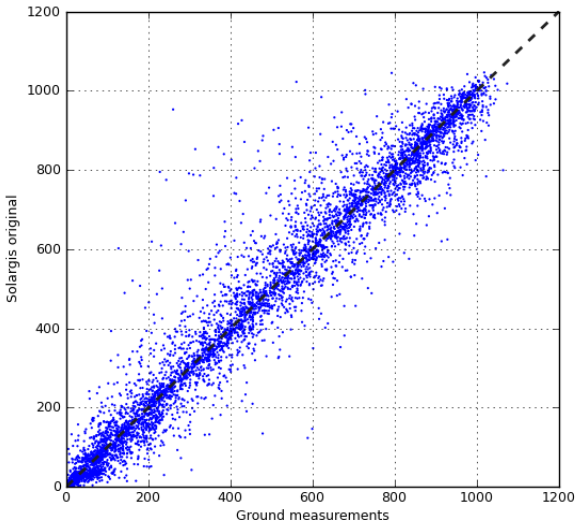

Hanimaadhoo: Original GHI

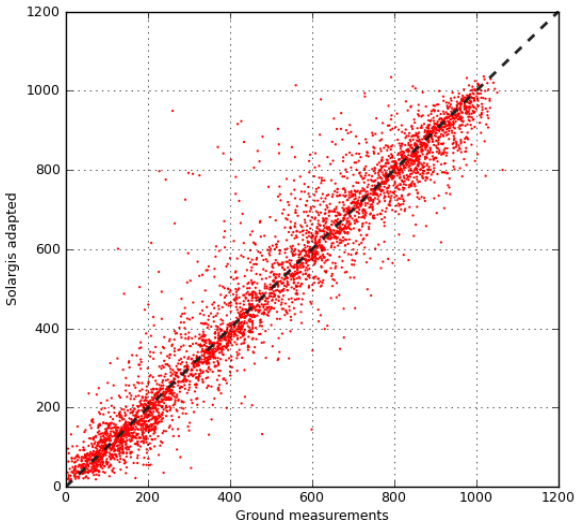

Hanimaadhoo: GHI after adaptation

Figure 4.1: Correction of DNI and GHI hourly values for Hanimaadhoo.
Left: original Solargis data, right: site-adapted Solargis data.
The X-axis represents the measured data and the Y-axis represents the satellite-derived data.

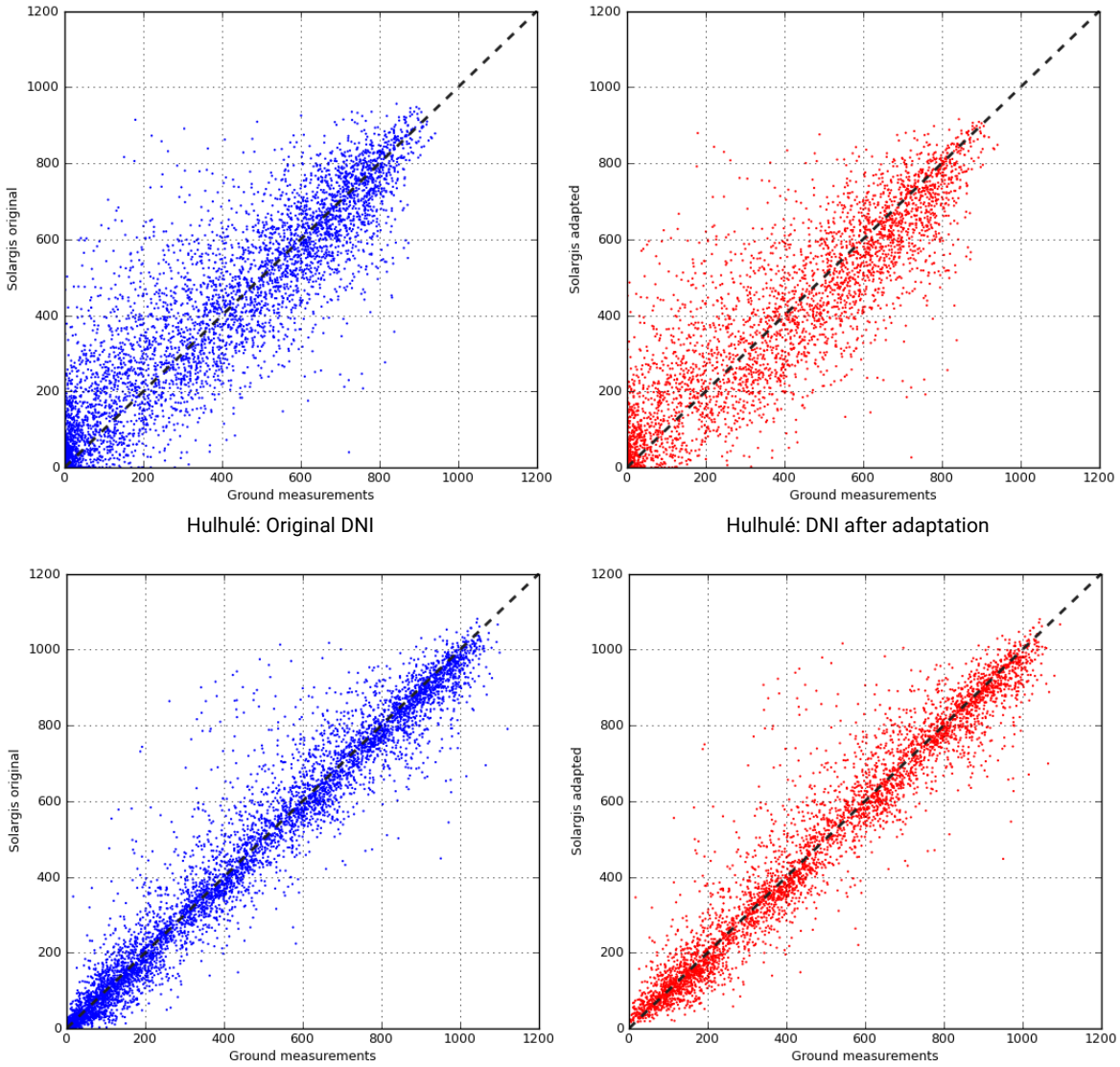

Hulhulé: Original DNI | Hulhulé: DNI after adaptation

Hulhulé: Original DNI | Hulhulé: DNI after adaptation

Figure 4.2: Correction of DNI and GHI hourly values for Hulhulé
Left: original Solargis data, right: site-adapted Solargis data.
The X-axis represents the measured data and the Y-axis represents the satellite-derived data.

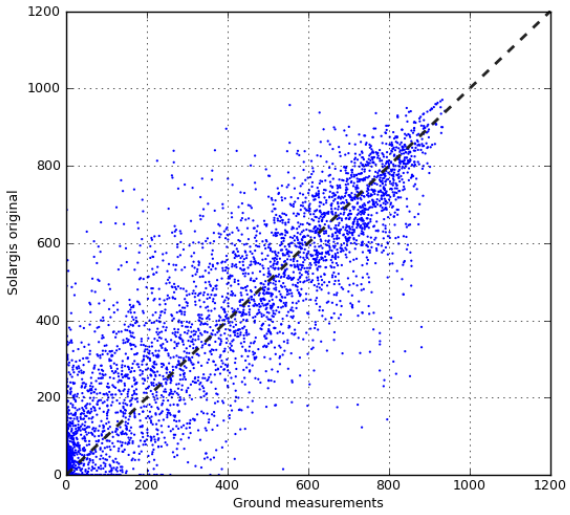

Kadhdhoo: Original DNI

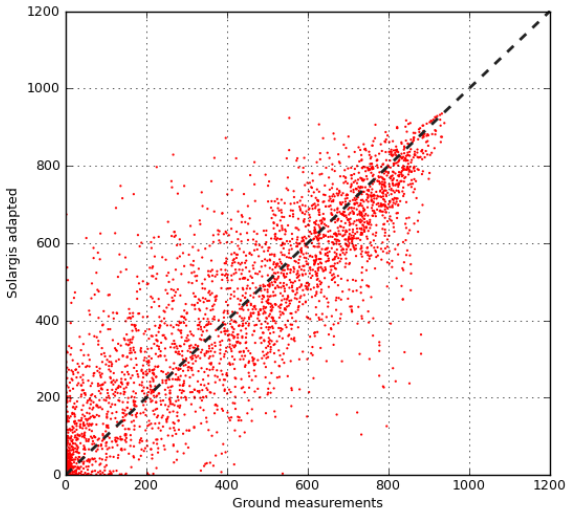

Kadhdhoo: DNI after adaptation

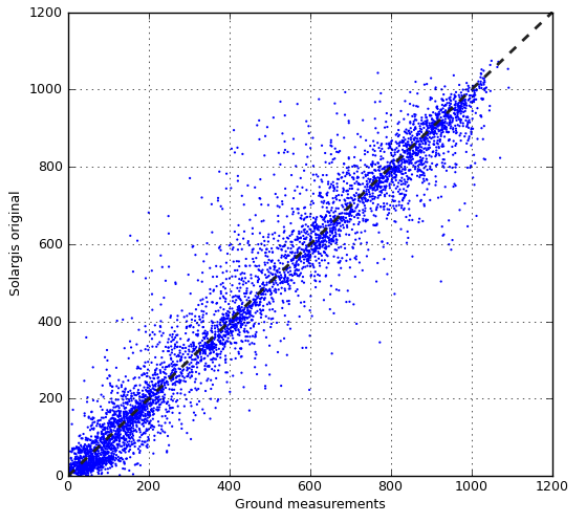

Kadhdhoo: Original DNI

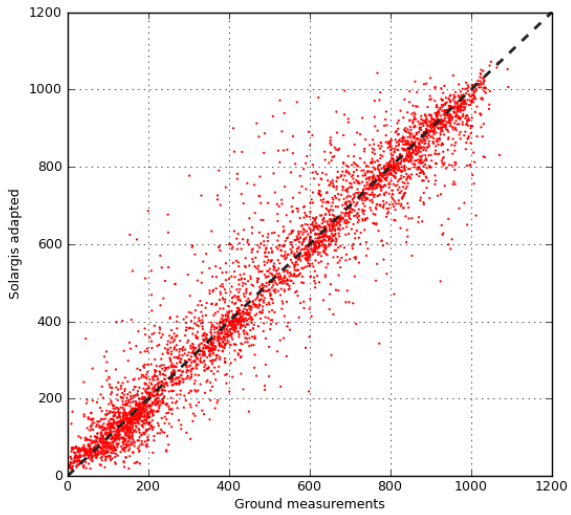

Kadhdhoo: DNI after adaptation

Figure 4.3: Correction of DNI and GHI hourly values for Kadhdhoo.
Left: original Solargis data, right: site-adapted Solargis data.
The X-axis represents the measured data and the Y-axis represents the satellite-derived data.

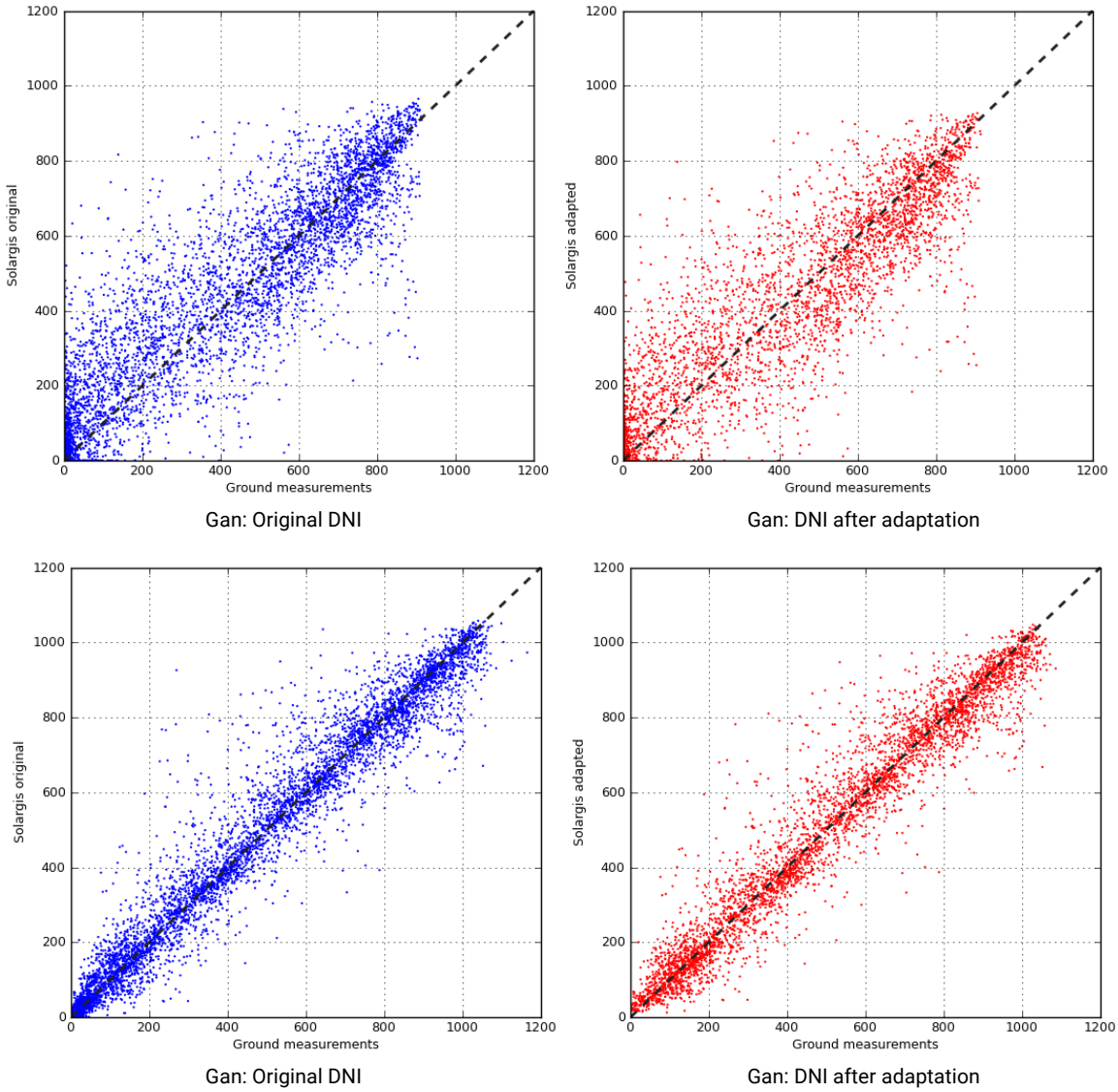

Figure 4.4: Correction of DNI and GHI hourly values for Gan.
Left: original Solargis data, right: site-adapted Solargis data.
The X-axis represents the measured data and the Y-axis represents the satellite-derived data.

The change of model GHI and DNI after adaptation is presented on an example of Hanimaadhoo (Figure 4.5). The change for GHI is negligible, the adapted DNI is slightly lower than original one. The other sites are very similar (Table 4.6).

The site-adapted model values better represent the geographical variability of DNI and GHI solar resource and they also improve the distribution and match of hourly values.

The measurements show that the model performs well in the region, and these results significantly improve the confidence about the reliability of the measured and modelled solar resource data for Maldives.

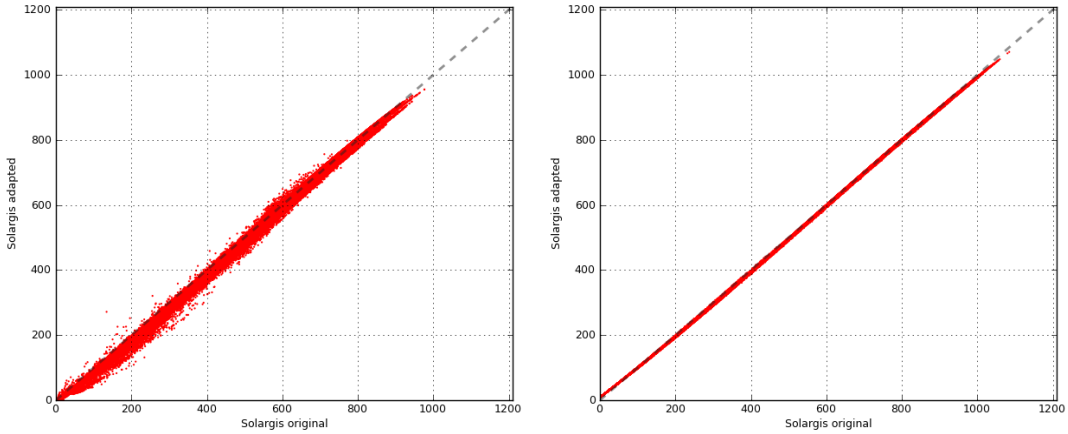

Figure 4.5: Comparison of Solargis original and site-adapted data for Hanimaadhoo site.
Left: DNI; Right: GHI; Data represent years 1999 to 2016.

Table 4.6 Comparison of long term average of yearly summaries of original and site-adapted values

Meteo station	**DNI annual values***			**GHI annual values***		
	Original	Site-adapted	Difference	Original	Site-adapted	Difference
	[kWh/m^2]	[kWh/m^2]	[%]	[kWh/m^2]	[kWh/m^2]	[%]
Hanimaadhoo	1521	1478	-2.8	2029	2020	-0.5
Hulhulé	1614	1520	-5.8	2048	2053	+0.2
Kadhdhoo	1678	1593	-5.1	2054	2056	+0.1
Gan	1742	1652	-5.1	2073	2061	-0.6

5 METEOROLOGICAL MODEL DATA

5.1 Meteorological model

For the territory of Maldives, the last 18 years of the Solargis model-based meteorological data is derived from the regional models. The meteorological data in Solargis database is derived from the two data sources: CFSR and CFSv2, with original characteristics specified in Table 5.1.

Table 5.1 Original source of Solargis meteorological data: models CFSR and CFSv2.

	Climate Forecast System Reanalysis (CFSR)	Climate Forecast System (CFSv2)
Time period	1999 to 2010	2011 to the present time
Original spatial resolution	30 x 35 km	19 x 22 km
Original time resolution	1 hour	1 hour

Table 5.2 shows meteorological parameters available in Solargis, their specifications and it also indicates, which of them have been delivered within this study. In general, the original spatial resolution of the models is enhanced to 1 km for air temperature and relative humidity by spatial disaggregation and use of the Digital Elevation Model SRTM-3, although for Maldives this correction has no effect. The spatial resolution of other parameters is unchanged.

Table 5.2 Solargis meteorological parameters delivered within this project

Meteorological parameter	Acronym	Unit	Time resolution	Spatial representation	Data delivered	Data validated
Air temperature at 2 metres (dry bulb temperature)	TEMP	°C	60 minute	1 km	Yes	Yes
Relative humidity at 2 metres	RH	%	60 minute	1 km	Yes	Yes
Wind speed at 10 metres	WS	m/s^2	60 minute	Original model	Yes	Yes
Wind direction at 10 metres	WD	°	60 minute	Original model	Yes	Yes
Atmospheric pressure	AP	hPa	60 minute	Original model	Yes	Yes
Precipitable water	PWAT		60 minute	Original model	Yes	No

Important note: meteorological parameters are derived from the numerical weather model outputs and they have lower spatial and temporal resolution. Thus, they do not represent the same accuracy as the solar resource data. Especially wind speed data has higher uncertainty, and it provides only overview information for solar energy projects. Thus, the **local microclimate of the site may deviate from the values derived from the Solargis global database.**

5.2 Validation of meteorological data

The validation procedure was carried out to compare the modelled data with ground-measurements from the 4 meteorological stations installed within the ESMAP project: Hanimaadhoo, Hulhulé, Kadhdhoo and Gan. In general, the data from the meteorological models represent larger area, and it is not capable to represent accurately the local microclimate created by small land mass of the islands in the atolls of the Maldives.

5.2.1 Air temperature at 2 metres

Air temperature is derived from the model outputs of both CSFR and CSFv2 meteorological models and recalculated at the spatial resolution of 1 km (Table 5.3 and Figures 5.1 to 5.4). Considering spatial and time interpolation, the deviation of the modelled values to the ground observations for hourly values can occasionally reach several degrees of Celsius.

Figures 5.1 to 5.4 show graphical representation of the model values accuracy at the meteorological stations. In general, the model matches the ground measurements well. Main issue identified is underestimation of daily temperature amplitude. This is caused by relatively small land mass of the islands (in comparison to the pixel size of the meteorological model). Model air temperature is driven mainly by the air temperature over the ocean, where the daily amplitude is lower than temperature amplitude at individual islands. Yet, the insufficiency of meteorological models ay have limited importance, as air temperature is changing only a little across the seasons and day time.

Table 5.3 Air temperature at 2 m: accuracy indicators of the model outputs [°C].

Meteorological station	CFSv2 model							
	Bias mean	Bias min	Bias max	Bias nigh-time	Bias day-time	RMSD hourly	RMSD daily	RMSD monthly
Hanimaadhoo	-0.7	0.9	-2.3	0.1	-1.6	1.6	0.9	0.8
Hulhulé	-0.9	0.4	-2.2	-0.2	-1.5	1.5	1.1	0.9
Kadhdhoo	-0.4	1.3	-2.2	0.5	-1.3	1.6	0.8	0.5
Gan	-0.4	1.2	-1.9	0.4	-1.2	1.5	0.8	0.5

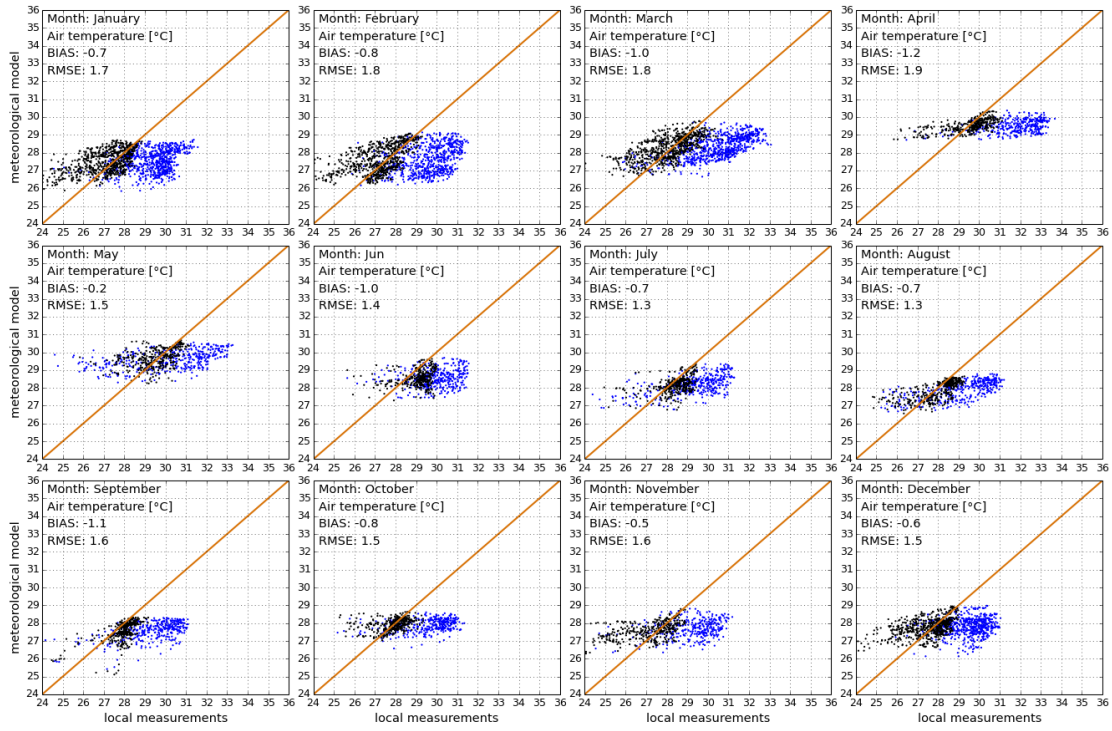

Figure 5.1: Scatterplots of air temperature at 2 m at Hanimaadhoo meteorological station.
Measured values (horizontal axis) and meteorological model values (vertical axis)
Blue: day-time, Black: night-time measurements

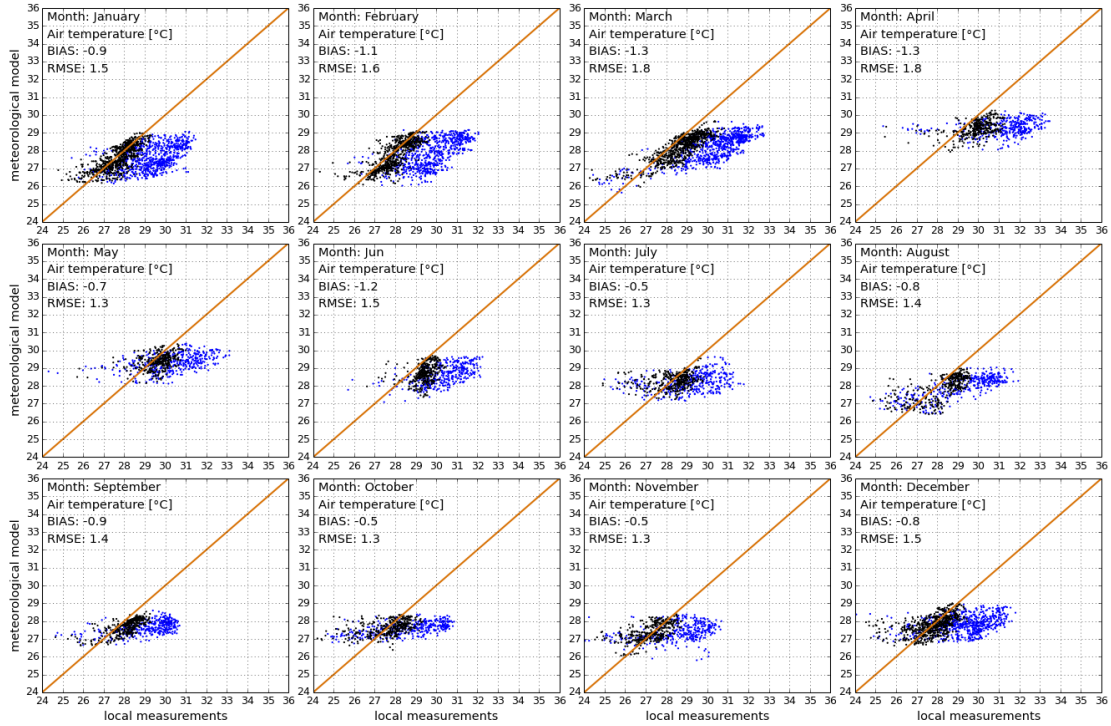

Figure 5.2: Scatterplots of air temperature at 2 m at Hulhulé meteorological station.
Measured values (horizontal axis) and meteorological model values (vertical axis)
Blue: day-time, Black: night-time measurements

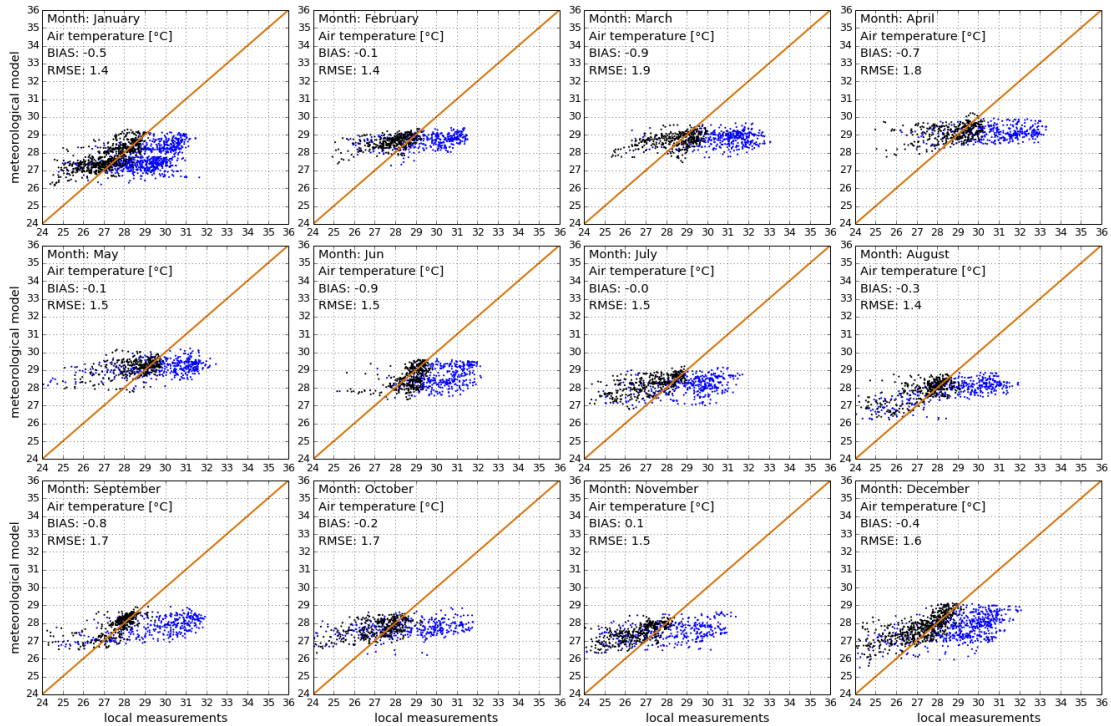

Figure 5.3: Scatterplots of air temperature at 2 m at Kadhdhoo meteorological station.
Measured values (horizontal axis) and meteorological model values (vertical axis)
Blue: day-time, Black: night-time measurements

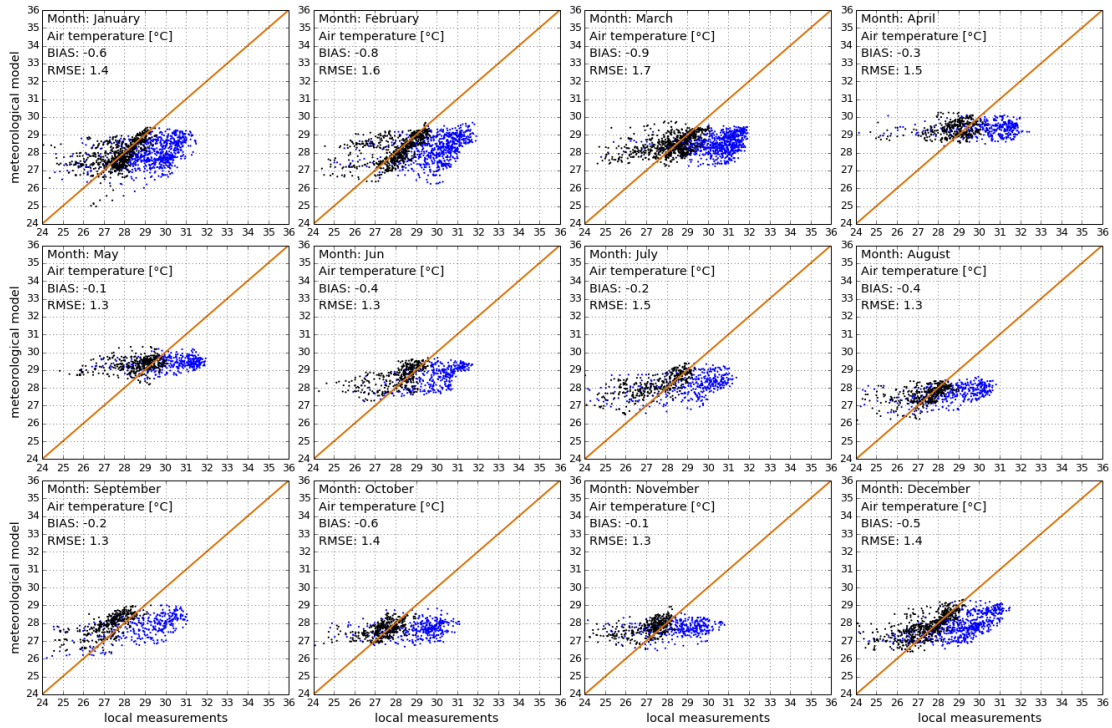

Figure 5.4: Scatterplots of air temperature at 2 m at Gan meteorological station.
Measured values (horizontal axis) and meteorological model values (vertical axis)
Blue: day-time, Black: night-time measurements

5.2.2 Relative humidity

Relative humidity is calculated from the specific humidity, air pressure and the site-adapted air temperature. The comparison of the model values with ground measurements at all 4 meteorological stations is shown in Table 5.4 and Figures 5.5 to 5.8. The issue identified is amplitude reduction of daily relative humidity. Yet, this effect is of limited importance, as relative humidity is quite stable across the seasons and day time.

Table 5.4 Relative humidity: accuracy indicators of the model outputs [%].

Meteorological station	CFSv2 model							
	Bias mean	Bias min	Bias max	Bias nigh-time	Bias day-time	RMSD hourly	RMSD daily	RMSD monthly
Hanimaadhoo	-7	-2	-12	-10	-4	9	7	7
Hulhulé	-5	0	-9	-7	-2	7	5	5
Kadhdhoo	-7	-3	-12	-10	-5	9	8	7
Gan	-7	-3	-13	-10	-4	9	8	7

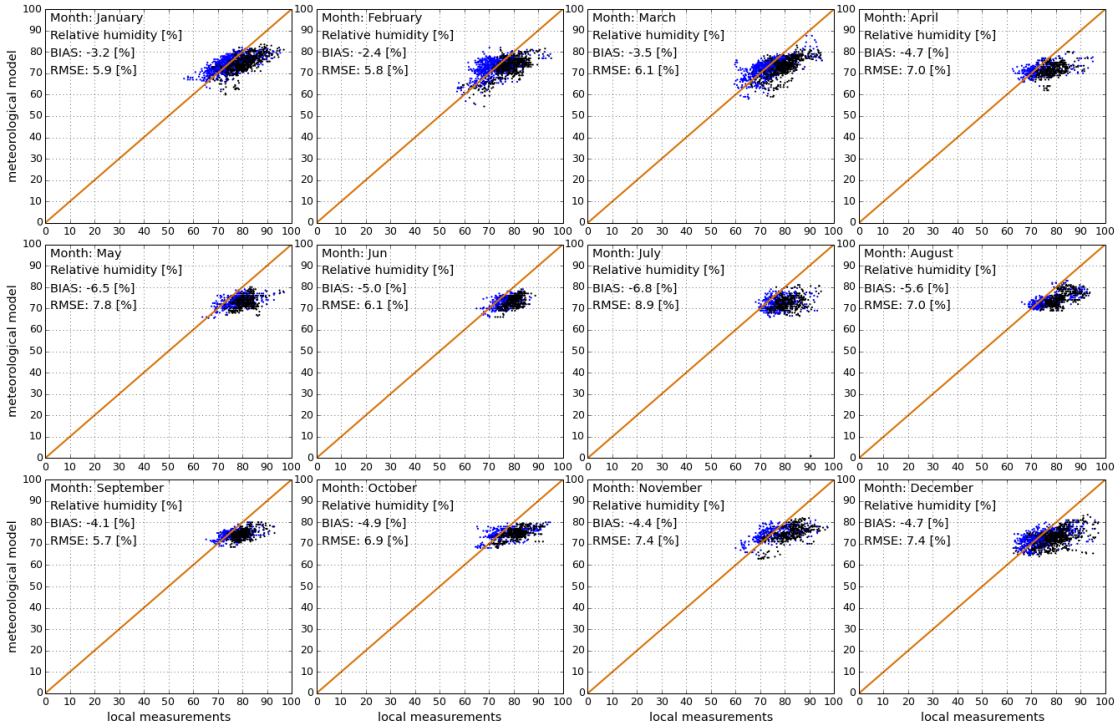

Figure 5.5: Scatterplots of relative humidity at 2 m at Hanimaadhoo meteorological station.
Measured values (horizontal axis) and meteorological model values (vertical axis).
Blue: day-time, black: night-time measurements.

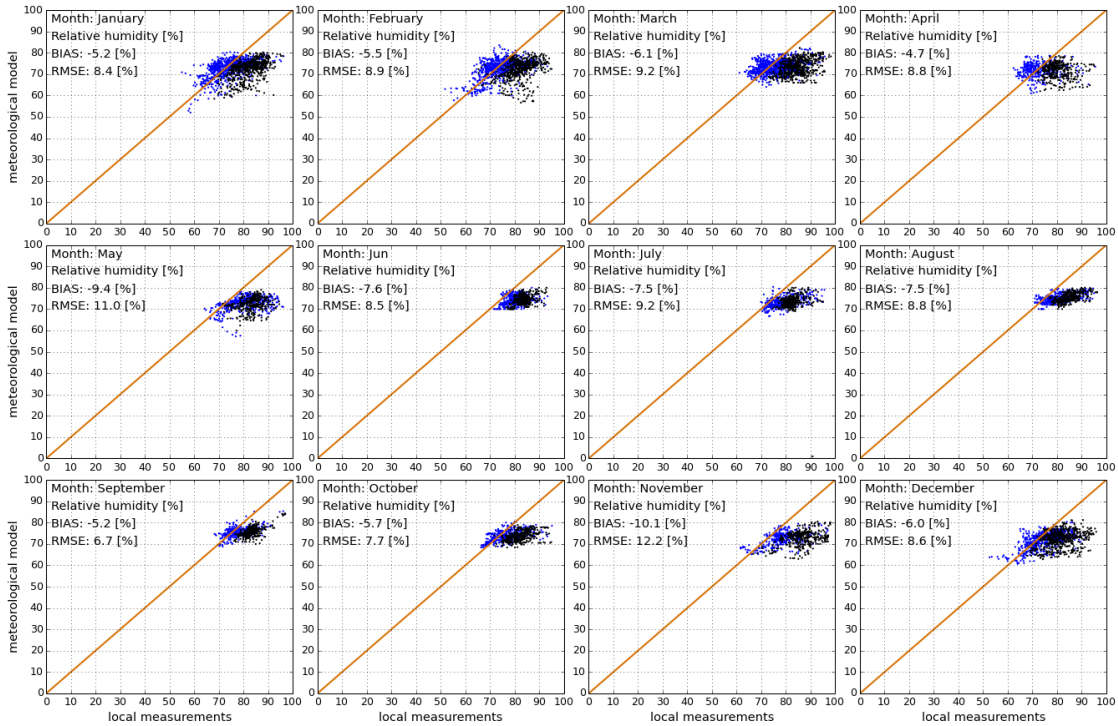

Figure 5.6: Scatterplots of relative humidity at 2 m at Hulhulé meteorological station.
Measured values (horizontal axis) and meteorological model values (vertical axis).
Blue: day-time, black: night-time measurements.

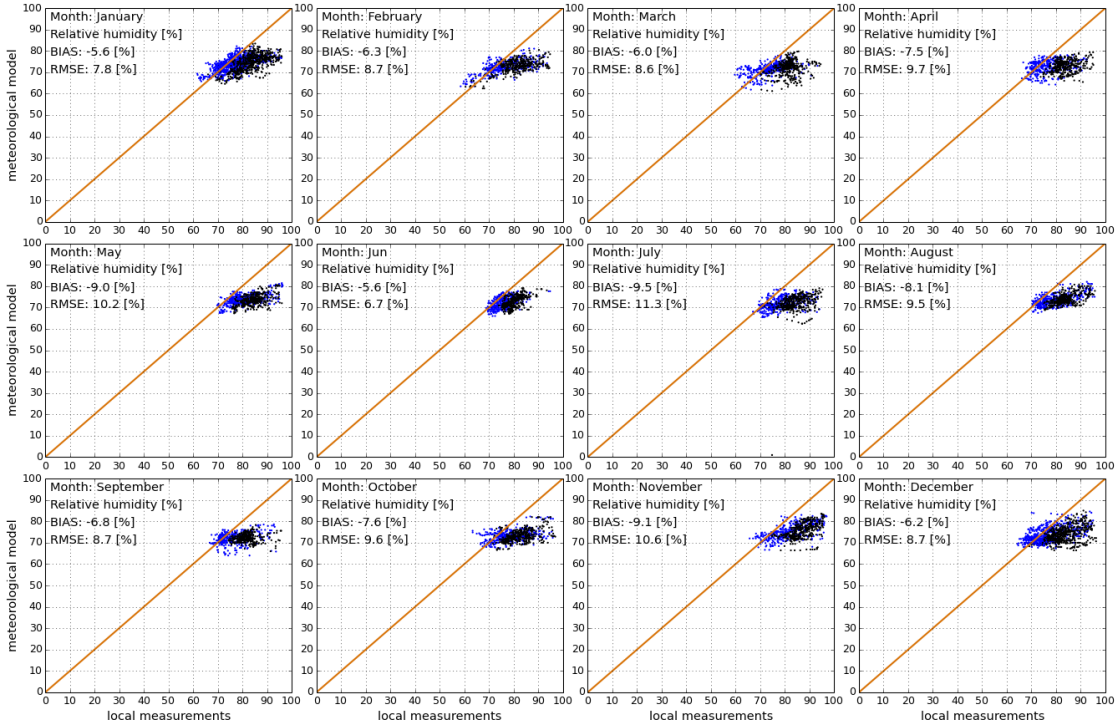

Figure 5.7: Scatterplots of relative humidity at 2 m at Kadhdhoo meteorological station.
Measured values (horizontal axis) and meteorological model values (vertical axis).
Blue: day-time, black: night-time measurements.

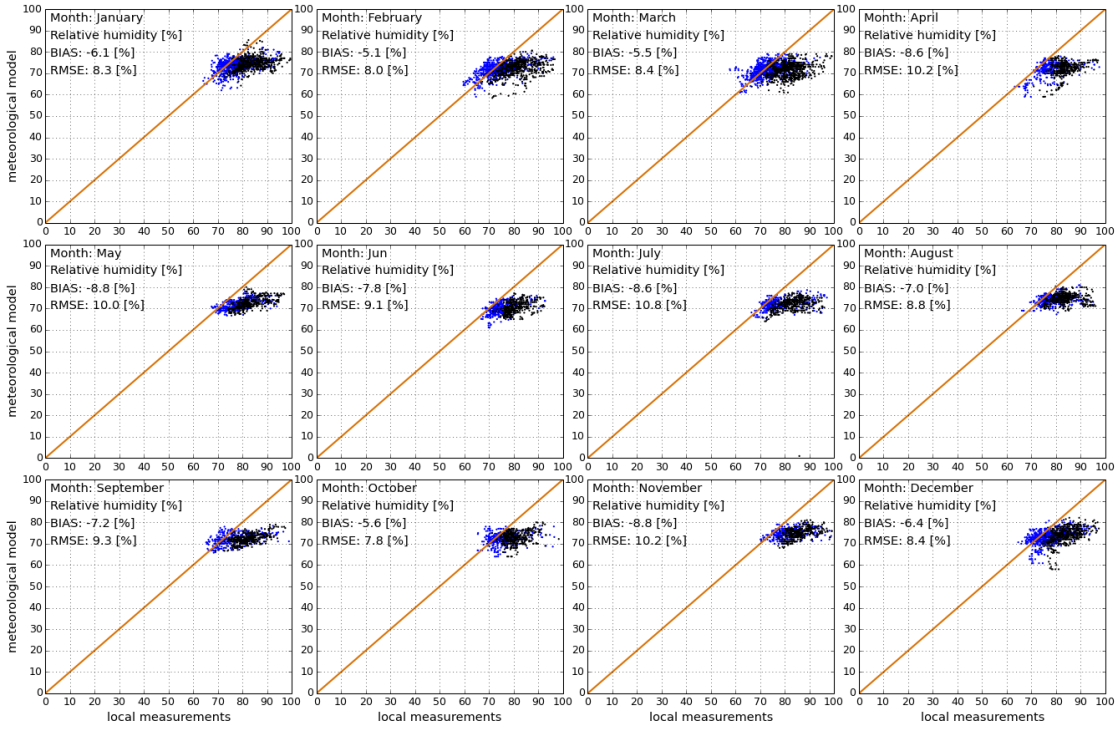

Figure 5.8: Scatterplots of relative humidity at 2 m at Gan meteorological station.
Measured values (horizontal axis) and meteorological model values (vertical axis).
Blue: day-time, black: night-time measurements.

5.2.3 Wind speed and wind direction at 10 metres

Wind speed and direction values delivered within Solargis data represent the height at 10 meters and they are calculated from the CFSR and CFSv2 models, from 10 m wind u- and v- components. The spatial resolution is kept as in the original data. The height of wind measurement is not given. Wind measurements take place **at the height of 3 metres, while the model data represent values at height of 10 m above ground**.

Comparison of the modelled wind speed with ground measurements is shown in Table 5.5 and Figures 5.9 to 5.12. The model values underestimate the wind conditions measured at the meteorological stations. Similarly to relative humidity, the data representation for wind speed and wind direction strongly depends on the local conditions; therefore the model values are only indicative and better characterize a larger region rather than the local microclimate. The important source of systematic difference is different height of the installed sensor (3 metres above ground), compared to the model assumptions (10 metres).

Table 5.5 Wind speed: accuracy indicators of the model outputs [m/s].

Meteorological station	CFSR and CFSv2 models							
	Bias mean	Bias min	Bias max	Bias nigh-time	Bias day-time	RMSD hourly	RMSD daily	RMSD monthly
Hanimaadhoo	2.9	2.4	3.2	3.1	2.6	3.2	3.1	3.2
Hulhulé	2.3	2.2	2.4	2.5	2.2	2.8	2.6	2.6
Kadhdhoo	3.0	2.5	3.2	3.1	2.8	3.4	3.3	3.1
Gan	1.4	1.5	1.4	1.8	1.1	2.1	1.9	1.5

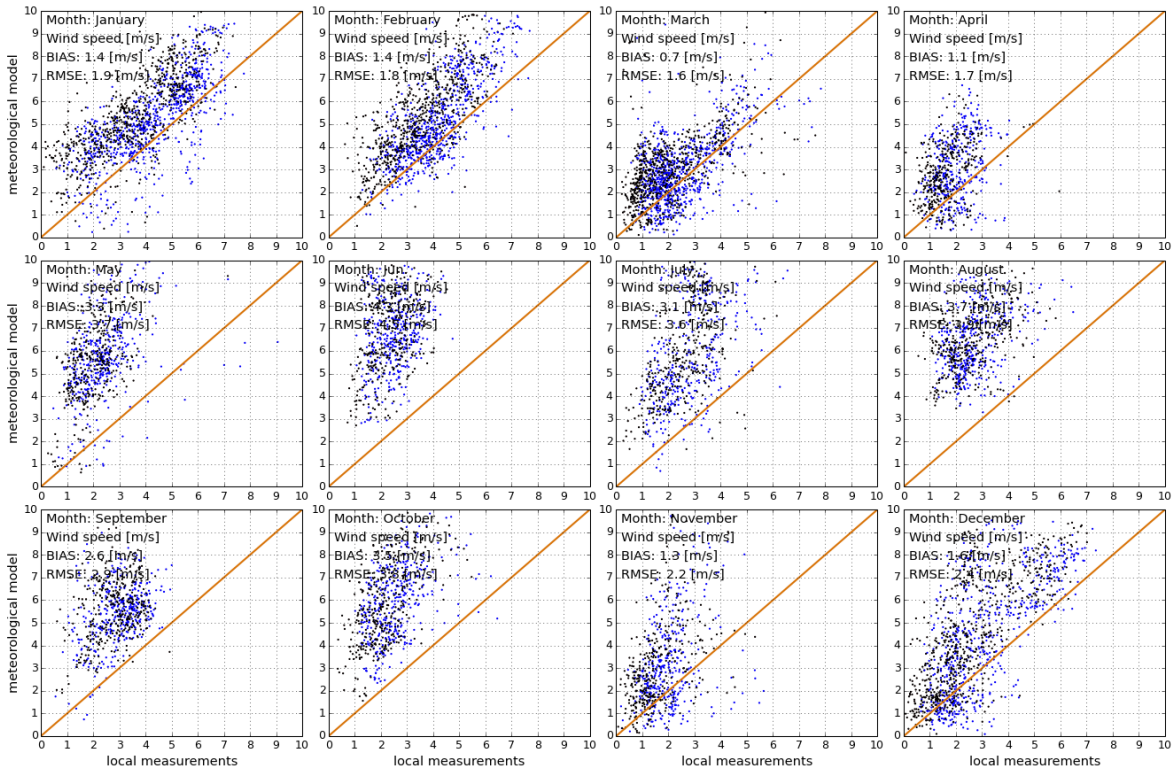

Figure 5.9: Scatterplots of wind speed at Hanimaadhoo meteorological station.
Measured values (horizontal axis) and meteorological model values (vertical axis).
Blue: day-time, black: night-time. (observations at 3 m heigth and model data at 10 m)

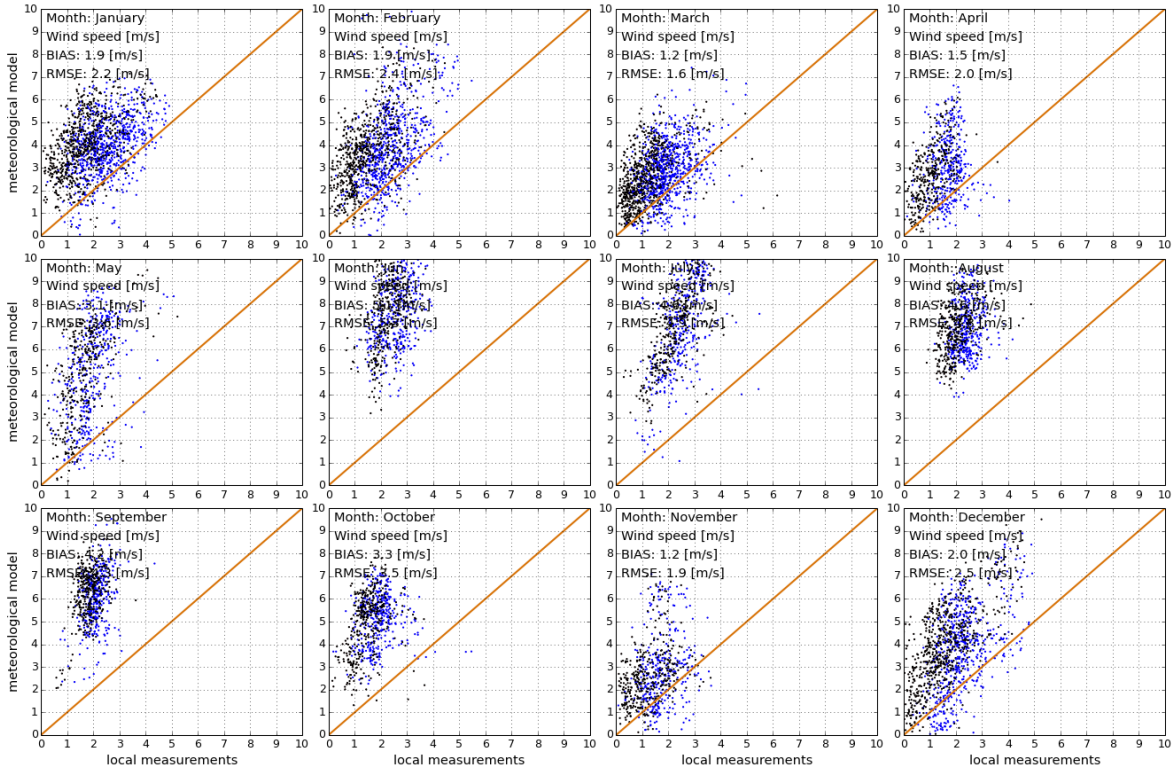

Figure 5.10: Scatterplots of wind speed at Hulhulé meteorological station.
Measured values (horizontal axis) and meteorological model values (vertical axis).
Blue: day-time, black: night-time. (observations at 3 m heigth and model data at 10 m)

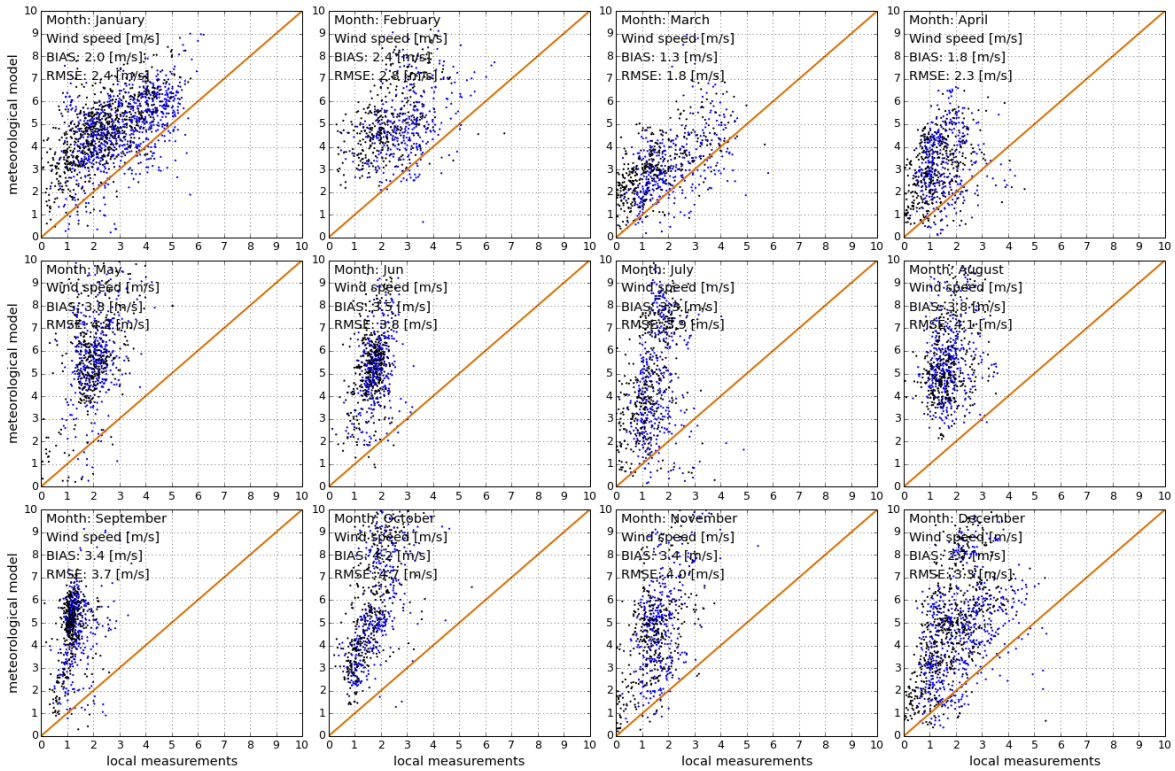

Figure 5.11: Scatterplots of wind speed at Kadhdhoo meteorological station.
Measured values (horizontal axis) and meteorological model values (vertical axis).
Blue: day-time, black: night-time. (observations at 3 m heigth and model data at 10 m)

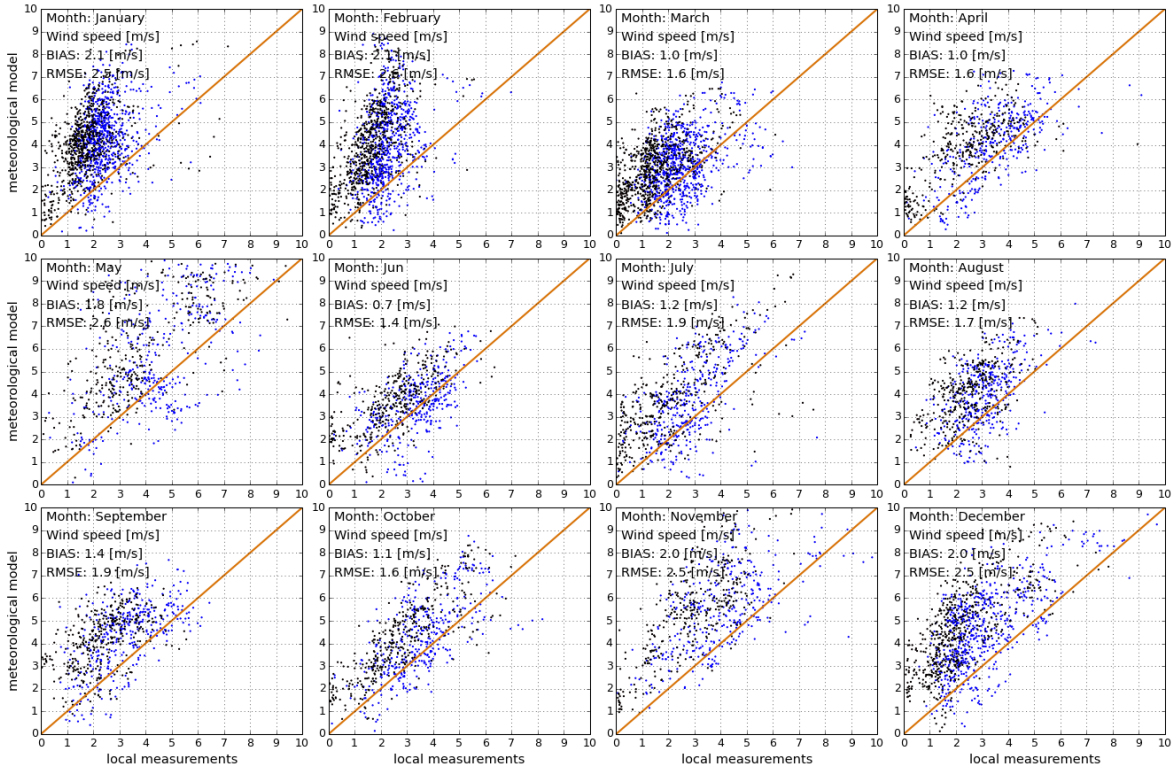

Figure 5.12: Scatterplots of wind speed at Gan meteorological station.
Measured values (horizontal axis) and meteorological model values (vertical axis).
Blue: day-time, black: night-time. (observations at 3 m heigth and model data at 10 m)

5.3 Uncertainty of meteorological model data

The meteorological parameters are derived from two very similar numerical meteorological models covering periods from 1999 to 2010 (CFSR model) and 2011 to 2016 (CFSv2). Considering the comparison results, the uncertainty of the estimate for the main meteorological parameters is summarised in Table 5.6.

It was found that the modelled air temperature fits reasonably well the measured data though (logically) due to the spatial resolution, the model daily amplitude is significantly smaller than amplitude of measured data.

Similarly to air temperature, relative humidity from the model exhibits much smaller daily amplitude than measured relative humidity. Wind speed data, obtained from the meteorological model, represents an area of larger region and this data is smoothed, in comparison to the point measurements collected at the meteorological sites. For all stations at Maldives wind speed is overestimated by the meteorological model. The reason is coarse resolution of the model and different elevation (observations at 3 m heigth and model data at 10 m)

Table 5.6 Expected uncertainty of modelled meteorological parameters at the project site.

	Unit	Annual	Monthly	Hourly
Air temperature at 2 m	°C	±1.0	±1.0	±2.0
Relative Humidity at 2 m	%	±8	±8	±15
Average wind speed at 10 m	m/s	+2.5	±3.0	±3.5

6 SOLAR RESOURCE: UNCERTAINTY OF LONGTERM ESTIMATES

6.1 Uncertainty of solar resource yearly estimate

The **uncertainty of site-adapted satellite-based GHI and DNI** is determined by the uncertainty of the model and of the ground measurements [7], more specifically it depends on:

1. Parameterization and adaptation of **numerical models integrated in Solargis** for the given data inputs and their ability to generate accurate results for various geographical and time-variable conditions:
    - Data inputs into Solargis model (accuracy of satellite data, aerosols and water vapour and Digital Terrain Model).
    - Clear-sky model and its capability to properly characterize various states of the atmosphere
    - Simulation accuracy of the satellite model and cloud transmittance algorithms, being able to properly distinguish different types of desert surface, clouds, fog, but also snow and ice.
    - Diffuse and direct decomposition models
    - Site adaptation methods.
2. Uncertainty of the **ground-measurements**, which is determined by:
    - Accuracy of the instruments
    - Maintenance practices, including sensor cleaning, calibration
    - Data post-processing and quality control procedures.

Accuracy statistics, such as bias and RMSD (Chapter 4.3) characterize accuracy of Solargis model in the given validation points, relative to the ground measurements. The validation statistics is affected by local geography and by quality and reliability of the ground-measured data. Therefore the validation statistics only indicates performance of the model in the region.

Solargis model uncertainty is compared to the high-quality data measured by the meteorological instruments. Representativeness of such data comparison (satellite and ground-measured) is determined by the precision of the measuring instruments, the maintenance and operational practices, and by quality control of the measured data – in other words, by the measurement accuracy achieved at each meteorological station.

From the user's perspective, the information about the model uncertainty has probabilistic nature. It generalizes the validation accuracy and it has to be considered at different confidence levels. The expert estimate of the calculation uncertainty in this report assumes 80% probability of occurrence of values.

The solar model uncertainty is discussed in Chapters 4 and 6.1. The main findings are summarized in Table 6.1. The site-adaptation procedure reduced uncertainty of estimate of all parameters. Chapter 6.3 evaluates combined uncertainty, in which also interannual variability is included (Chapter 6.2).

Even though the physical reductionfo themodel uncertainty is seen to vbe low, important component of the uncertainty reduction in Table 6.1 is dramatically increased confidence in the data values.

Table 6.1 Uncertainty of the model estimates for original and site-adapted annual long-term values (Considers 80% probability of occurrence)

Uncertainty of longterm annual values	Acronym	Uncertainty of the original Solargis model	Uncertainty of the Solargis model after site adaptation
Global Horizontal Irradiation	GHI	±5.0%	±3.5%
Direct Normal Irradiance	DNI	±11.0%	±6.0%

6.2 Uncertainty due to interannual variability of solar radiation

Weather changes in cycles and has also stochastic nature. Therefore annual solar radiation in each year can deviate from the long-term average in the range of few percent. The estimation of the interannual variability below shows the magnitude of this change. The uncertainty of GHI and DNI prediction is highest if only one single year is considered, but when averaged for a longer period, weather oscillations even out and approximate to the long-term average.

In this report, the **interannual variability** is calculated from the unbiased standard deviation *stdev* of GHI and DNI over **18 years**, considering, in the long-term, the normal distribution of the annual sums for *n* years, where x_i is any particular year and $\bar{x}$is longterm yearly average. Due to the limited number of years of available data, for the calculation we apply simplified assumption of normal distribution of yearly values:

$$stdev = \sqrt{\frac{1}{n-1}\sum_{i=1}^{n}(x_i - \bar{x})^2}$$

Tables 6.2 and 6.3 show GHI and DNI values that are to be exceeded at P90 for a consecutive number of years. The variability (var_n) for a number of years (n) is calculated from the unbiased standard deviation (*stdev*):

$$var_n = \frac{stdev}{\sqrt{n}}$$

The uncertainty, which characterises 80% probability of *occurrence* (U_{var}), is calculated from the variability (var_n), multiplying it with 1.28155:

$$uncert = 1.28155\ var$$

The lower boundary (negative value) of uncertainty represents 90% probability of *exceedance*, and it is used for calculating the P90 value.

Table 6.2 Annual GHI that should be exceeded with 90% probability in the period of 1 to 10 (25) years

Hanimaadhoo | Years	**1**	**2**	**3**	**4**	**5**	**6**	**7**	**8**	**9**	**10**	**25**
Variability [±%]	1.3	0.9	0.8	0.7	0.6	0.5	0.5	0.5	0.4	0.4	0.3
Uncertainty P90 [±%]	1.7	1.2	1.0	0.9	0.8	0.7	0.6	0.6	0.6	0.5	0.3
Minimum GHI P90	**1985**	**1995**	**2000**	**2002**	**2004**	**2005**	**2007**	**2007**	**2008**	**2009**	**2013**

Hulhulé | Years	**1**	**2**	**3**	**4**	**5**	**6**	**7**	**8**	**9**	**10**	**25**
Variability [±%]	1.5	1.0	0.9	0.7	0.7	0.6	0.6	0.5	0.5	0.5	0.3
Uncertainty P90 [±%]	1.9	1.3	1.1	1.0	0.9	0.8	0.7	0.7	0.6	0.6	0.4
Minimum GHI P90	**2014**	**2025**	**2030**	**2033**	**2035**	**2037**	**2038**	**2039**	**2040**	**2040**	**2045**

Kadhdhoo | Years	**1**	**2**	**3**	**4**	**5**	**6**	**7**	**8**	**9**	**10**	**25**
Variability [±%]	2.0	1.4	1.1	1.0	0.9	0.8	0.7	0.7	0.7	0.6	0.4
Uncertainty P90 [±%]	2.5	1.8	1.5	1.3	1.1	1.0	1.0	0.9	0.8	0.8	0.5
Minimum GHI P90	**2004**	**2019**	**2026**	**2030**	**2032**	**2034**	**2036**	**2037**	**2038**	**2039**	**2045**

Gan | Years	**1**	**2**	**3**	**4**	**5**	**6**	**7**	**8**	**9**	**10**	**25**
Variability [±%]	2.0	1.4	1.2	1.0	0.9	0.8	0.8	0.7	0.7	0.6	0.4
Uncertainty P90 [±%]	2.6	1.8	1.5	1.3	1.2	1.1	1.0	0.9	0.9	0.8	0.5
Minimum GHI P90	**2008**	**2024**	**2031**	**2035**	**2038**	**2040**	**2041**	**2043**	**2044**	**2045**	**2051**

Table 6.3 Annual DNI that should be exceeded with 90% probability in the period of 1 to 10 (25) years.

Hanimaadhoo | Years	**1**	**2**	**3**	**4**	**5**	**6**	**7**	**8**	**9**	**10**	**25**
Variability [±%]	3.6	2.5	2.1	1.8	1.6	1.5	1.3	1.3	1.2	1.1	0.7
Uncertainty P90 [±%]	4.6	3.2	2.6	2.3	2.0	1.9	1.7	1.6	1.5	1.4	0.9
Minimum DNI P90	**1411**	**1431**	**1439**	**1445**	**1448**	**1451**	**1453**	**1455**	**1456**	**1457**	**1465**

Hulhulé | Years	**1**	**2**	**3**	**4**	**5**	**6**	**7**	**8**	**9**	**10**	**25**
Variability [±%]	3.9	2.8	2.3	2.0	1.7	1.6	1.5	1.4	1.3	1.2	0.8
Uncertainty P90 [±%]	5.0	3.5	2.9	2.5	2.2	2.0	1.9	1.8	1.7	1.6	1.0
Minimum DNI P90	**1444**	**1466**	**1476**	**1482**	**1486**	**1489**	**1491**	**1493**	**1494**	**1496**	**1505**

Kadhdhoo | Years	**1**	**2**	**3**	**4**	**5**	**6**	**7**	**8**	**9**	**10**	**25**
Variability [±%]	4.1	2.9	2.4	2.1	1.9	1.7	1.6	1.5	1.4	1.3	0.8
Uncertainty P90 [±%]	5.3	3.8	3.1	2.7	2.4	2.2	2.0	1.9	1.8	1.7	1.1
Minimum DNI P90	**1508**	**1533**	**1544**	**1550**	**1555**	**1558**	**1561**	**1563**	**1564**	**1566**	**1576**

Gan | Years	**1**	**2**	**3**	**4**	**5**	**6**	**7**	**8**	**9**	**10**	**25**
Variability [±%]	4.1	2.9	2.3	2.0	1.8	1.7	1.5	1.4	1.4	1.3	0.8
Uncertainty P90 [±%]	5.2	3.7	3.0	2.6	2.3	2.1	2.0	1.8	1.7	1.6	1.0
Minimum DNI P90	**1566**	**1591**	**1603**	**1609**	**1614**	**1617**	**1620**	**1622**	**1624**	**1625**	**1635**

We can interpret the above Table 6.2 and 6.3 on the example of Hulhulé site:

i. GHI interannual variability at P90 of 1.9% has to be considered for any single year in Hulhule. In other words, assuming that the long-term average is 2053 kWh/m^2, it is expected (with 90% probability) that annual GHI exceeds, at any single year, the value of 2014 kWh/m^2.

ii. Within a period of three consecutive years, it is expected at P90 that annual average of GHI exceeds value of 2030 kWh/m^2;

iii. For a period of 25 years, it is expected at 90% probability that due to interannual variability the estimate of the long-term annual DNI average will deviate within the range of ±1.0% in Hulhulé. Thus assuming that the estimate of the long-term average is 1520 kWh/m^2, it can be expected at P90 that *due to variability of weather*, it should be at least 1505 kWh/m^2.

It is to be underlined that prediction of the future irradiation is based on the analysis of the recent historical data (period 1999 to 2016). Future weather changes may include man-induced or natural events such as volcano eruptions, which may have impact on this prediction.

Based on the existing scientific knowledge [20, 21], an effect of **extreme volcano eruptions**, with an emission of large amount of stratospheric aerosols, can be estimated on the example of Pinatubo event in 1991 (the second largest volcano eruption in 20th century). It can be expected that in such a case, the annual DNI in the affected year can decrease by approx. 16% or more, compared to the long-term average, still influencing another two consecutive years. In the same way, the volcano eruption of the comparable size may reduce long-term average estimate of DNI by about 4%. The decrease of GHI is much lower; the annual value in the particular year of eruption could be reduced by about 2% compared to the long-term average.

6.3 Combined uncertainty

In this Chapter, the combined uncertainty of the annual GHI and DNI values is quantified. Taking into account uncertainties of both types of data (satellite and ground measured), the combined effect of two components of the uncertainty of the site-adapted GHI and DNI values has to be considered.

1. **Uncertainty of the estimate** (U_{est}) of the annual solar resource values, which is ±3.5% for GHI and ±6.0% for DNI (Chapter 6.1);
2. **Interannual variability** (U_{var}) in any particular year, due to changing weather. In four Maldivian sites, it varies from ±1.7% to ±2.6% for GHI and from ±4.6% to ±5.3% for DNI. The uncertainty due to weather variability decreases over the time with square root of the number of years (Chapter 6.2).

The two above-mentioned uncertainties combine in U_c (see Glossary), which represents a conservative expectation of the minimum GHI and DNI assuming various number of years *N* (Tables 6.4 and 6.5). Considering

a simplified assumption of normal distribution of the annual values, probability of exceedance can be calculated at different confidence levels. GHI and DNI minimum annual values expected for combined uncertainty in any single year are shown on Figure 6.2 and 6.3.

Table 6.4 Combined probability of exceedance of annual GHI for uncertainty of the estimate ±3.5%.

Nr. of years	Uncertainty of estimate	Interanual variability	Combined uncertainty	Expected minimum | **Hanimaadhoo** [kWh/m^2]								
N	[±%]	N years [±%]	P90 [±%]	P01	P05	P10	P25	P50	P75	P90	P95	P99
1	3.5	1.7	3.9	2162	2120	2098	2061	2020	1978	1941	1919	1877
5	3.5	0.8	3.6	2151	2112	2092	2058	2020	1981	1947	1927	1888
10	3.5	0.5	3.5	2149	2111	2091	2057	2020	1982	1948	1928	1890
25	3.5	0.3	3.5	2148	2111	2091	2057	2020	1982	1949	1928	1891

Nr. of years	Uncertainty of estimate	Interanual variability	Combined uncertainty	Expected minimum | **Hulhulé** [kWh/m^2]								
N	[±%]	N years [±%]	P90 [±%]	P01	P05	P10	P25	P50	P75	P90	P95	P99
1	3.5	1.9	4.0	2201	2158	2134	2096	2053	2010	1971	1948	1904
5	3.5	0.9	3.6	2187	2148	2127	2092	2053	2014	1979	1958	1918
10	3.5	0.6	3.6	2185	2146	2126	2091	2053	2014	1980	1959	1920
25	3.5	0.4	3.5	2184	2145	2125	2091	2053	2015	1980	1960	1921

Nr. of years	Uncertainty of estimate	Interanual variability	Combined uncertainty	Expected minimum | **Kadhdhoo** [kWh/m^2]								
N	[±%]	N years [±%]	P90 [±%]	P01	P05	P10	P25	P50	P75	P90	P95	P99
1	3.5	2.5	4.3	2217	2170	2144	2102	2056	2009	1967	1942	1895
5	3.5	1.1	3.7	2193	2153	2131	2095	2056	2016	1980	1959	1918
10	3.5	0.8	3.6	2190	2150	2129	2095	2056	2017	1982	1961	1922
25	3.5	0.5	3.5	2188	2149	2128	2094	2056	2017	1983	1962	1924

Nr. of years	Uncertainty of estimate	Interanual variability	Combined uncertainty	Expected minimum | **Gan** [kWh/m^2]								
N	[±%]	N years [±%]	P90 [±%]	P01	P05	P10	P25	P50	P75	P90	P95	P99
1	3.5	2.6	4.4	2224	2177	2151	2109	2061	2014	1972	1946	1898
5	3.5	1.2	3.7	2199	2159	2137	2101	2061	2021	1985	1964	1923
10	3.5	0.8	3.6	2196	2157	2136	2100	2061	2022	1987	1966	1927
25	3.5	0.5	3.5	2194	2155	2134	2100	2061	2023	1989	1968	1929

Table 6.5 Combined probability of exceedance of annual DNI for uncertainty of the estimate ±6.0%.

Nr. of years	Uncertainty of estimate	Interanual variability	Combined uncertainty	Expected minimum | **Hanimaadhoo** [kWh/m^2]								
N	[±%]	N years [±%]	P90 [±%]	P01	P05	P10	P25	P50	P75	P90	P95	P99
1	6.0	4.6	7.5	1681	1621	1590	1537	1478	1420	1367	1335	1276
5	6.0	2.0	6.3	1649	1599	1572	1528	1478	1429	1385	1358	1308
10	6.0	1.4	6.2	1644	1596	1570	1526	1478	1430	1387	1361	1313
25	6.0	0.9	6.1	1641	1594	1568	1526	1478	1431	1389	1363	1316

Nr. of years	Uncertainty of estimate	Interanual variability	Combined uncertainty	Expected minimum | **Hulhulé** [kWh/m^2]								
N	[±%]	N years [±%]	P90 [±%]	P01	P05	P10	P25	P50	P75	P90	P95	P99
1	6.0	5.0	7.8	1735	1672	1638	1582	1520	1457	1401	1367	1304
5	6.0	2.2	6.4	1696	1645	1617	1571	1520	1469	1422	1395	1343
10	6.0	1.6	6.2	1691	1641	1614	1569	1520	1470	1425	1399	1349
25	6.0	1.0	6.1	1688	1638	1612	1568	1520	1471	1427	1401	1352

Nr. of years	Uncertainty of estimate	Interanual variability	Combined uncertainty	Expected minimum | **Kadhdhoo** [kWh/m^2]								
N	[±%]	N years [±%]	P90 [±%]	P01	P05	P10	P25	P50	P75	P90	P95	P99
1	6.0	5.3	8.0	1824	1756	1720	1660	1593	1525	1465	1429	1361
5	6.0	2.4	6.5	1779	1725	1695	1647	1593	1539	1490	1461	1406
10	6.0	1.7	6.2	1773	1720	1692	1645	1593	1540	1493	1465	1412
25	6.0	1.1	6.1	1769	1717	1690	1644	1593	1542	1496	1468	1416

Nr. of years	Uncertainty of estimate	Interanual variability	Combined uncertainty	Expected minimum | **Gan** [kWh/m^2]								
N	[±%]	N years [±%]	P90 [±%]	P01	P05	P10	P25	P50	P75	P90	P95	P99
1	6.0	5.2	7.9	1890	1821	1783	1721	1652	1583	1521	1484	1414
5	6.0	2.3	6.4	1845	1789	1759	1708	1652	1596	1546	1516	1459
10	6.0	1.6	6.2	1839	1784	1755	1706	1652	1598	1549	1520	1466
25	6.0	1.0	6.1	1835	1781	1753	1705	1652	1599	1552	1523	1470

This analysis is based on the data representing a history of year 1999 to 2016, and on the expert extrapolation of the related weather variability. This report may not reflect possible man-induced climate change or occurrence of extreme events such as large volcano eruptions in the future (see the last paragraph in Chapter 6.2).

Graphical visualisation of Tables 6.4 and 6.5 on the example of Hulhulé Airport is shown in Figures 6.1 and 6.2, where the expected probabilities of exceedance (different Pxx scenarios) are drawn on the cumulatove distribution curve showing yearly GHI amd DNI values.

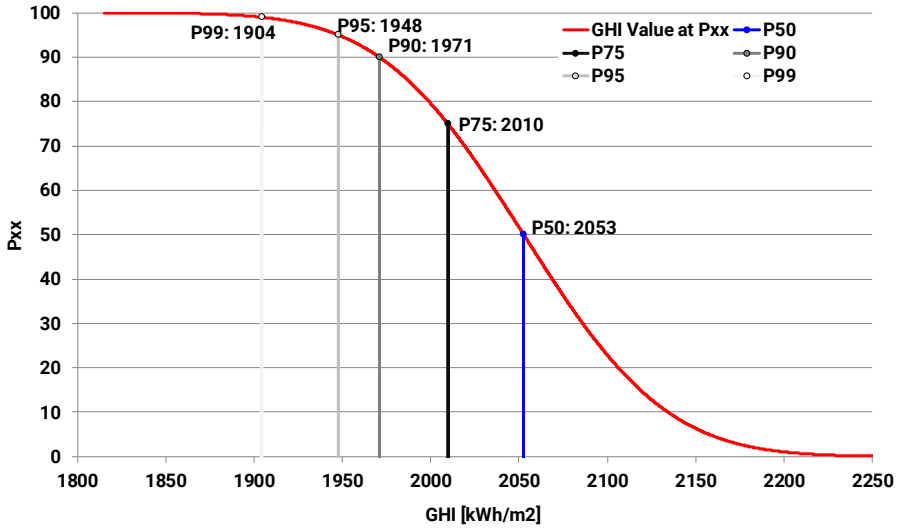

Figure 6.1: Expected Pxx values for GHI at Hulhulé Airport

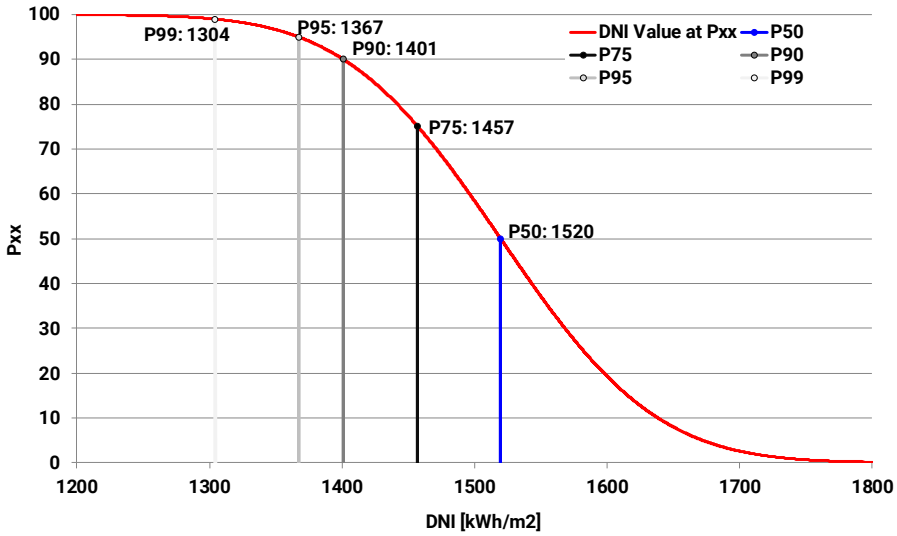

Figure 6.2: Expected Pxx values for DNI at Hulhulé Airport

7 TIME SERIES AND TYPICAL METEOROLOGICAL YEAR DATA

7.1 Delivered data sets

Table 7.1 Parameters in the delivered site-adapted time series and TMY data (hourly time step)

Parameter	Acronym	Unit	TS	TMY P50	TMY P90
Global horizontal irradiance	GHI	W/m^2	X	X	X
Direct normal irradiance	DNI	W/m^2	X	X	X
Diffuse horizontal irradiance	DIF	W/m^2	X	X	X
Global tilted irradiance (at optimum angle)	GHI	W/m^2	X	-	-
Solar azimuth	SA	°	X	X	X
Solar elevation	SE	°	X	X	X
Air temperature at 2 metres	TEMP	°C	X	X	X
Wind speed at 10 metres	WS	m/s	X	X	X
Wind direction at 10 metres	WD	°	X	X	X
Relative humidity	RH	%	X	X	X
Air Pressure	AP	hPa	X	X	X
Precipitable Water	PWAT	kg/m^2	X	X	X

7.2 TMY method

The Typical Meteorological Year (TMY) data sets are delivered, together with Solargis time series data and this report. TMY contains hourly data derived from the time series covering complete 18 years (1999 to 2016). The data history of 18 years is compressed into one year (Figure 7.1 to 7.3) following two criteria:

- Minimum difference between statistical characteristics (annual average, monthly averages) of TMY and long-term time series. This criterion is given about 80% weighting.
- Maximum similarity of monthly Cumulative Distribution Functions (CDF) of TMY and full-time series, so that occurrence of typical hourly values is well represented for each month. This criterion is given about 20% weighting.

TMY P50 data set is constructed on the monthly basis. For each month the long-term average monthly value and cumulative distribution for each parameters is calculated: Direct Normal Irradiance (DNI), Global Horizontal Irradiance (GHI), Diffuse Horizontal Irradiance (DIF) and Air Temperature (TEMP). Following the monthly data for each individual year from the set of 18 years are compared to the long-term parameters. The monthly data from the year, which resembles the long-term parameters more closely, is selected. The procedure is repeated for all 12 months, and the TMY is constructed by concatenating the selected months into one artificial (but representative) year.

The method for calculation **P90** data set is based on the TMY P50 method. It has been modified in a way of how a candidate month is selected. The search for set of twelve candidates is repeated in iteration until a condition of minimization of difference between annual P90 value and annual average of new TMY is reached (instead of minimization of differences in monthly means and CDFs, as applied in P50 case). Once the selection converges to minimum difference, the TMY is created by concatenation of selected months. The P90 annual values are calculated for each confidence limit – from the combined uncertainty of estimate and inter-annual variability, which can occur in any year (Chapter 6.3).

To derive TMY that fits specific needs of the selected energy application the different weights are given to individual parameters – thus highlighting important properties. In solar energy applications, the higher importance is given to GHI and DNI. In assembling TMY P50, the values of DNI, GHI, DIF and TEMP are only considered, where the weights are set as follows: 0.9 is given to DNI, 0.3 to GHI, 0.02 to diffuse horizontal irradiance, and 0.07 to air temperature (divided by the total of 1.29).

To derive solar resource parameters with an **hourly time step**, the original satellite data with time resolution of 30-minutes were aggregated by time integration. The meteorological parameters are available in the original 1-hourly time step. The TMY datasets were constructed from solar radiation and meteorological data (Chapters 4 and 5). Time zone was adjusted to Maldives Time MVT (UTC +05:00).

More about the Solargis TMY method in [22].

7.3 Results

Two data sets are derived from the Solargis historical time series for the four sites: P50 and P90. In graphts and tables below we show the values for Hulhulé meteorological site, in order to present the methodology of TMY data calculation.

Important note: Due to the inherent features of the underlying methods, monthly values in TMY data set in Tables 7.2 to 7.4 do not fit to the values generated from full time series (Figures 7.1 to 7.3).

Table 7.2 Monthly and yearly long-term GHI averages as calculated from time series and from TMY representing P50, and P90 cases at Hulhulé site

Global Horizontal Irradiation [kWh/m^2]	1	2	3	4	5	6	7	8	9	10	11	12	Year
Time series (18 years)	178	182	208	184	167	157	161	169	163	176	153	155	2053
TMY for P50 case	178	176	204	187	165	157	166	170	157	176	161	154	2053
TMY for P90 case	172	177	206	175	157	140	158	168	155	167	144	151	1971

Table 7.3 Monthly and yearly long-term DNI averages as calculated from time series and from TMY representing P50, and P90 cases at Hulhulé site

Direct Normal Irradiation [kWh/m^2]	1	2	3	4	5	6	7	8	9	10	11	12	Year
Time series (18 years)	143	151	169	146	120	107	106	109	104	131	115	119	1520
TMY for P50 case	142	151	169	146	121	107	106	109	103	132	115	119	1520
TMY for P90 case	135	146	166	136	103	85	104	107	95	120	97	107	1401

Table 7.4 Monthly and yearly long-term TEMP averages as calculated from time series and from TMY representing P50, and P90 cases at Hulhulé site

Air temperature [°C]	1	2	3	4	5	6	7	8	9	10	11	12	Year
Time series (18 years)	27.5	27.7	28.2	28.7	28.7	28.4	28.2	28.0	27.9	27.9	27.7	27.5	28.0
TMY for P50 case	27.2	27.5	28.4	28.2	28.4	28.7	28.0	28.1	27.9	27.9	28.2	27.5	28.0
TMY for P90 case	27.5	27.5	28.2	28.7	28.6	28.5	28.1	27.9	27.8	28.0	27.6	27.5	28.0

As an example o finterpretation of the tables above, the TMY data sets for P50 and P90 can be described as:

1. **P50 TMY** data set represents, for each month, the average climate conditions and the most representative cumulative distribution function, therefore extreme situations (e.g. extremely cloudy weather) are not represented in this dataset. The long-term annual summary of GHI and DNI are considered as the most critical parameters to consider, and in this data set P50 **GHI value is 2053 kWh/m^2** and **DNI value is 1520 kWh/m^2.**

2. **P90 TMY** data set represents for each month the climate conditions, which after summarization GHI and DNI for the whole year results in the value *equal or close to P90* derived by the analysis of uncertainty of the estimate and of the interannual variability for any single year (Chapter 6.3). Thus TMY for P90 represents generally a conservative estimate, i.e. a year with the long-term value of **GHI of 1971 kWh/m^2** and **DNI of 1401 kWh/m^2**.

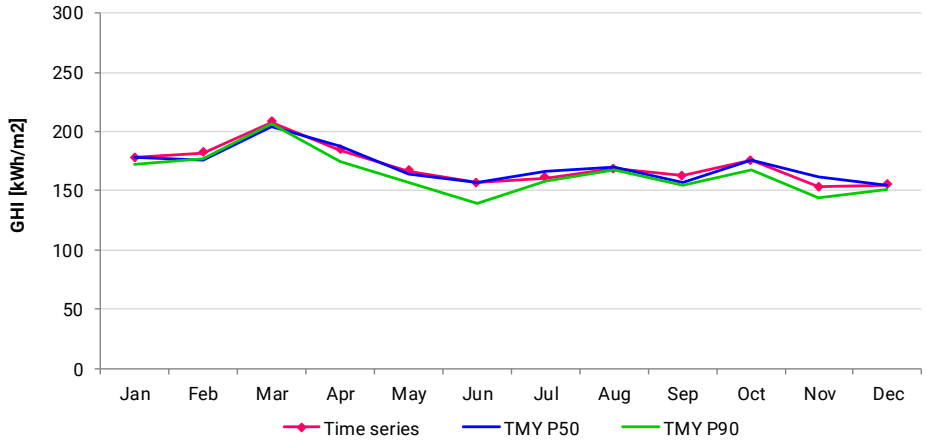

Figure 7.1: GHI monthly values derived from time series and TMY P50 and P90 at Hulhulé site.

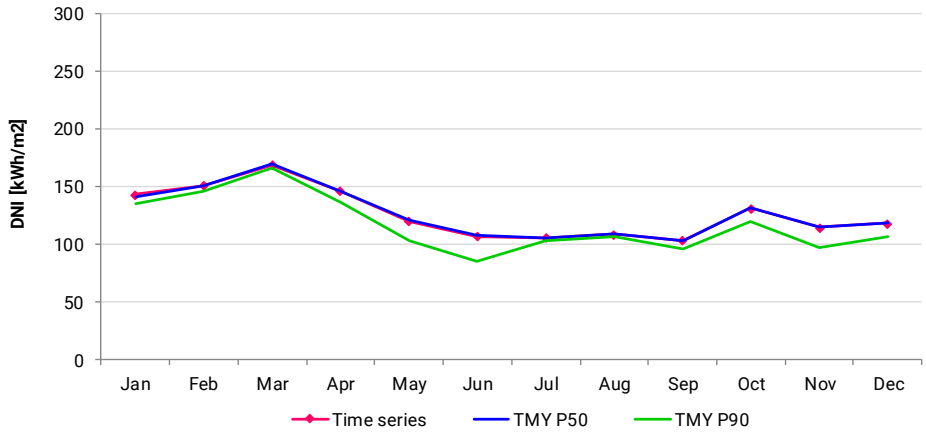

Figure 7.2: DNI monthly values derived from time series and TMY P50 and P90 at Hulhulé site.

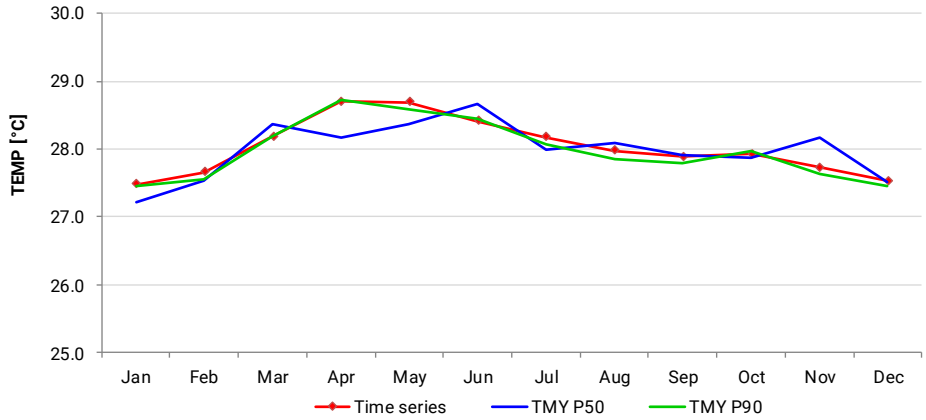

Figure 7.3: TEMP monthly values derived from time series and TMY P50 and P90 at Hulhulé site

It is important to note that the data reduction in the TMY data set is not possible without loss of information contained in the original multiyear time series. Therefore **time series data are considered as the most accurate reference suitable for the statistical analysis of solar resource and meteorological parameters of the site.**

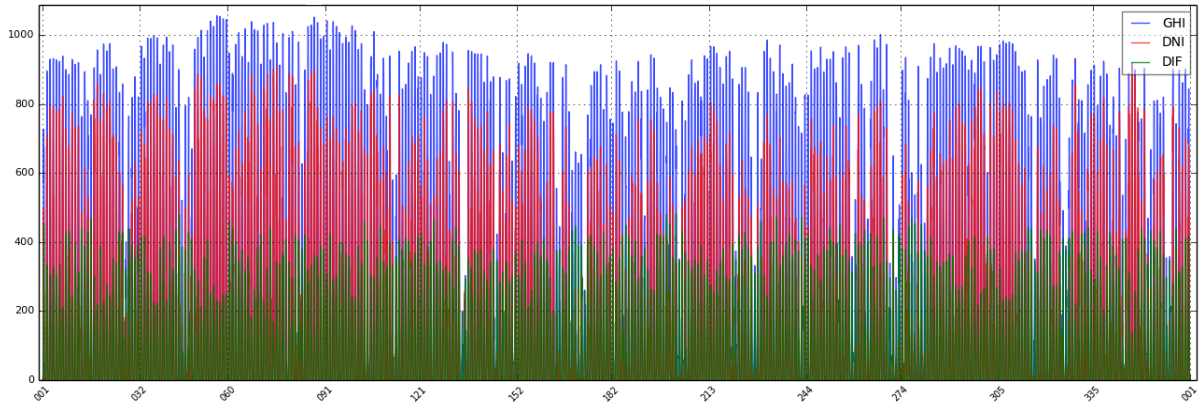

Figure 7.4: Seasonal profile of GHI, DNI and DIF for Typical Meteorological Year P50 Hulhulé site: X-axis – day of the year; Y-axis – solar irradiance W/m^2

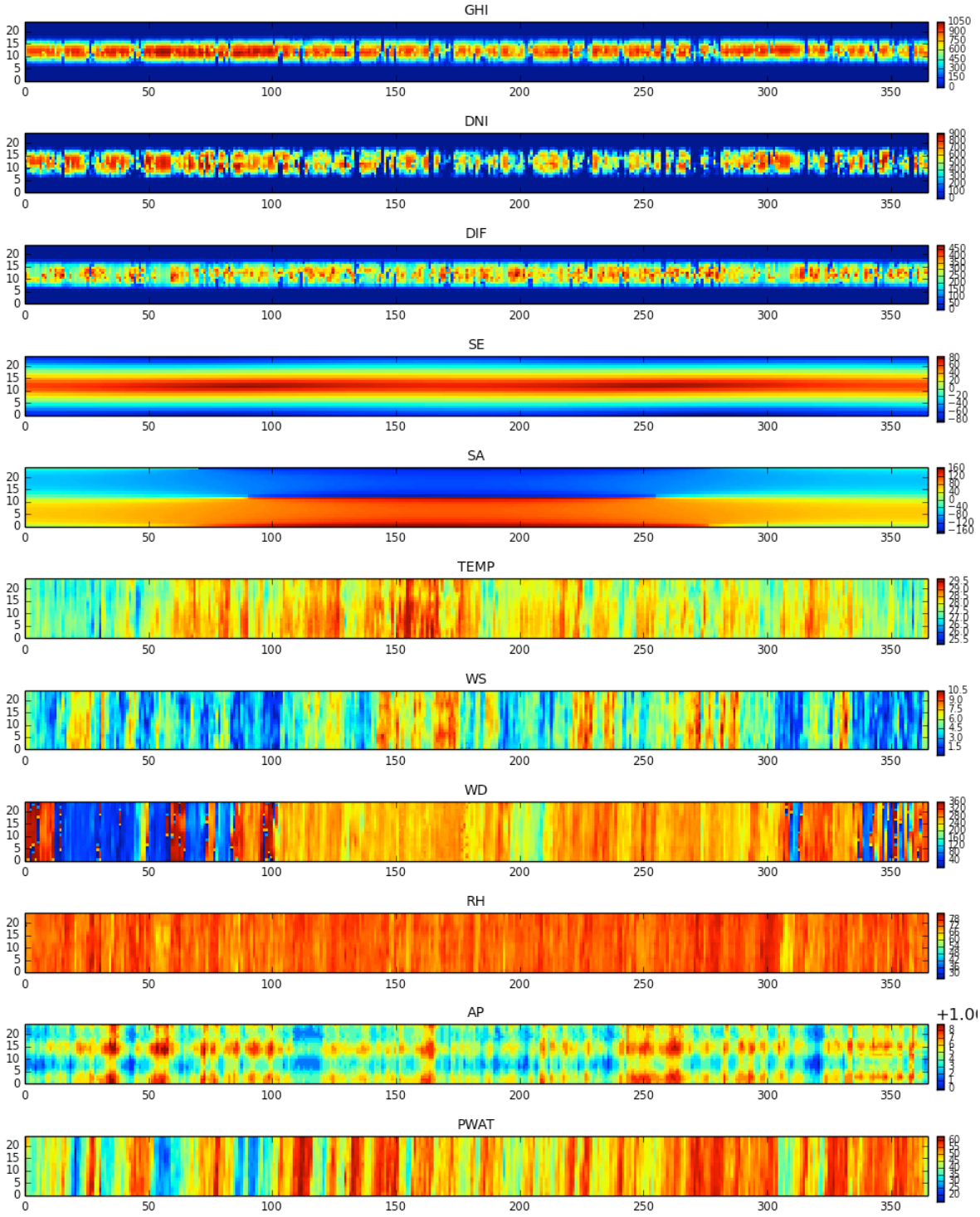

Figure 7.5: Snapshot of Typical Meteorological Year for P50 for Hulhulé

8 CONCLUSIONS

This report accompanies delivery of site-specific solar resource and meteorological data for four sites, where solar meteorological stations have been installed and operated during the year 2016. The measurement campaign is ongoing, and the same data exercise will be repeated after concluding of 24 months measurements, with expectation for reducing som more the data uncertainty.

The measured data used in site-adaptation of the Solargis model. As a result, reliable historical time series and TMY data is computed and provided in formats ready to use in standard phovotoltaic energy simulation software. The reliability of the delivered data is high and it can be used for energy evaluation of any project in Maldives and also for bankable assessment.

ANNEX 1: SITE RELATED DATA STATISTICS

Yearly summaries of solar and meteorological parameters

Statistics for site adapted model yearly values representing 18 years (2999 to 2016).

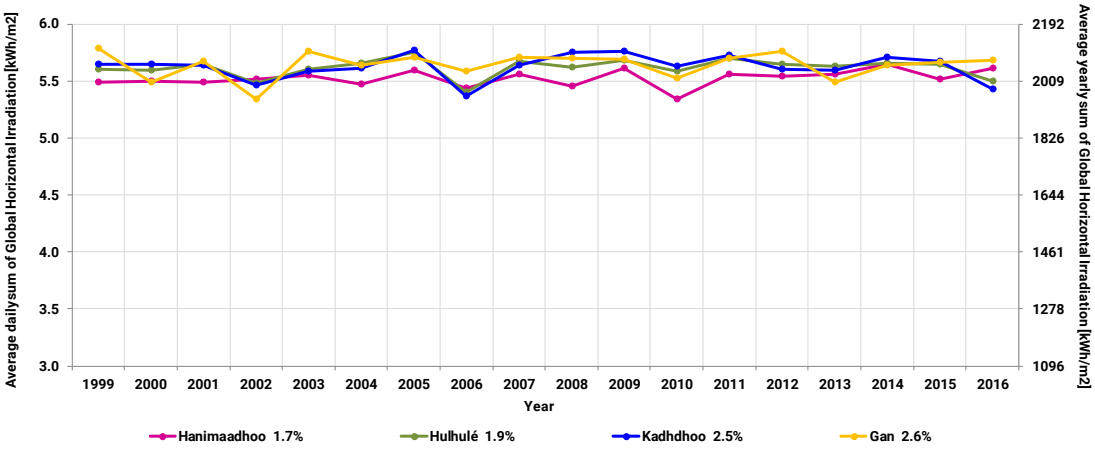

Figure I: Interannual variability of site-adapted yearly GHI [kWh/m^2].
Annual average (*avg*, solid line) and standard deviation (value behind the names of sites).

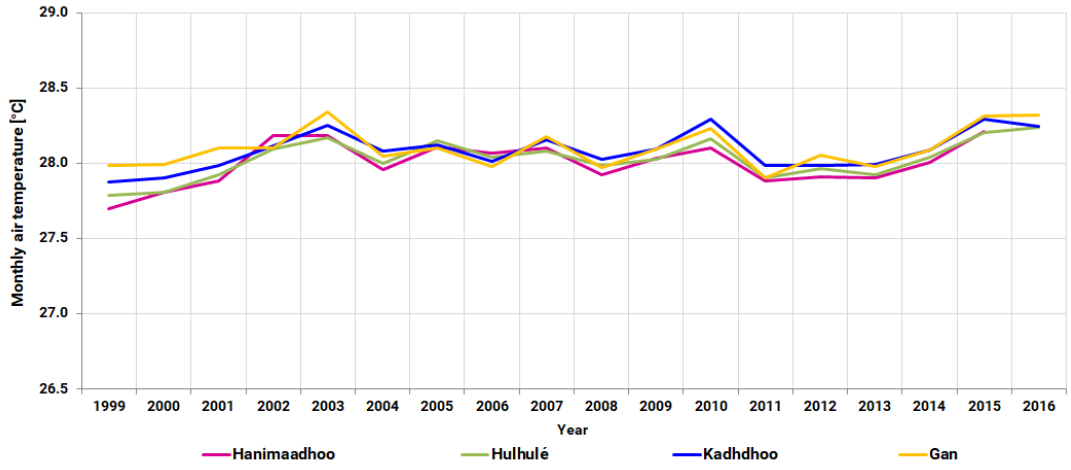

Figure II: Interannual variability of site-adapted yearly DNI [kWh/m^2].
Annual average (*avg*, solid line) and standard deviation (value behind the names of sites).

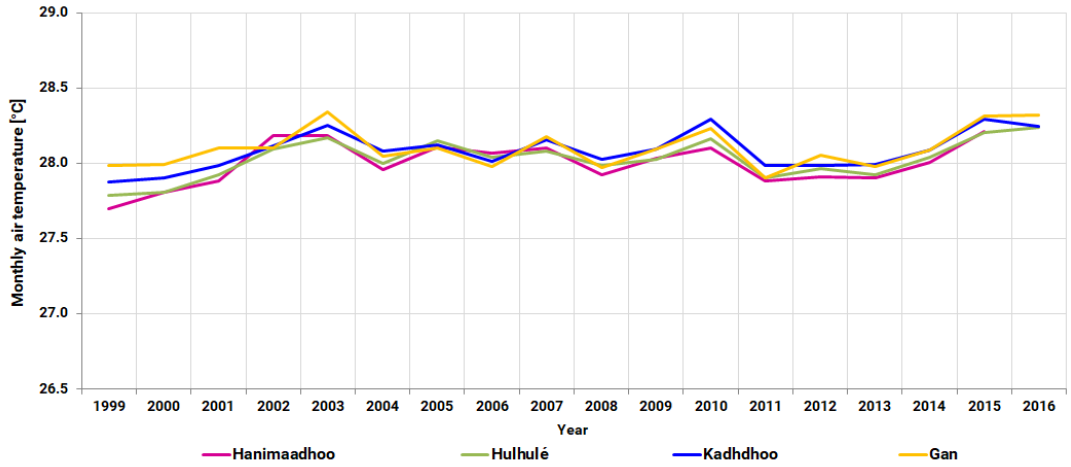

Figure III: Interannual variability of yearly TEMP [°C].
Annual average (*avg*, solid line).

Monthly summaries of solar and meteorological parameters

The graphs compare (site-adapted) monthly model time series compared to long-term averages.

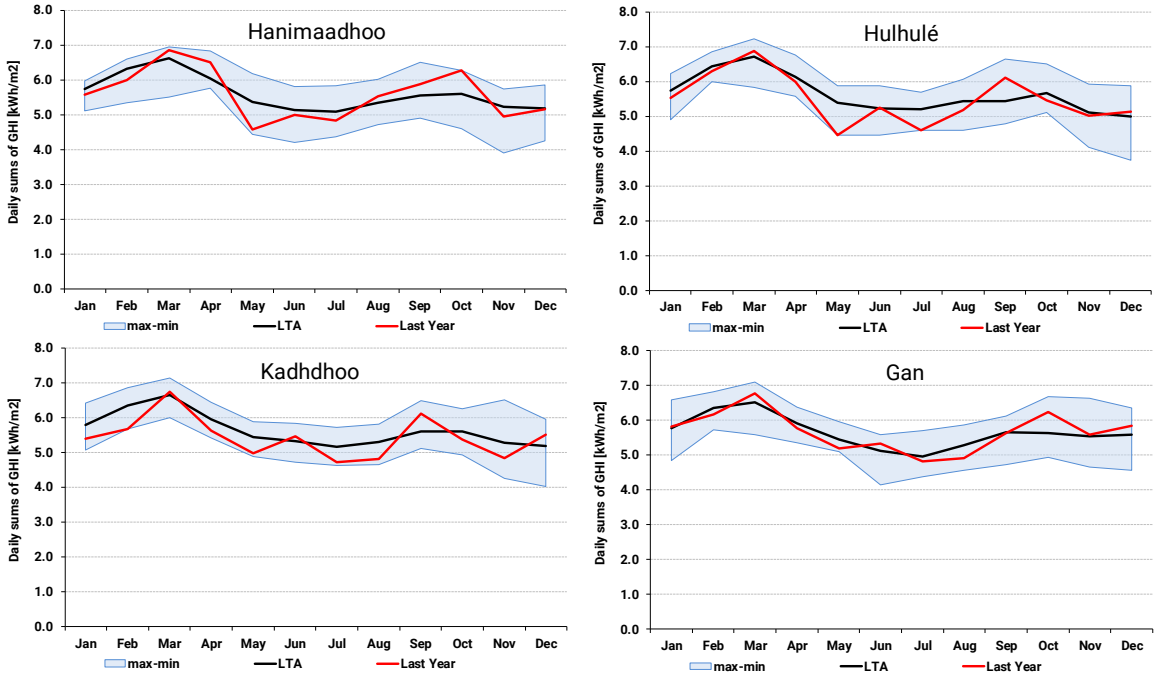

Figure IV: GHI monthly averages [kWh/m^2].
Monthly average shown as solid line; min/max monthly values as as boundary lines; last 12 months in red.

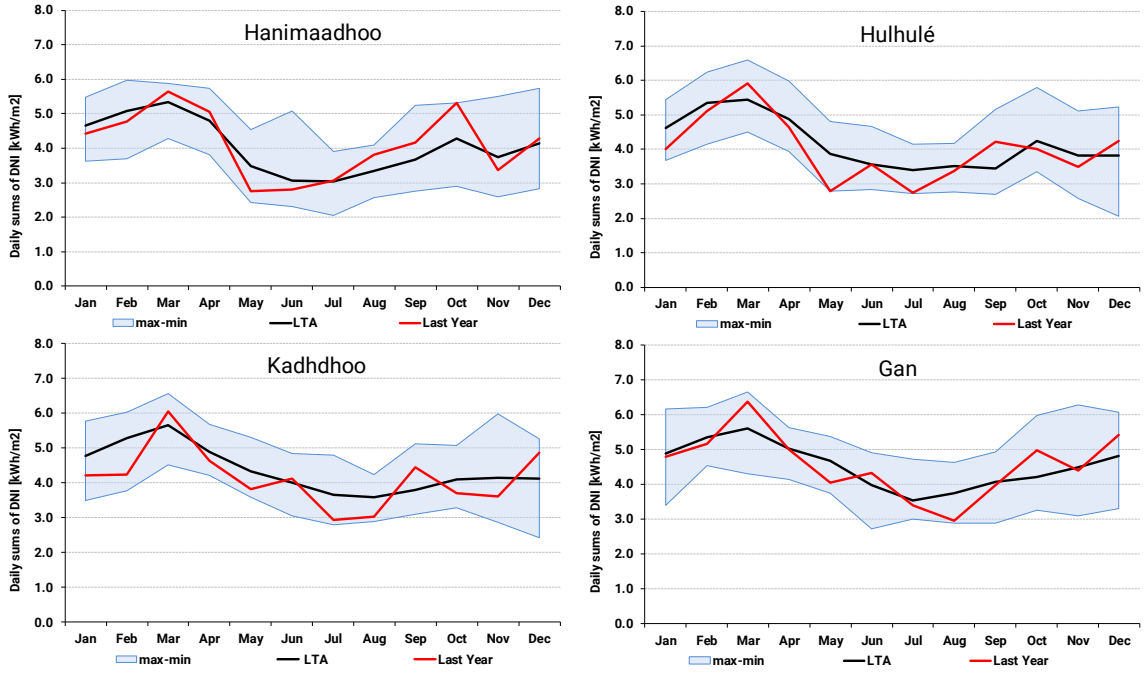

Figure V: DNI monthly averages [kWh/m^2].
Monthly average shown as solid line; min/max monthly values as boundary lines; last 12 months shown in red.

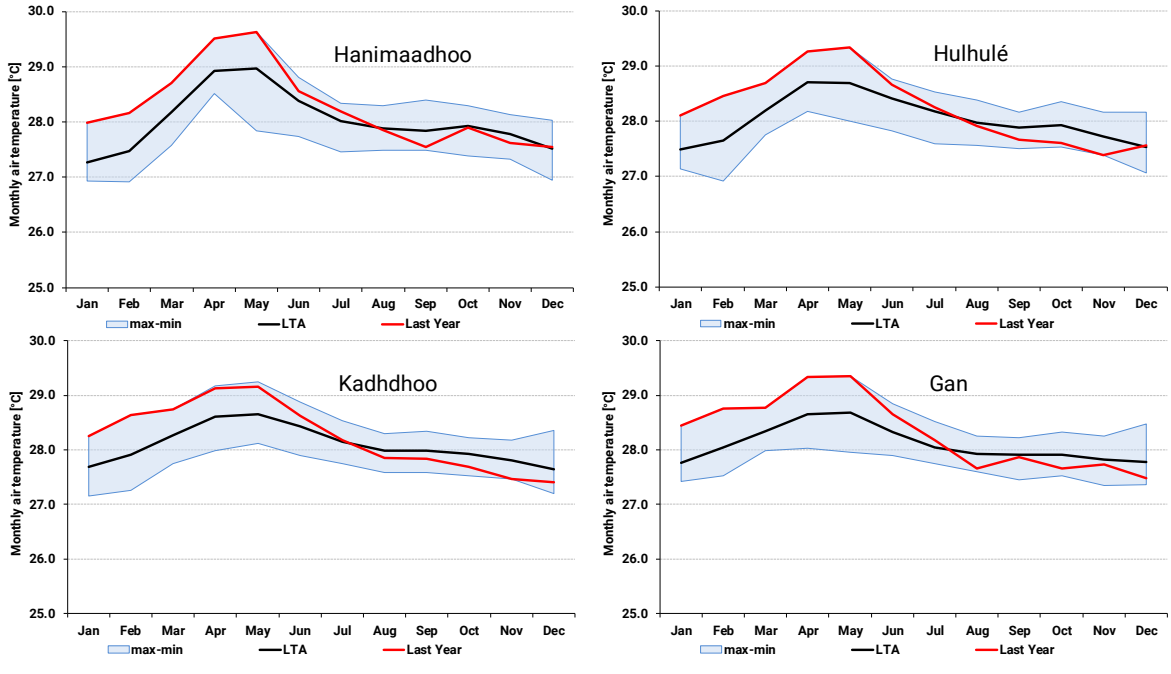

Figure VI: TEMP monthly averages [°C].
Monthly average shown as solid line; min/max onthly values as boundary lines; last 12 months shown in red.

Frequency of occurrence of GHI and DNI daily model values for a period 1999 to 2016

The histograms below show occurrence statistics of daily values derived from the satellite-based time series for GHI and DNI. The time covered in the graphs below is 18 complete calendar years (1999 to 2016). The occurrence is calculated separately for each month.

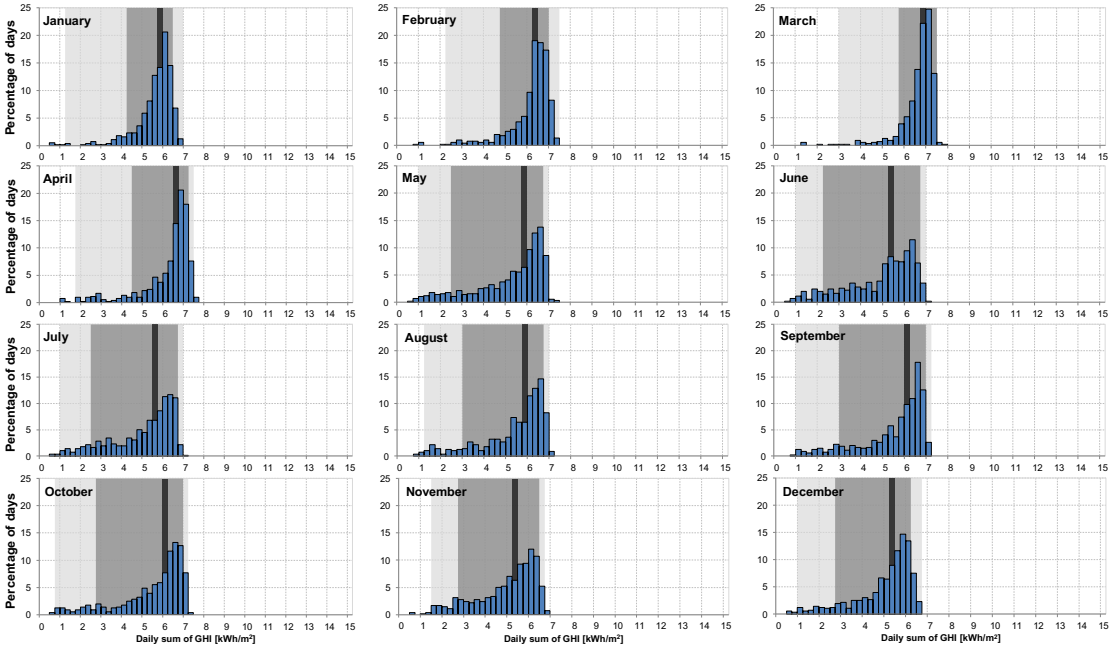

Figure VII: Histograms of daily summaries of Global Horizontal Irradiation in Hanimaadhoo.

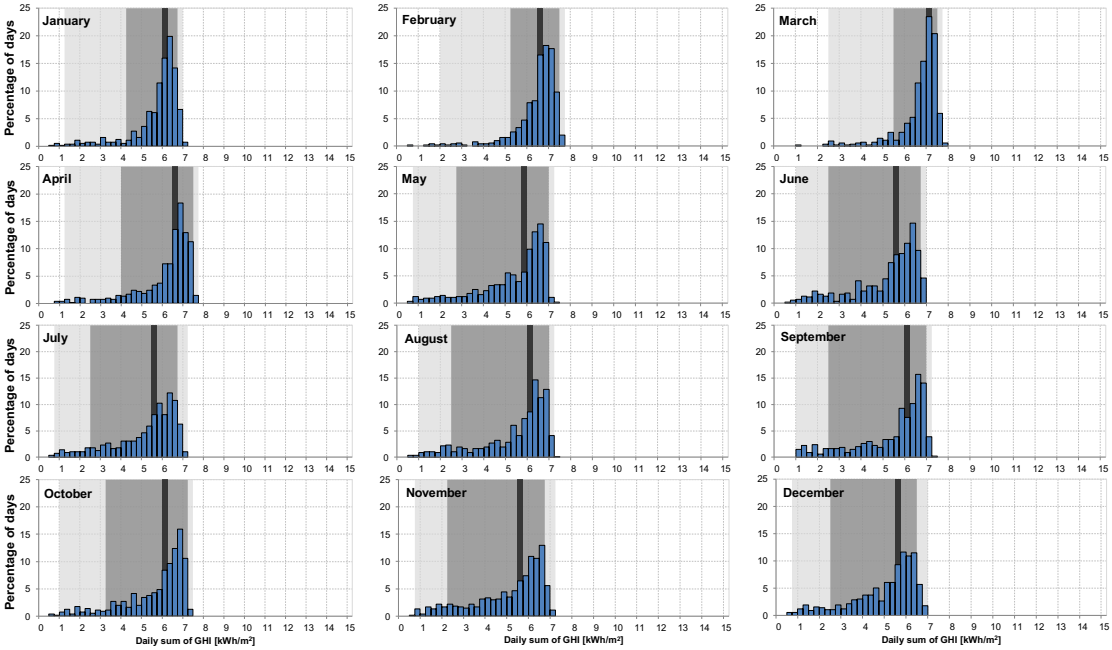

Figure VIII: Histograms of daily summaries of Global Horizontal Irradiation in Hulhulé.

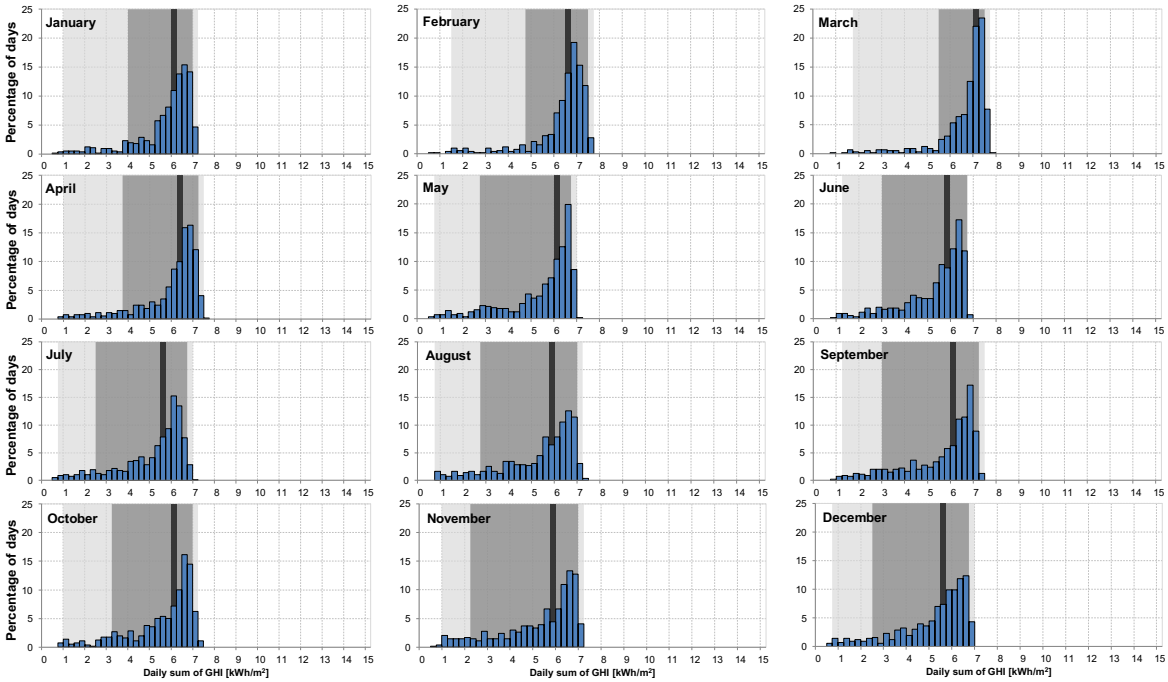

Figure IX: Histograms of daily summaries of Global Horizontal Irradiation in Kadhdhoo.

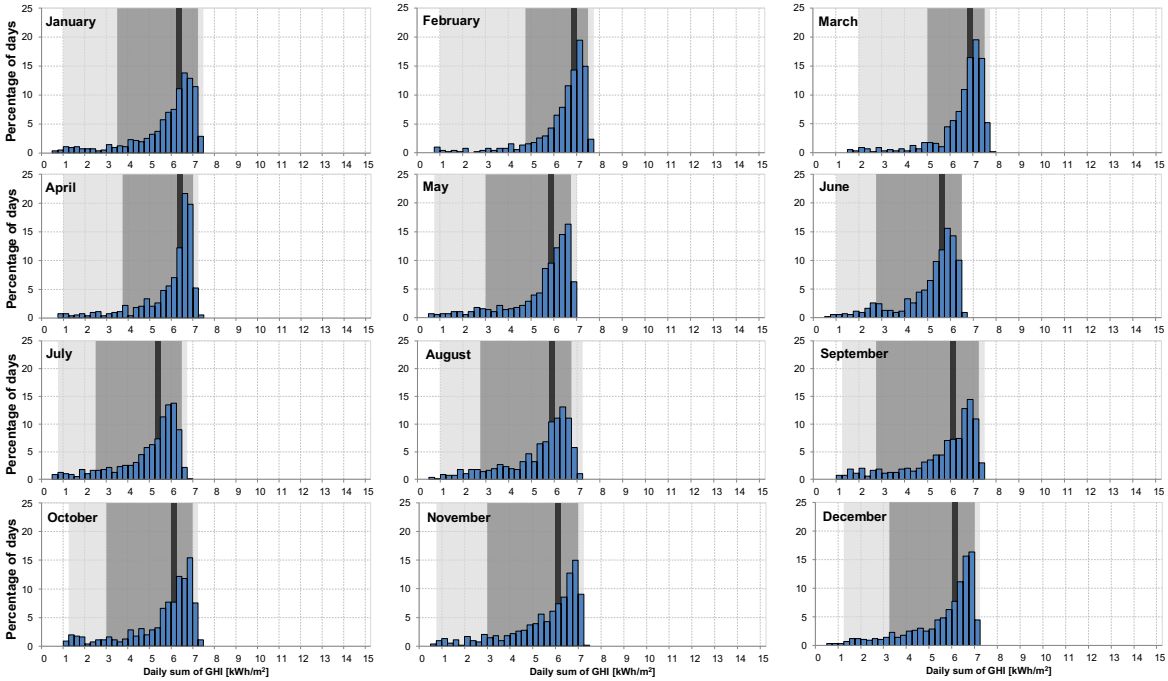

Figure X: Histograms of daily summaries of Global Horizontal Irradiation in Gan.

Figures VII to X show histograms of **daily GHI** summaries for each month as calculated from Solargis time series representing the years 1999 to 2016. The distribution of daily values is not symmetric: median is drawn by the vertical line, and percentiles P_{10}, P_{25}, and P_{75}, and P_{90} are displayed with dark grey and light grey colour bands, respectively. The percentiles P_{10} and P_{90} show 80% occurrence of daily values within each month and percentiles P_{25} and P_{75} show 50% occurrence.

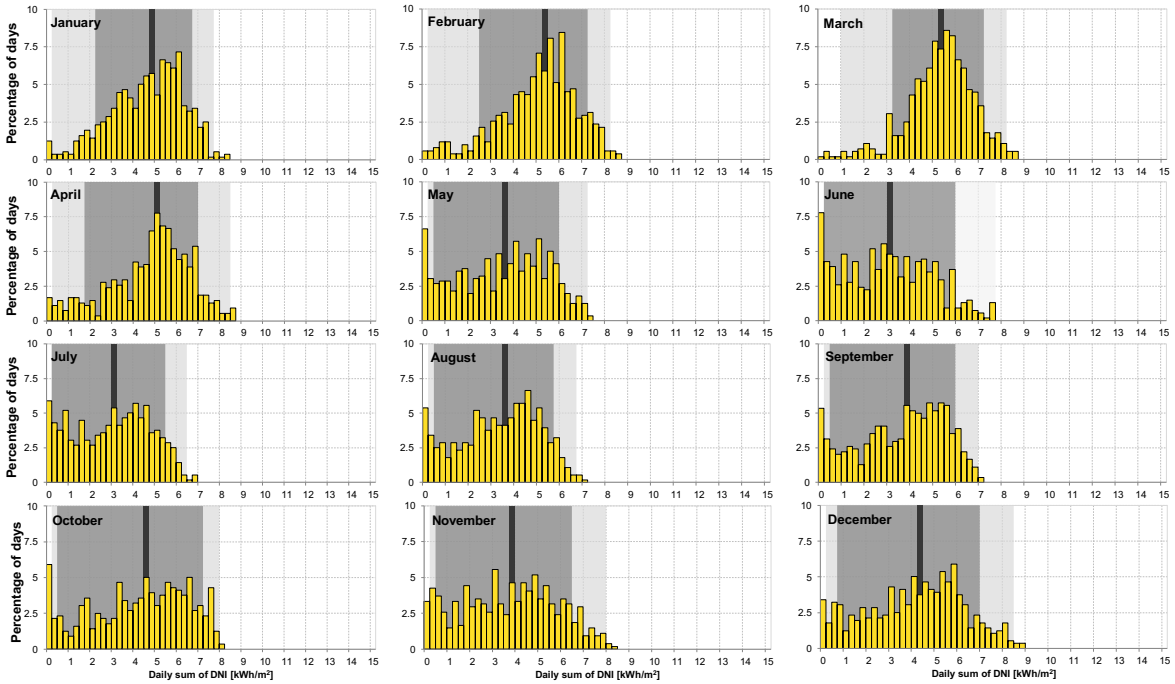

Figure XI: Histograms of daily summaries of Direct Normal Irradiation in Hanimaadhoo.

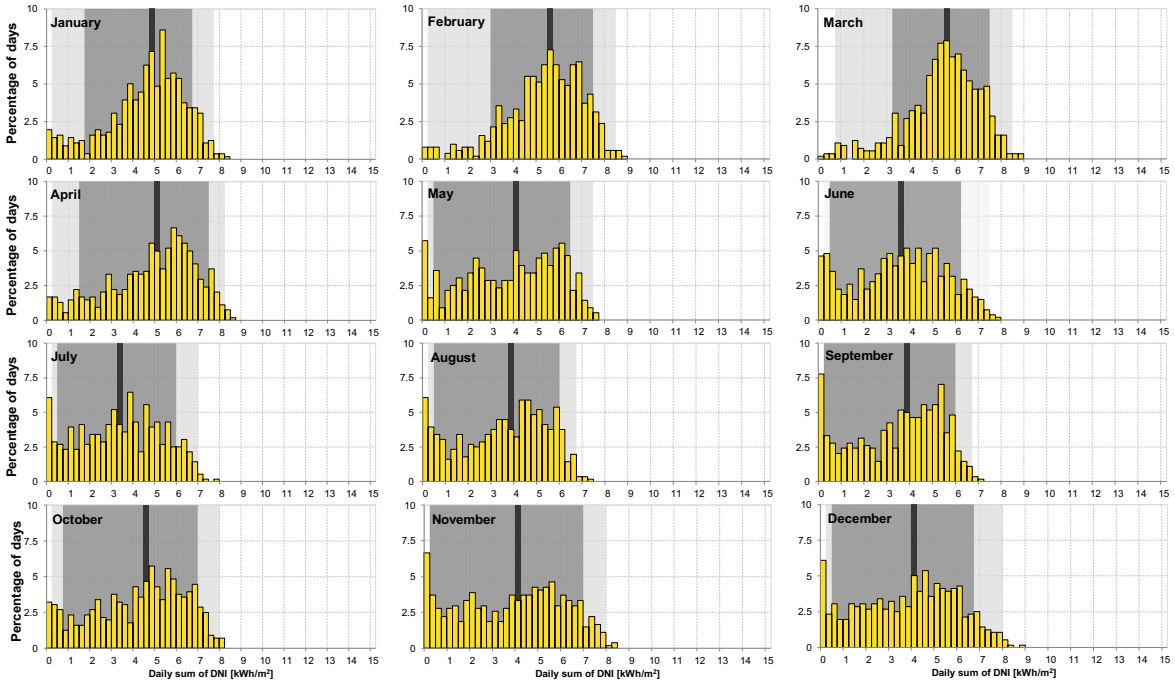

Figure XII: Histograms of daily summaries of Direct Normal Irradiation in Hulhulé.

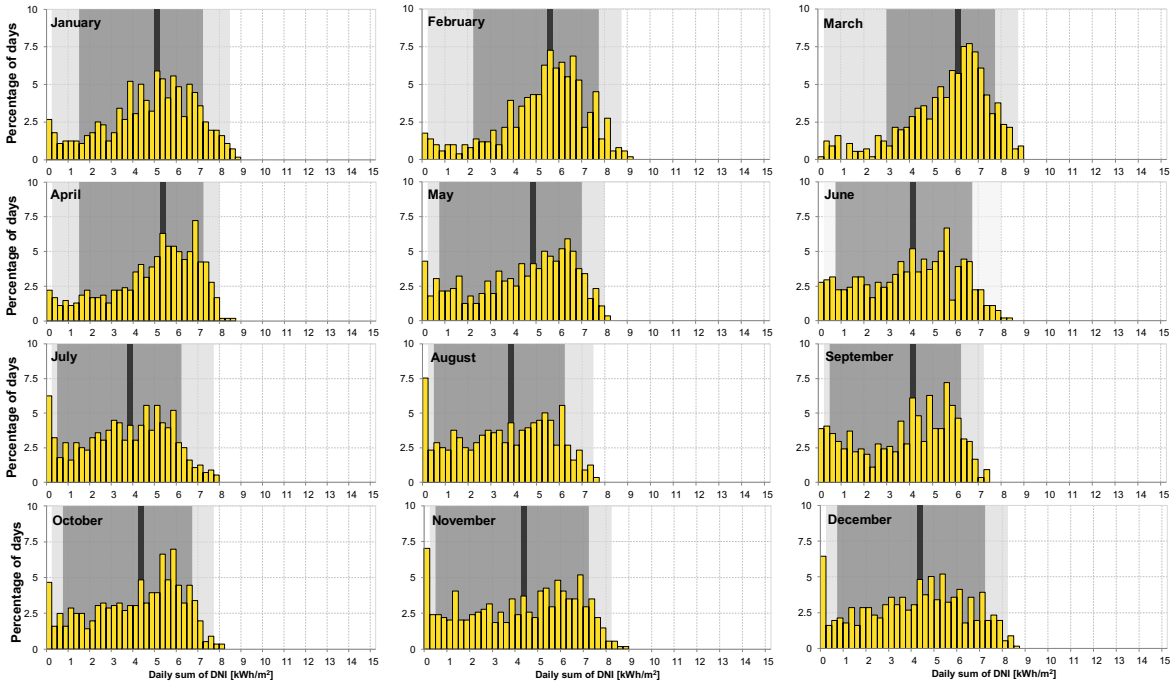

Figure XIII: Histograms of daily summaries of Direct Normal Irradiation in Kadhdhoo.

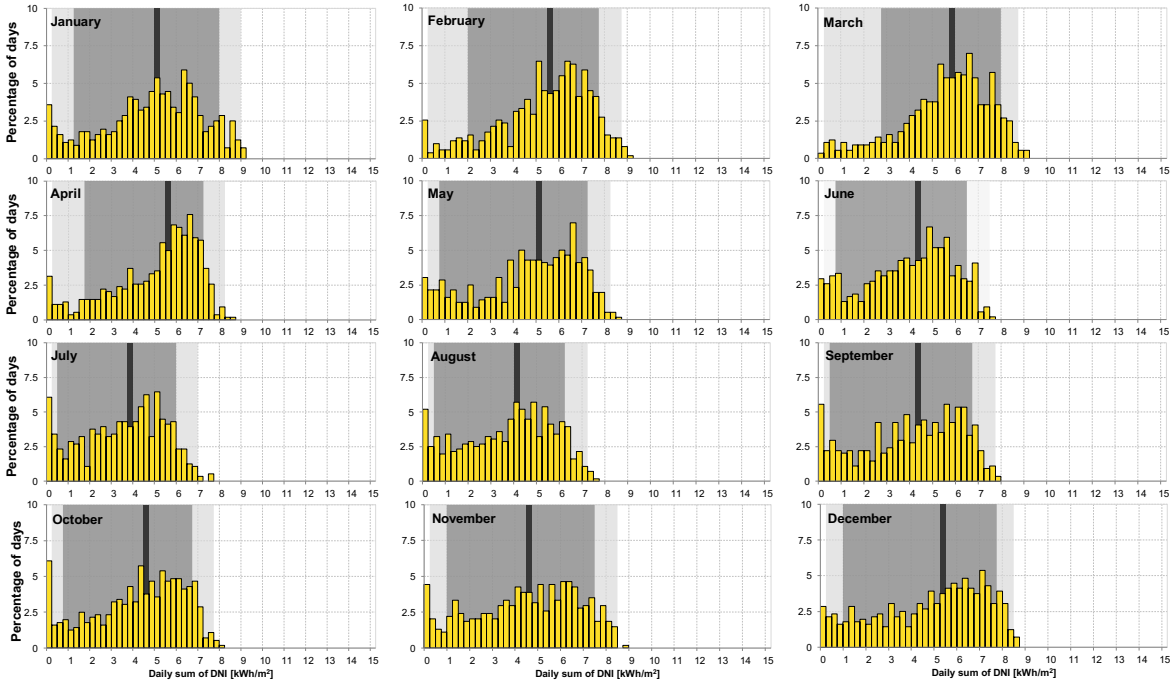

Figure XIV: Histograms of daily summaries of Direct Normal Irradiation in Gan.

Figures XI to XIV show histograms of **daily DNI** summaries for each month as calculated from Solargis time series representing the years 1999 to 2016. The distribution of daily values is not symmetric: median is drawn by the vertical line, and percentiles P_{10}, P_{25}, and P_{75}, and P_{90} are displayed with dark grey and light grey colour bands, respectively. The percentiles P_{10} and P_{90} show 80% occurrence of daily values within each month and percentiles P_{25} and P_{75} show 50% occurrence.

Frequency of occurrence of GHI and DNI 30-minute model values for a period 1999 to 2016

The histograms below show occurrence statistics of 30-minute values derived from the satellite-based time series for GHI and DNI. The time covered in the graphs below is 18 complete calendar years (1999 to 2016). The occurrence is calculated separately for each month.

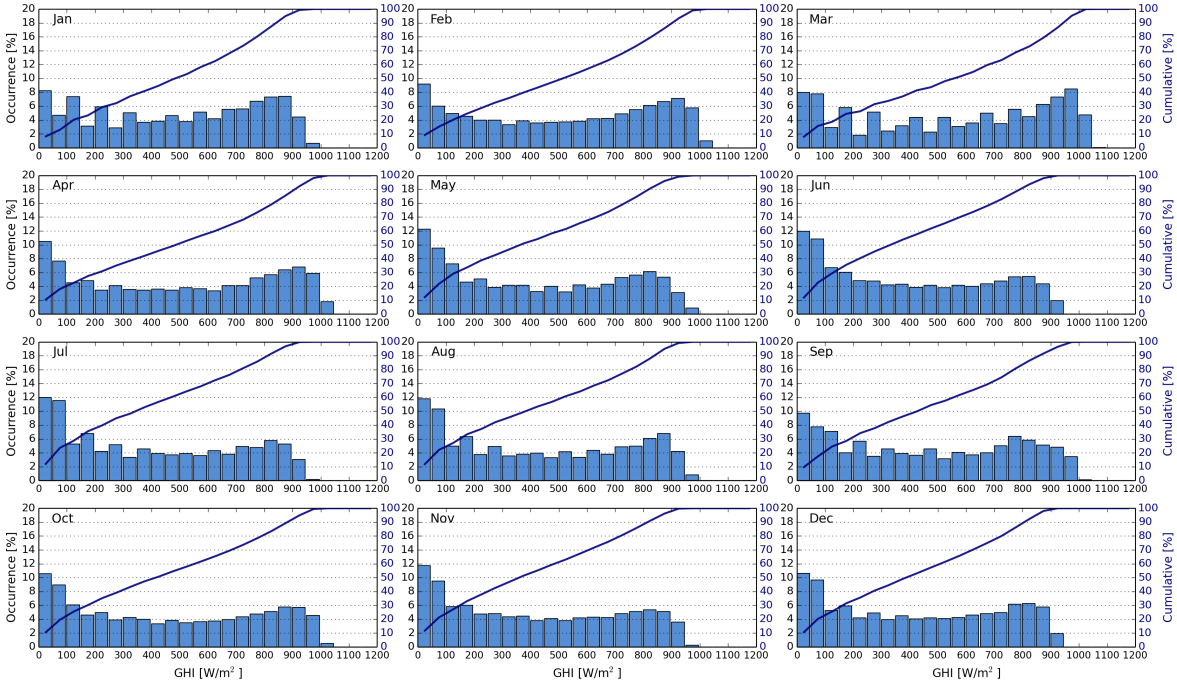

Figure XV: Histograms and cumulative distribution function of 30-minute GHI in Hanimaadhoo

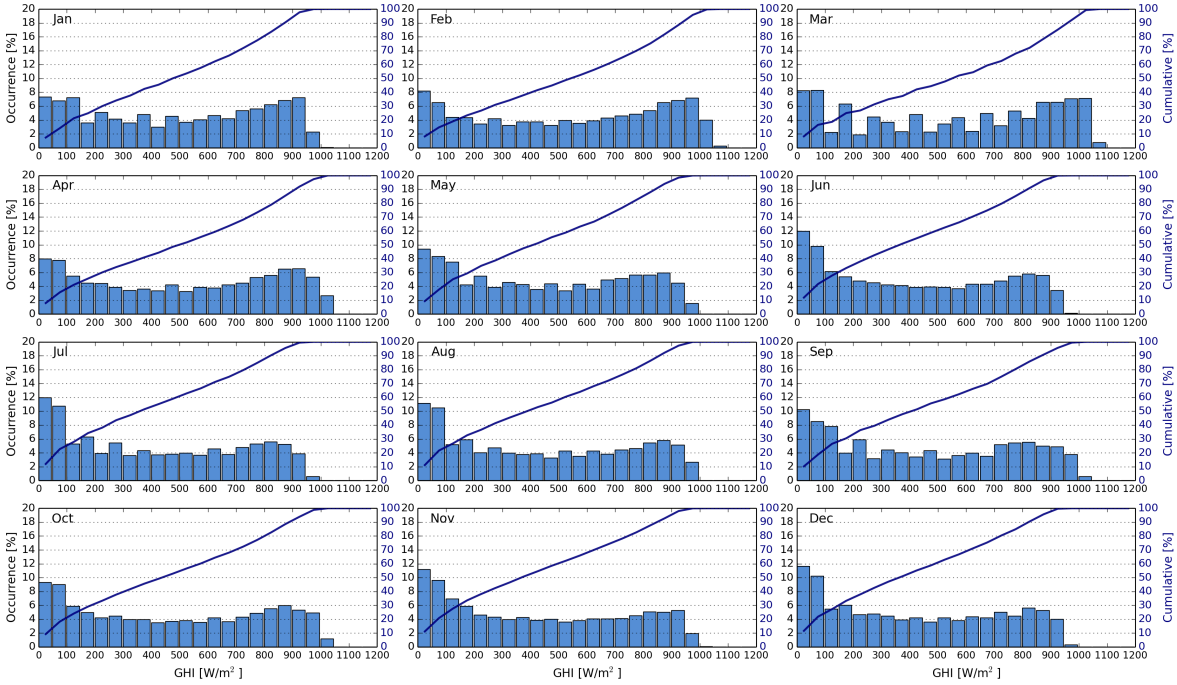

Figure XVI: Histograms and cumulative distribution function of 30-minute GHI in Hulhulé

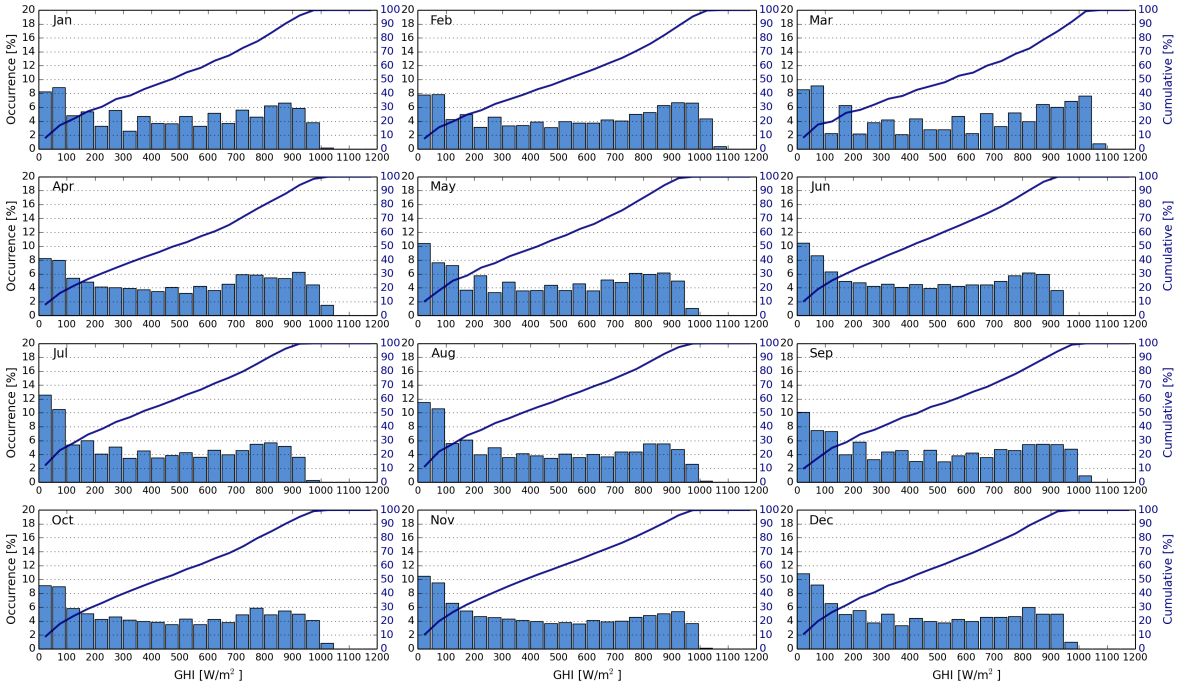

Figure XVII: Histograms and cumulative distribution function of 30-minute GHI in Kadhdhoo

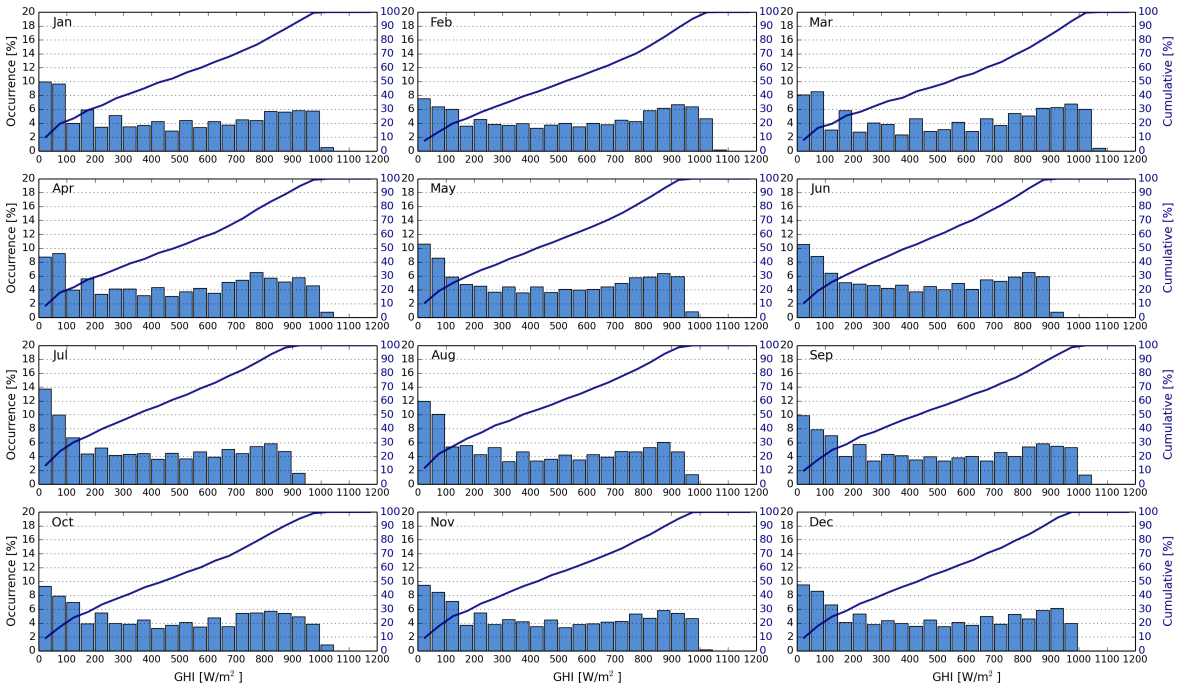

Figure XVIII: Histograms and cumulative distribution function of 30-minute GHI in Gan

Figures XV to XVIII show monthly histograms (bars) and cumulative distribution (line) of 30-minute GHI values, calculated from Solargis time series. The values represent the occurrence of GHI values within 50 W/m^2 bins, ranging from 0 to 1200 W/m^2.

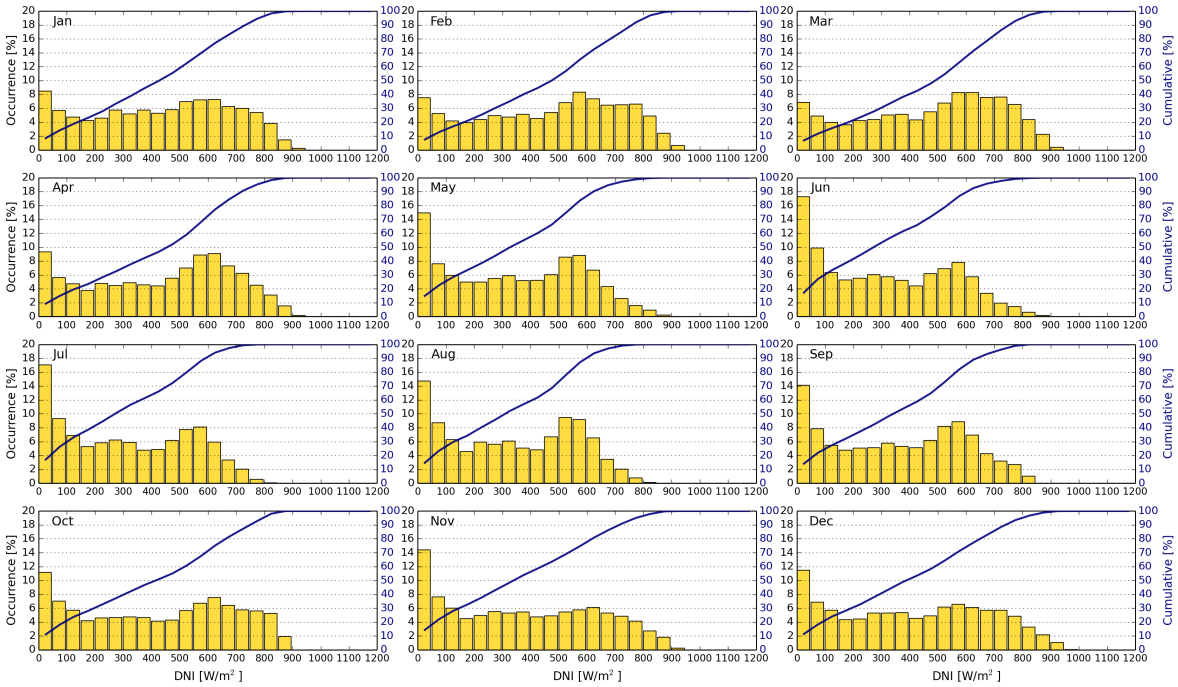

Figure XIX: Histograms and cumulative distribution function of 30-minute DNI in Hanimaadhoo

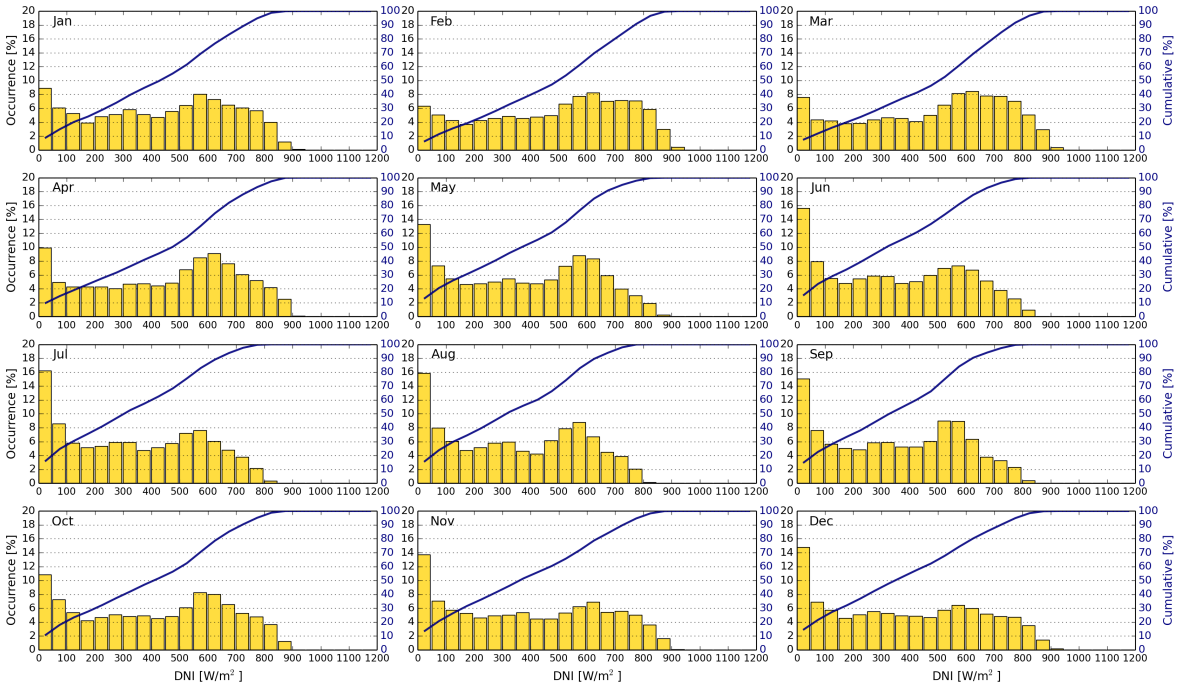

Figure XX: Histograms and cumulative distribution function of 30-minute DNI in Hulhulé

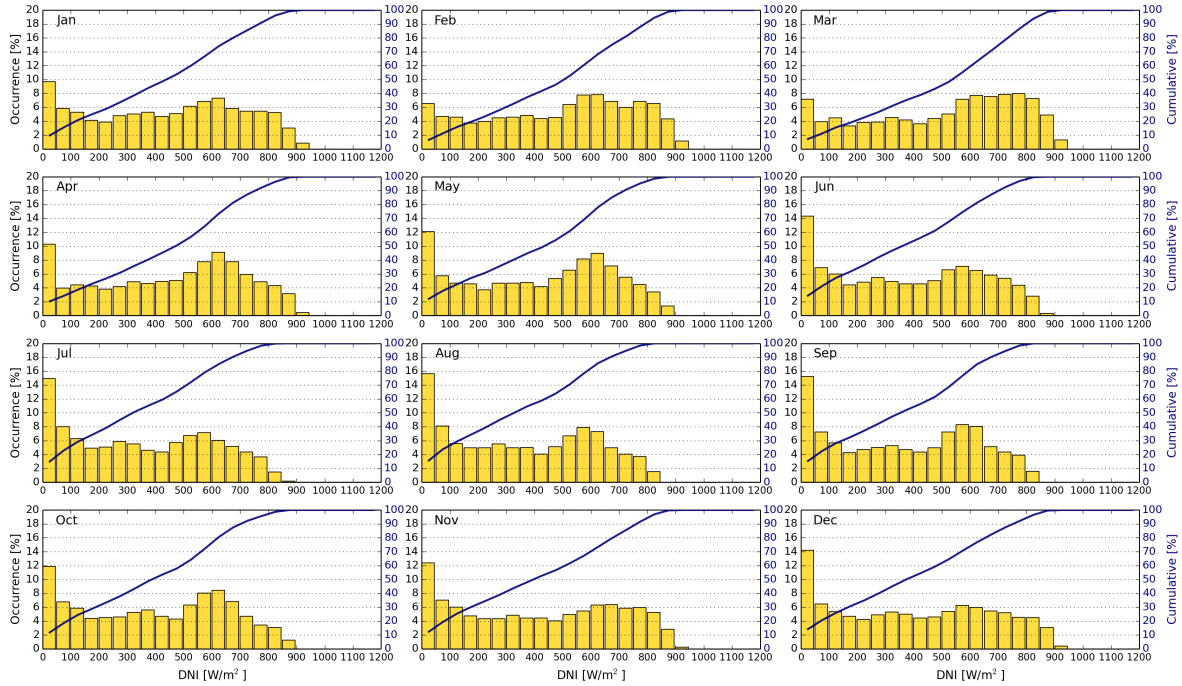

Figure XXI: Histograms and cumulative distribution function of 30-minute DNI in Kadhdhoo

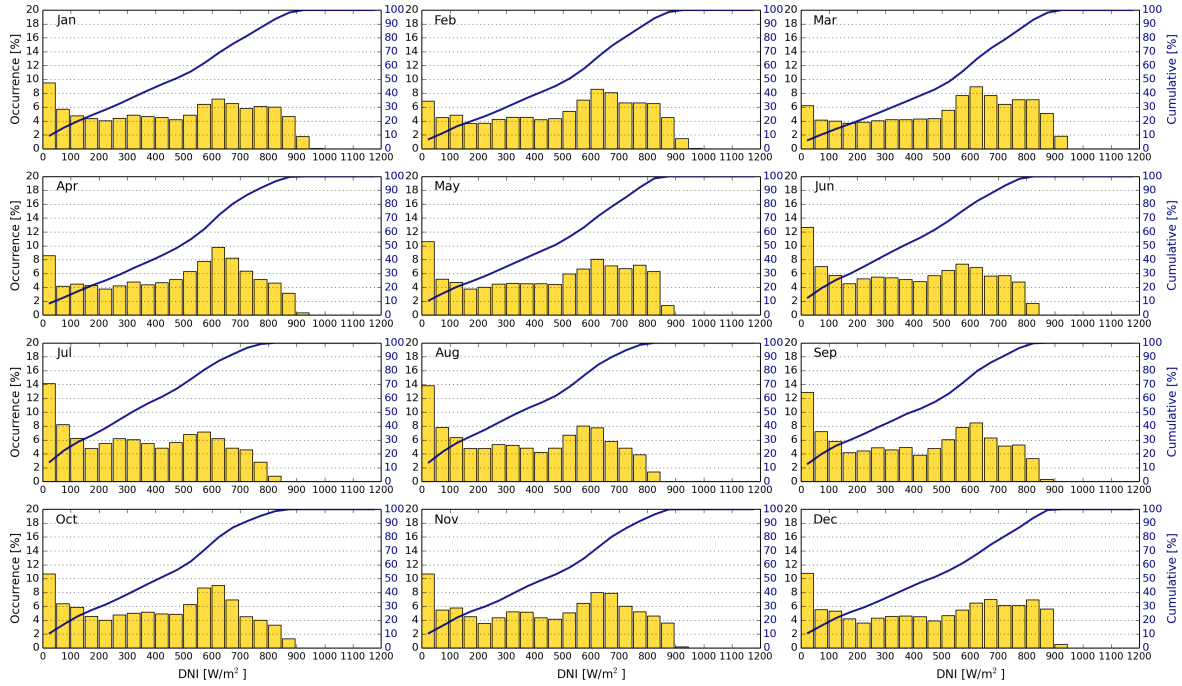

Figure XXII: Histograms and cumulative distribution function of 30-minute DNI in Gan

Figures XIX to XXII show monthly histograms (bars) and cumulative distribution (line) of 30-minute DNI values, calculated from Solargis time series. The values represent the occurrence of DNI values within 50 W/m^2 bins, ranging from 0 to 1200 W/m^2.

Frequency of occurrence of GHI and DNI measured and model values representing year 2016

Figures XXIII to XXX show histograms comparing the measured values with the model GHI and DNI data. The period covered in these histogram is last 12-months (one full year of data, i.e. from 1 Jan 2016 to 31 Dec 2016):

- 1-minute measured vs. 30-min satellite-based model values
- 30-minute measured (aggregated from 1-min) vs. 30-min satellite-based values
- Daily measured (aggregated from 1-min) vs. daily satellite-based model values

Aggregation process deals with the missing values in the ground measurement in three steps:

1. Only those 1-minute measured data values that passed through quality control (Chapter 3.3) is taken into account (satellite time series does not have gaps.);
2. Aggregation of 1-minute measured data values into 30-minute slots (equivalent to satellite time slots) is applied if more than 15 valid data-points is available, otherwise the 30-minute data slot is ignored in further statistical comparison;
3. Daily aggregation of measured data represents the same 30-minute time slots in a day (passing through the two steps above), as those in the satellite-based data. Incorrect data slots found in the measurements are excluded in both the measured and model data.

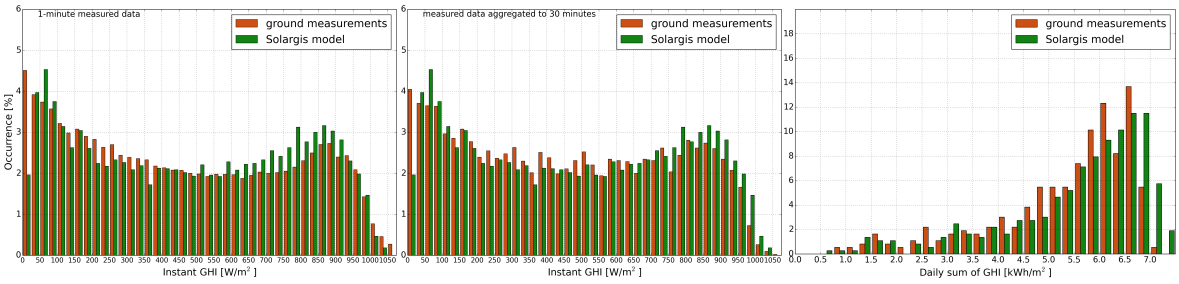

Figure XXIII: Measured vs. satellite-based GHI values in Hanimaadhoo
1-minute measured vs. 30-min satellite-based values.
30-minute measured (aggregated from 1-min) vs. 30-min satellite-based values
Daily measured (aggregated from 1-min) vs. daily satellite-based values

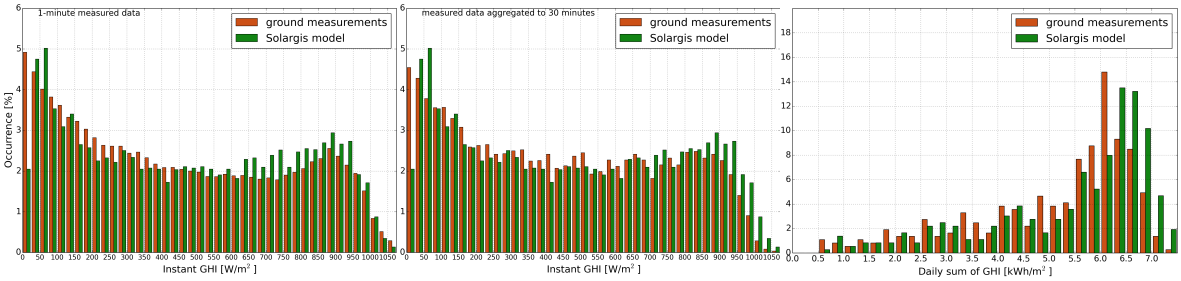

Figure XXIV: Measured vs. satellite-based GHI values in Hulhulé
1-minute measured vs. 30-min satellite-based values.
30-minute measured (aggregated from 1-min) vs. 30-min satellite-based values
Daily measured (aggregated from 1-min) vs. daily satellite-based values

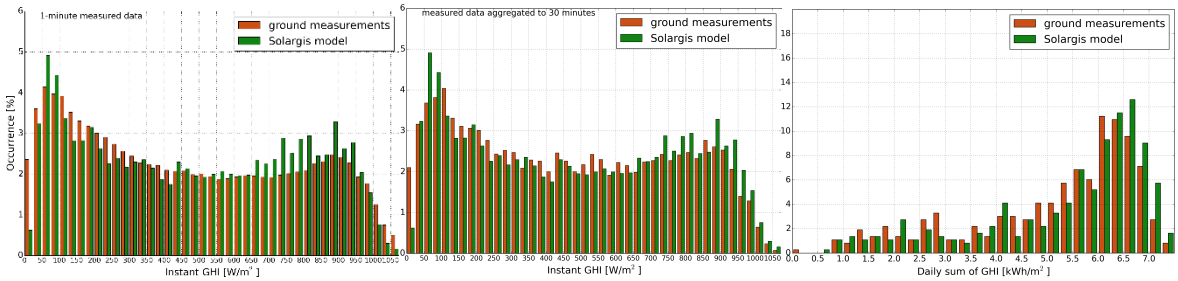

Figure XXV: Measured vs. satellite-based GHI values in Kadhdhoo
1-minute measured vs. 30-min satellite-based values.
30-minute measured (aggregated from 1-min) vs. 30-min satellite-based values
Daily measured (aggregated from 1-min) vs. daily satellite-based values

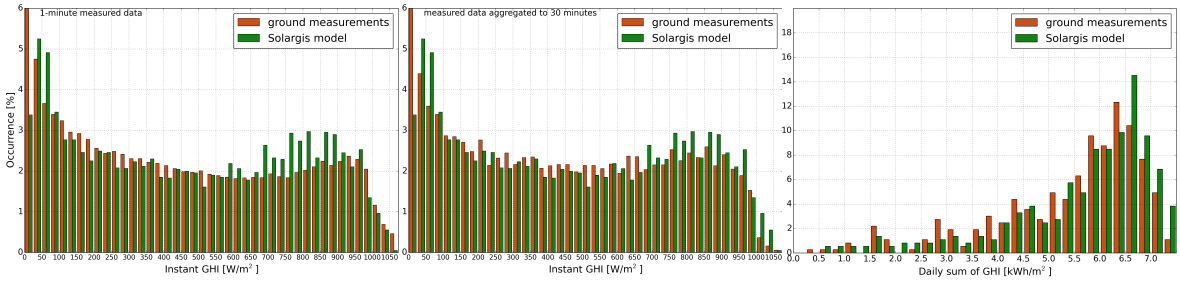

Figure XXVI: Measured vs. satellite-based GHI values in Gan
1-minute measured vs. 30-min satellite-based values.
30-minute measured (aggregated from 1-min) vs. 30-min satellite-based values
Daily measured (aggregated from 1-min) vs. daily satellite-based values

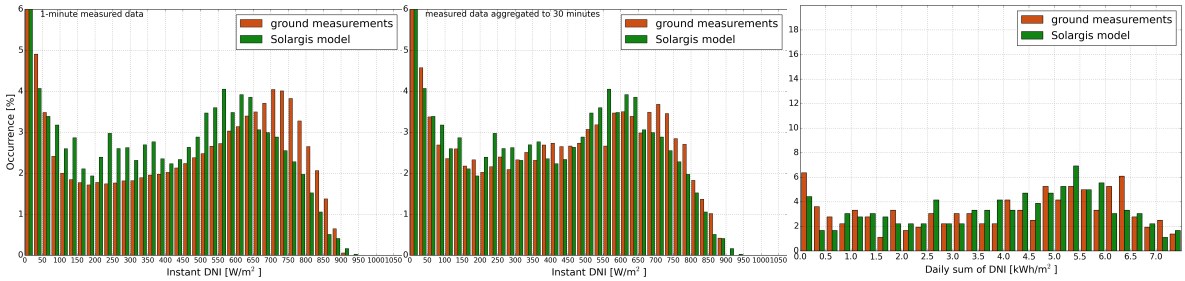

Figure XXVII: Measured vs. satellite-based DNI values in Hanimaadhoo
1-minute measured vs. 30-min satellite-based values.
30-minute measured (aggregated from 1-min) vs. 30-min satellite-based values
Daily measured (aggregated from 1-min) vs. daily satellite-based values

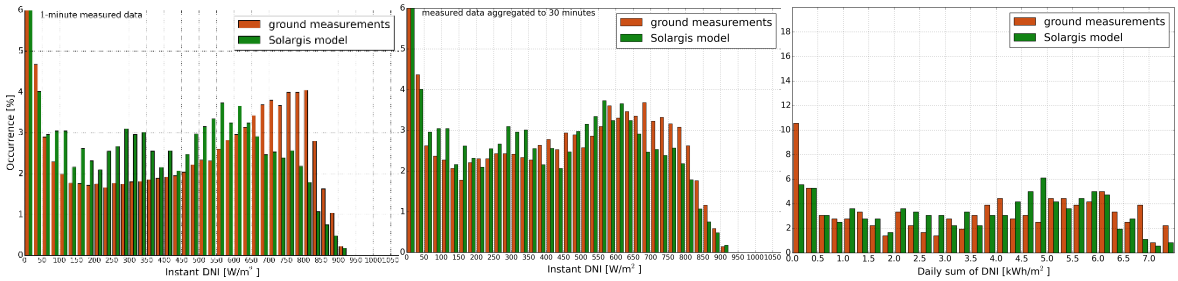

Figure XXVIII: Measured vs. satellite-based DNI values in Hulhulé
1-minute measured vs. 30-min satellite-based values.
30-minute measured (aggregated from 1-min) vs. 30-min satellite-based values
Daily measured (aggregated from 1-min) vs. daily satellite-based values

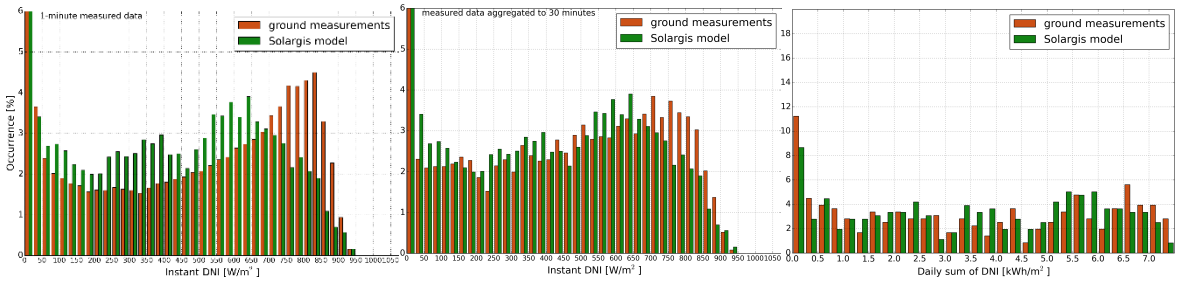

Figure XXIX: Measured vs. satellite-based DNI values in Kadhdhoo
1-minute measured vs. 30-min satellite-based values.
30-minute measured (aggregated from 1-min) vs. 30-min satellite-based values
Daily measured (aggregated from 1-min) vs. daily satellite-based values

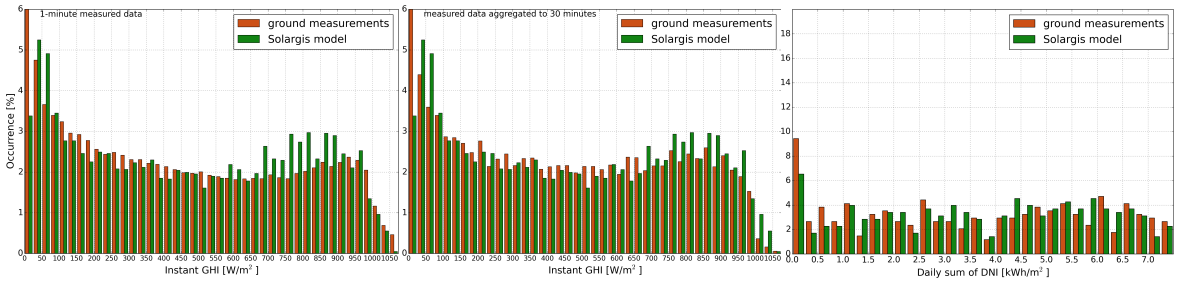

Figure XXX: Measured vs. satellite-based DNI values in Gan
1-minute measured vs. 30-min satellite-based values.
30-minute measured (aggregated from 1-min) vs. 30-min satellite-based values
Daily measured (aggregated from 1-min) vs. daily satellite-based values

Frequency of occurrence of GHI and DNI ramps

Figures XXXI to XXXVIII show histograms of instantaneous changes (ramps) calculated from the measurements and compared to the instantaneous changes calculated fro the model data. Figures show both negative (-) and positive (+) changes. Two versions for GHI and DNI are shown:

- Ramps calculated from 1-minute measured values compared to ramps calculated from 30-minute satellite-based data (figure on the left)
- Ramps calculated from 30-minute aggregated valid measurement compared to ramps calculated from 30-minute satellite-based data (figure on the right).

Occurrence of gaps in the measurements is managed in the same way as described about in this Chapter:

1. For measurements, only those 1-minute data values (measurements) that passed through quality control (Chapter 3.3) is taken into account (satellite time series does not have gaps.);
2. For measurements, the aggregation (averaging) of 1-minute measured data values into 30-minute slots (equivalent to satellite time slots) is applied if more than 15 valid data-points is available, otherwise the 30-minute data slot is ignored in further statistical comparison;

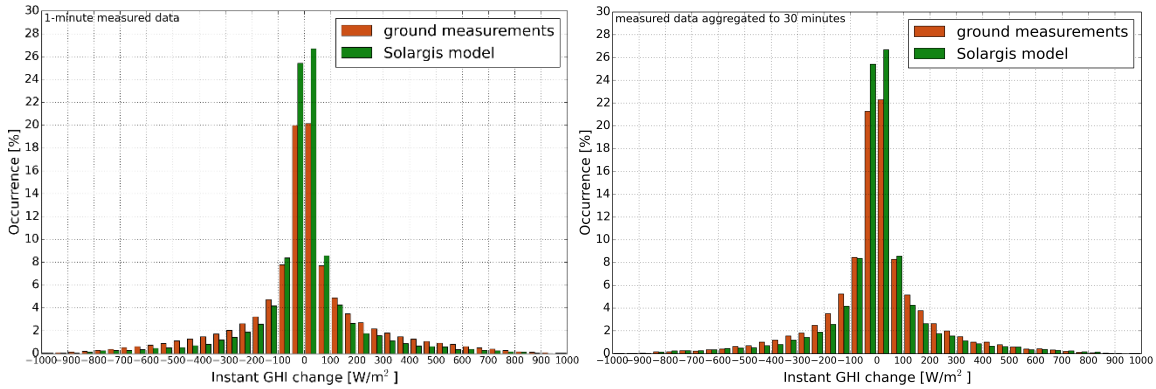

Figure XXXI: 1-minute and 30-minute GHI ramps (measured and satellite data) at Hanimaadhoo.

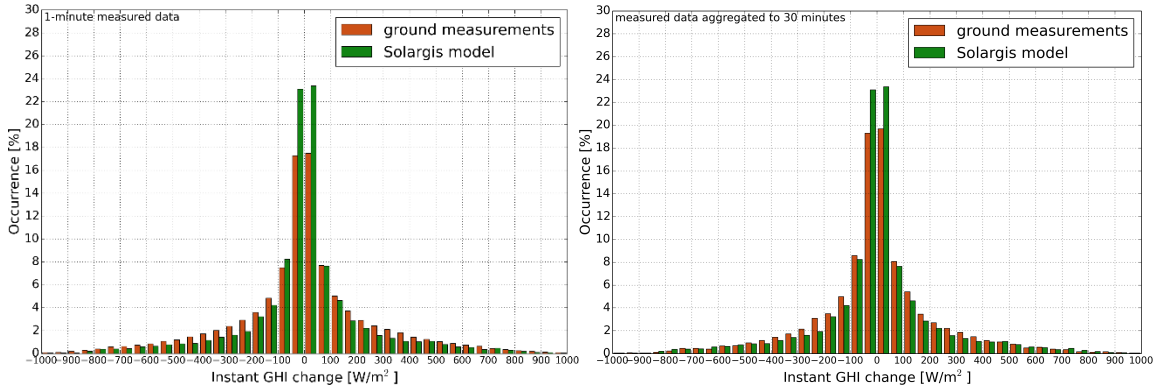

Figure XXXII: 1-minute and 30-minute GHI ramps (measured and satellite data) at Hulhulé

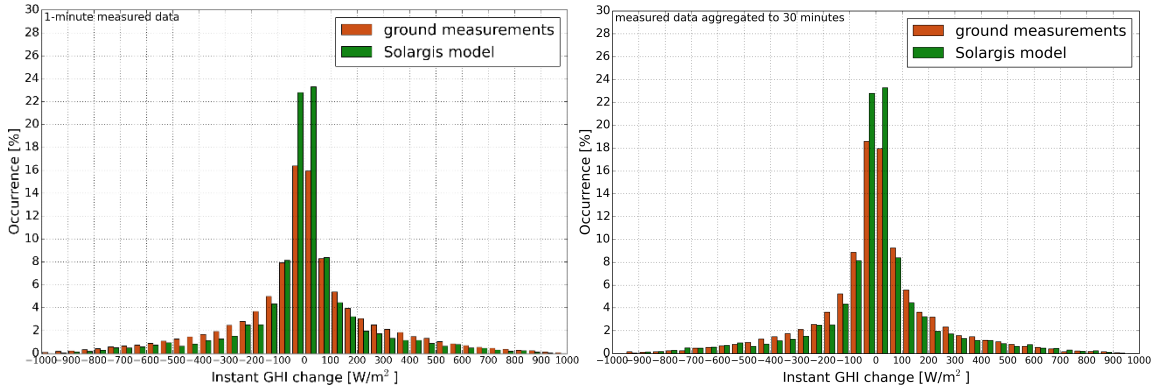

Figure XXXIII: 1-minute and 30-minute GHI ramps (measured and satellite data) at Kadhdhoo

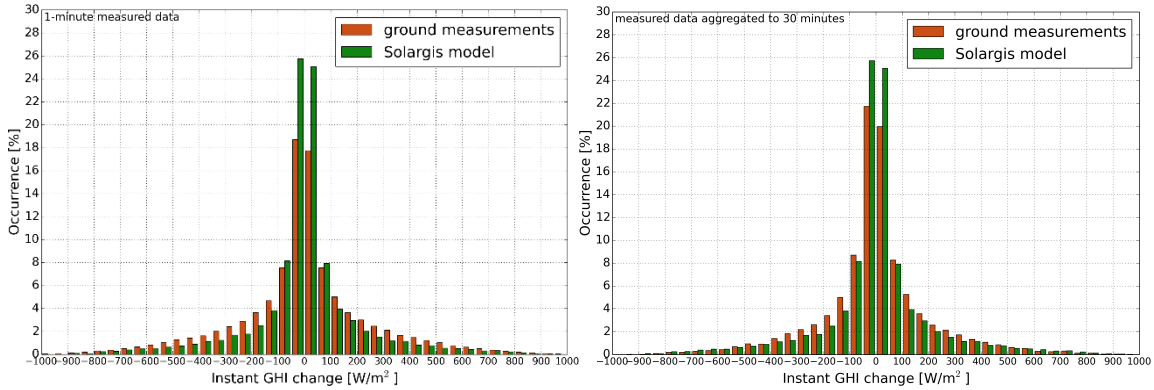

Figure XXXIV: 1-minute and 30-minute GHI ramps (measured and satellite data) at Gan

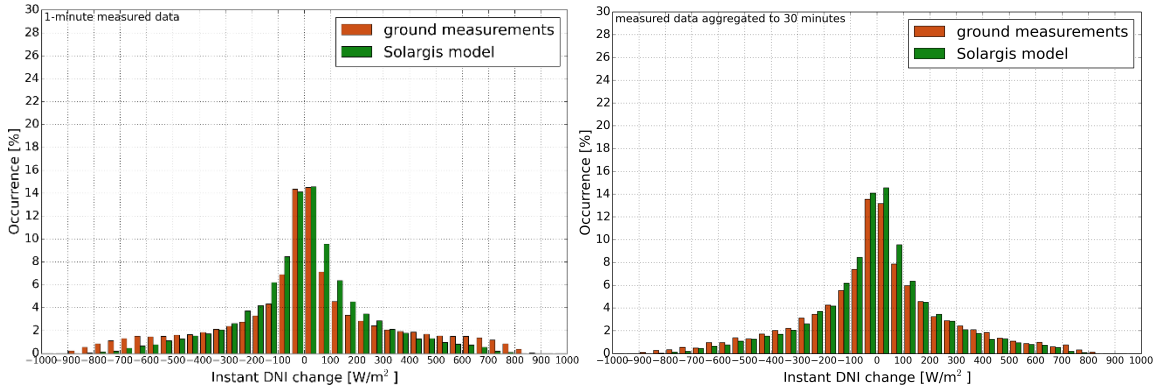

Figure XXXV: 1-minute and 30-minute DNI ramps (measured and satellite data) at Hanimaadhoo

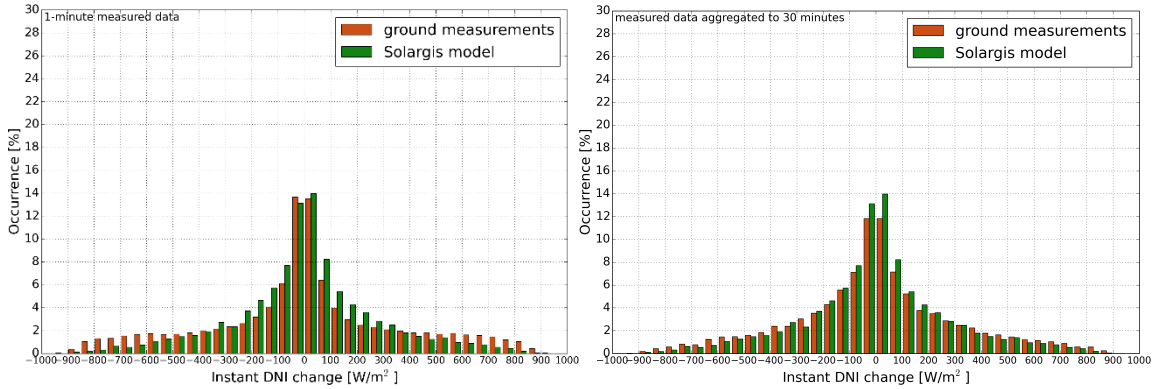

Figure XXXVI: 1-minute and 30-minute DNI ramps (measured and satellite data) at Hulhulé

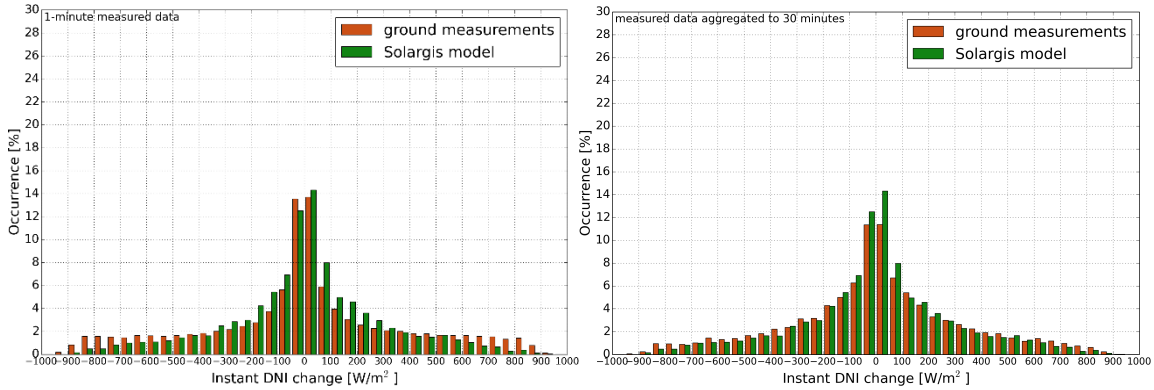

Figure XXXVII: 1-minute and 30-minute DNI ramps (measured and satellite data) at Kadhdhoo

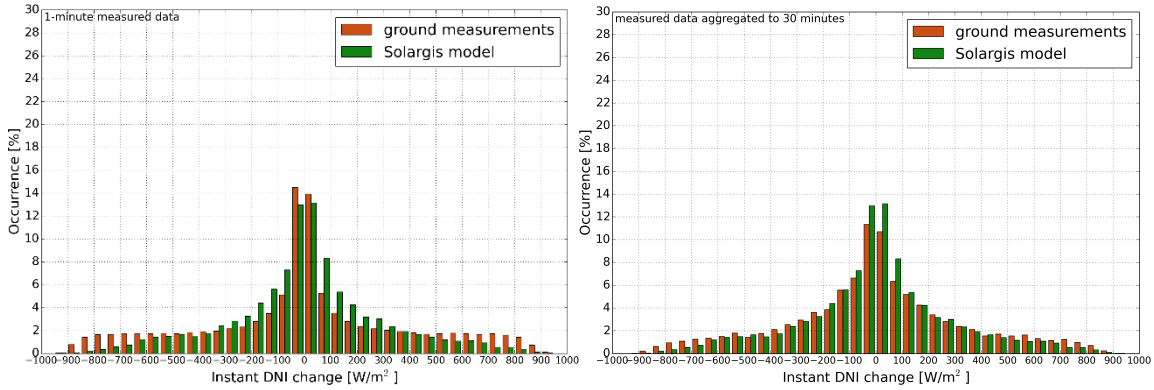

Figure XXXVIII: 1-minute and 30-minute DNI ramps (measured and satellite data) at Gan

LIST OF FIGURES

LIST OF TABLES

REFERENCES

[1] NREL, 1993. User's Manual for SERI_QC Software-Assessing the Quality of Solar Radiation Data. NREL/TP-463-5608. Golden, CO: National Renewable Energy Laboratory.

[2] Younes S., Claywell R. and Muneer T, 2005. Quality control of solar radiation data: Present status and proposed new approaches. Solar Energy 30, 1533-1549.

[3] Perez R., Cebecauer T., Šúri M., 2013. Semi-Empirical Satellite Models. In Kleissl J. (ed.) Solar Energy Forecasting and Resource Assessment. Academic press. http://www.sciencedirect.com/science/article/pii/B9780123971777000024

[4] Cebecauer T., Šúri M., Perez R., High performance MSG satellite model for operational solar energy applications. ASES National Solar Conference, Phoenix, USA, 2010. http://solargis.com/assets/publication/2010/Cebecauer-Suri-Perez--ASES2010--High-performance-MSG-satellite-model-for-operational-solar-energy-applications.pdf

[5] Šúri M., Cebecauer T., Perez P., 2010. Quality Procedures of Solargis for Provision Site-Specific Solar Resource Information. Conference SolarPACES 2010, September 2010, Perpignan, France. http://solargis.com/assets/publication/2010//Suri-Cebecaue--Perez-SolarPACES2010--Quality-procedures-of-solargis-for-provision-site-specific-solar-resource-information.pdf

[6] Cebecauer T., Suri M., Gueymard C., Uncertainty sources in satellite-derived Direct Normal Irradiance: How can prediction accuracy be improved globally? Proceedings of the SolarPACES Conference, Granada, Spain, 20-23 Sept 2011.

[7] http://solargis.com/assets/publication/2011/Cebecauer-Suri-Gueymard--SolarPACES2011--Uncertainty-sources-in-satellite-derived-direct-normal-irradiance--How-can-prediction-accuracy-be-improved-globally.pdf

[8] Suri M., Cebecauer T., 2014. Satellite-based solar resource data: Model validation statistics versus user's uncertainty. ASES SOLAR 2014 Conference, San Francisco, 7-9 July 2014. http://solargis.com/assets/publication/2014//Suri-Cebecauer--ASES-Solar2014--Satellite-Based-Solar-Resource-Data--Model-Validation-Statistics-Versus-User-Uncertainty.pdf

[9] Ineichen P., A broadband simplified version of the Solis clear sky model, 2008. Solar Energy, 82, 8, 758-762.

[10] Benedictow A. et al. 2012. Validation report of the MACC reanalysis of global atmospheric composition: Period 2003-2010, MACC-II Deliverable D83.1.

[11] Molod, A., Takacs, L., Suarez, M., and Bacmeister, J., 2015: Development of the GEOS-5 atmospheric general circulation model: evolution from MERRA to MERRA2, Geosci. Model Dev., 8, 1339-1356, doi:10.5194/gmd-8-1339-2015

[12] GFS model. http://www.nco.ncep.noaa.gov/pmb/products/gfs/

[13] CFSR model. https://climatedataguide.ucar.edu/climate-data/climate-forecast-system-reanalysis-cfsr/

[14] CFSv2 model http://www.cpc.ncep.noaa.gov/products/CFSv2/CFSv2seasonal.shtml

[15] Cano D., Monget J.M., Albuisson M., Guillard H., Regas N., Wald L., 1986. A method for the determination of the global solar radiation from meteorological satellite data. Solar Energy, 37, 1, 31–39.

[16] Perez R., Ineichen P., Maxwell E., Seals R. and Zelenka A., 1992. Dynamic global-to-direct irradiance conversion models. ASHRAE Transactions-Research Series, pp. 354-369.

[17] Perez, R., Seals R., Ineichen P., Stewart R., Menicucci D., 1987. A new simplified version of the Perez diffuse irradiance model for tilted surfaces. Solar Energy, 39, 221-232.

[18] Ruiz-Arias J.A., Cebecauer T., Tovar-Pescador J., Šúri M., 2010. Spatial disaggregation of satellite-derived irradiance using a high-resolution digital elevation model. Solar Energy, 84,1644-57. http://www.sciencedirect.com/science/article/pii/S0038092X10002136

[19] Zelenka A., Perez R., Seals R., Renne D., 1997. Effective Accuracy of Satellite-Derived Hourly Irradiances. Theoretical Appl. Climatology, 62, 199-207.

[20] Espinar B., Ramírez L., Drews A., Beyer H. G., Zarzalejo L. F., Polo J., Martín L., Analysis of different comparison parameters applied to solar radiation data from satellite and German radiometric stations. Solar Energy, 83, 1, 118-125, 2009.

[21] Lohmann S., Schillings C., Mayer B., Meyer R., 2006. Long-term variability of solar direct and global radiation derived from ISCCP data and comparison with reanalysis data, Solar Energy, 80, 11, 1390-1401.

[22] Gueymard C., Solar resource assessment for CSP and CPV. Leonardo Energy webinar, 2010. http://www.leonardo-energy.org/webfm_send/4601

[23] Cebecauer T., Šúri M., 2015. Typical Meteorological Year Data: Solargis Approach. Energy Procedia, Volume 69, 1958-1969. http://dx.doi.org/10.1016/j.egypro.2015.03.195

SUPPORT INFORMATION

Background on Solargis

The primary business of the company Solargis is in providing support to the site qualification, planning, financing and operation of solar energy systems. We are committed to increase efficiency and reliability of solar technology by expert consultancy and access to our databases and customer-oriented services.

The company builds on experience in solar energy and photovoltaics for 17 years. We strive for development and operation of new generation high-resolution quality-assessed global databases with focus on solar resource and energy-related weather parameters. We are operating simulation, management and control tools, map products, and services for fast access to high quality information needed for system planning, performance assessment, forecasting and management of distributed power generation.

Company Solargis operates a set of online services, integrated within Solargis® information system, which includes data, maps, software, and geoinformation services for solar energy.

Legal information

Considering the nature of climate fluctuations, interannual and long-term changes, as well as the uncertainty of measurements and calculations, company Solargis cannot take guarantee of the accuracy of estimates. Company Solargis has done maximum possible for the assessment of climate conditions based on the best available data, software and knowledge. Solargis® is the registered trademark of company Solargis. Other brand names and trademarks that may appear in this study are the ownership of their respective owners.

ISO 9001
LL-C (Certification)

Solargis is ISO 9001:2008 certified company for quality management.

Authors:	Marcel Suri
	Tomas Cebecauer
	Branislav Schnierer
	Artur Skoczek
	Daniel Chrkavy
	Nada Suriova
Maps:	Juraj Betak
	Veronika Madlenakova
Project manager:	Nada Suriova
Approved by:	Marcel Suri


SOLARGIS